

Facoltà di Scienze MM. FF. NN.

Dr. Massimiliano Rolandi

**ENGINEERING-GEOLOGICAL STUDY OF  
DEBRIS SLIDE – DEBRIS FLOW TRIGGERING  
MECHANISM IN THE ISCHIA ISLAND**

Project funded by the Italian Ministry Of University and Research (MIUR) and developed at the Department of Geosciences of “Virginia Polytechnic and State University” and Department of Earth Sciences “Federico II University” of Naples.

**Advisory Board**

R.J. Bodnar

Pantaleone De Vita

B. De Vivo

# **CHAPTER 1**

## **1.1. INTRODUCTION**

In recent years several catastrophic landslides took place in the Campania District, Italy. These provoked the loss of human lives and millions of Euros in damages.

On May 5 and 6 1998, hundreds of landslides were triggered on the “Pizzo D’Alvano” relief belonging to the Sarno Mountains. These stroke the towns of Sarno, Siano, Quindici and Bracigliano, located at the foot of the mountain, causing 159 deaths and damages to the local structures economy.

The following year, on December 16, fifteen shallow landslides occurred on a relief close to the Town of Cervinara, after a period of intense rainfall. This was a minor event with respect to that of Sarno Mountains, but still it caused fatalities.

More recently, on 30 April 2006 on the Island of Ischia, an analogous event occurred on the “Monte di Vezzi”. On the slopes belonging to this relief, five shallow landslides were triggered after intense rainfall. Also in this case the loss of four human lives has been recorded.

Several analogies can be found between the “Monte di Vezzi” landslides and the events previously occurred in Sarno and Cervinara. The pyroclastic soils that are involved in the landslides are mostly coarse pumice and fine ash. The pumice layer in primary deposits is always on top of ashy layers. Therefore, the contact interface represents a hydraulic discontinuity where seepage flow is likely to arise. Moreover, landslides took place during or after periods of relatively intense rainfall. However, it should be noted that these landslides occurred in different geological settings. In the first case the geological setting is characterized by heterogeneous pyroclastic deposits that lay on volcanic bedrock; in the case of Sarno and Cervinara the pyroclastic soil are deposited on top of carbonate bedrock.

With the present doctorate thesis it is meant to give a contribution to the interpretation of the triggering mechanism of shallow landslides occurring in pyroclastic soils. The study area that is deemed to be ideal for this purpose is “Monte di Vezzi”, Ischia.

The purposes of this research project are:

1. To put in evidence the relevant factors of susceptibility characterizing the failed slopes in the research area.
2. To give a previous estimate of the soil strength parameters mobilized at the limit equilibrium.
3. To propose the methodology adopted in the present research as a suitable, economically affordable and reliable mean to approach the study of debris slide-debris flow phenomena.
4. To define the geologic model of the slope. This will represent the basis for a complete formulation of a triggering mechanism.
5. To experiment engineering geological methods and criteria leading to the draft of initial landslide susceptibility map.

This research study will mainly include the following field and desk analyses:

1. Engineering geological field analyses for the identification of the main factors of susceptibility that will be included in the geological model of the slope. More specifically these will include: evaluation of the soil stratigraphy in situ; soil sampling for the evaluation of mechanical and index properties in the laboratory; in situ infiltration tests for the evaluation of the hydraulic conductivity of each layer; in situ penetrometric tests to obtain a preliminary estimate of soil strength;

detailed in situ measurements of the scar topography. This latter are fundamental for the execution of the landslide back analysis.

2. Laboratory testing to evaluate index and mechanical properties of the soils involved in the instability.

This will include: direct shear tests on undisturbed soil samples to evaluate peak and residual shear strength parameters; infiltration tests on undisturbed soil samples to evaluate the hydraulic conductivity of each layer.

3. Back analysis of the initial failure with the aim of estimating the pore pressure necessary to trigger the landslide (in terms of water table height).

This research study has been developed also at the “Virginia Polytechnic Institute and State University”, Blacksburg Virginia-USA. It is part of a more extensive project, funded by the Italian Ministry Of University and Research (MIUR). This project is developed between the department of Geosciences of the previously mentioned University, and “Department of Earth Sciences” Federico II University, Naples, and has the main goal of internationalization of the research.

The heads the international research project are Prof. Benedetto De Vivo, professor of Geochemistry at the Department of Earth Sciences of the Federico II University Naples and Prof. Robert. J. Bodnar, distinguished professor of Geochemistry at the Department of Geosciences of Virginia Polytechnic Institute and State University of Blacksburg. The supervisor of the project is Prof. Pantaleone De Vita, associate professor of Engineering Geology at the “Department of Earth Sciences” of the Federico II University Naples.

## **1.2. GEOLOGICAL SETTING OF CAMPANIA SURROUNDING VOLCANIC DISTRICTS**

The tectonic evolution of the Apennine is believed to occur in two phases: the first one that goes from the upper Oligocene to mid Miocene is characterized by the convergence of the European and African-Adriatic plate takes place. The second phase that goes from the upper Tortonian to the Quaternary, by the roll back of the lithosphere of the Ionic plate generated the thrusts of the chain and the formation of the Tyrrhenian basin. The roll back is a passive subduction of a plate with respect to another. This is due to an increase in weight of one plate that plunges into the mantle and stretches the other plate. This complex mechanism of passive subduction of the Ionic plate generates in turn a counterclockwise rotational shift of the Tyrrhenian plate that has two main consequences: the aperture of the Tyrrhenian Sea. The overtopping of the Tyrrhenian lithosphere on the Ionic lithosphere resulting ultimately in the formation of the Apennine chain and the stretching of the crust that is lacerated with following magma lift up in the central Tyrrhenian zone.

The Campanian Plane and the Garigliano Plane are two depressions whose formation started during the Pliocene and continued throughout the following 5 million years due to the sinking of carbonate Apennine platforms. The carbonate plates not collapsed emerge at the sides of the Planes bordering them (Aurunci-Monte Massico, Northern side and Monti Lattari, South side). The carbonate blocks collapsed unevenly with parts more depressed (graben) and parts less depressed (horst). The two depressions have subsequently been filled by volcanic sediments. Some investigations, aimed to the discover of geothermal sources that have been conducted in proximity of the town of Parete, revealed the presence of an ancient volcanic activity in the Campanian Plane (Di Girolamo et al 1976). A scheme of the recent volcanic activity (< di 1000.000 years) in the Campanian and Garigliano Plane is presented in figure 1.1.

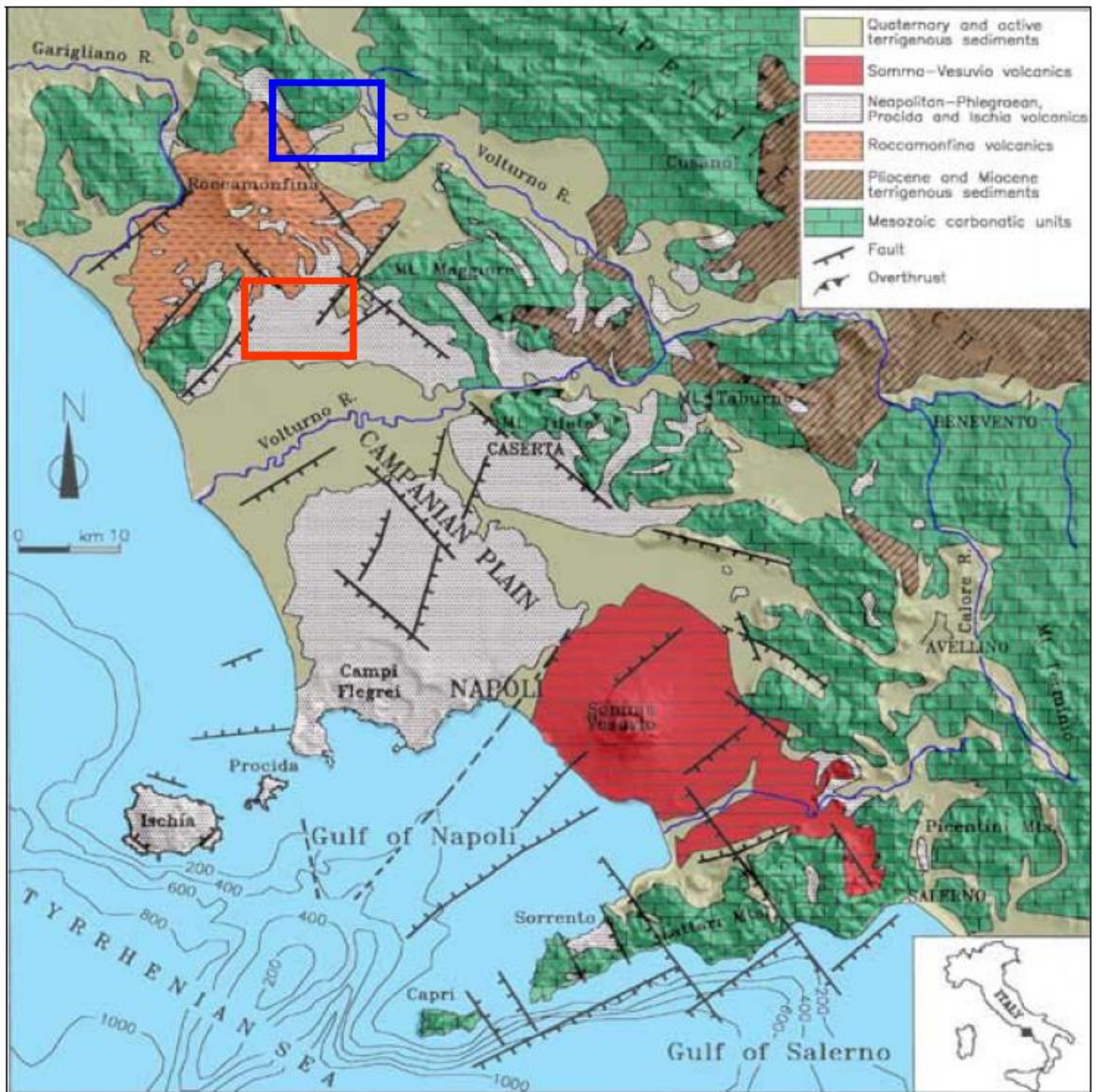


Fig. 1.1: Geology of the surroundings of the volcanic districts in Campania

In the Garigliano Plane the oldest volcanic activity occurred at Roccamonfina volcano (600.000 and 100.000 years bp). A synthetic outline of the volcanic activity in the Campanian Plane is the following:

- Ancient explosive volcanism of the Campanian Plane: six different eruptions belong to this category. These occurred from 300.000 to 39.000 years bp (Rolandi et al 2003). These eruptions are associated to the late tectonic activity leading to the Apennine formations and originated from centers located in the Campanian Plane. Numerous centers are present with a past volcanic activity older than 50.000 years in the area of the Campanian Plane north of the Gulf of Naples (Miliscola Volcano, Cuma and Punta Marmolite Cupola) or In the Ischia Island (Monte Epomeo Eruption, 55.000 ybp and Monte di Vezzi eruption 130.000 ybp).
- Campanian Ignimbrite Eruption, 39.000 ybp: this is the most violent eruption occurred in the Campanian volcanic district. The centre of the eruption according to Rosi e Sbrana (1983) is located in the Phlegrean Fields whereas according to Rolandi et al. (2003) the first fissures manifested in the Campanian Plane. In this case the eruptive centers are located in the north, middle and south sector of the Plane.
- From 39.000 to present, the volcanic activity is concentrated in the active areas of the Phlegrean fields and Somma-Vesuvio.  
In the Phlegrean Field, the most relevant eruption is that of Yellow Neapolitan Tuff occurred 15.000 ybp. This led to the formation of the Phlegrean Caldera, inside of which there is a volcanic field where about 30 small eruptions occurred over the time, the last of which is that of Monte Nuovo, 1538.

The recent volcanic activity of the Somma-Vesuvio started after the Campanian Ignimbrite eruption of 39.000 ybp. The Somma volcano was built over 10.000 years and has been disrupted by seven Plinian eruptions. Among these, one of the most powerful and disruptive has been that of 79 a.C. (Avellino eruption) after which the caldera was formed. After the Avellino eruption the volcanic activity has been of low to medium explosive intensity (Interplinian phase Rolandi et al, 1993) that happens in between of two Plinian eruptions and precedes a period of repose in the volcanic activity. The middle age Interplinian phase, following to the 472 a.C., which has ended in 1139, has lead to the formation of the Vesuvio volcanic cone inside the caldera of the Somma. After a period characterized by no volcanic activity, there has been the most recent Plinian eruption in 1631. The following most recent Interplinian phase has lasted 300 years and has been characterized by a peculiar cyclic activity (Vesuvian Cycles). The last cycle started in 1913 and was closed by the 1944 Eruption.

The “Monte di Vezzi” is a top flat relief trending in the anti Apennine direction that is located in the south-eastern part of the Ischia Island and that characterizes its orography. It is a former volcanic center whose past activity is associated to a NE-SW trending set of faults. The volcanic dome that represents the main structure of the relief is composed of several successions that are belonging to the two main cycles of the Ischia Island volcanic activity, separated by the Mount Epomeo green tuff eruption (Chiesa *et alii* 1987; Vezzoli, 1988).

The 6 April 2006 five landslides took place in the Piano Liguori formation, the more recent volcanic deposit (6 ky), that is a relatively thick non homogeneous succession of fine volcanic ash and coarse lapilli, covering a welded scoria formation and interested by pedogenetic processes.

The relieves surrounding the Campania Plain are composed by a several hundred meters thick sequence formed during the Cretaceous and characterized by calcareous, dolomite and marly litho types. They result widely fractured, as a consequence of the Miocene tectonic phases, and interested by karstic processes that influenced both morphology and hydrogeology (Celico & Guadagno, 1998). Such ridges form monocline structures gently dipping in the SE direction. The morphological configuration of these ridges has also been influenced by the Pliocene and subordinately by the Quaternary, tectonic stretching phases. These latter activities, that generated two sets of normal faults trending NW-SE and NE-SW, characterized the Campania Apennine relieves, with typical steep slopes morphology derived from fault-line scarps evolution. A common feature to all the relieves located in the south-east area of the Somma-Vesuvio eruptive center, is the presence of a pyroclastic soil cover, deposited on the carbonate slopes, formed by ash-fall deposits erupted from the volcano. The ash-fall soils were air-transported mainly eastward according to the dispersion axes of each eruption. This process determined the actual stratigraphy, characterized by a non homogeneous sequence composed by coarse (predominantly pumice) and fine (ashy) layers. The pyroclastic soils on the mountains of this area are mainly belonging to the eruptions of Sarno, Ottaviano and Avellino (17.000y BP, 8.000y BP and 3.500y BP respectively) and to the eruptions of 79 DC, 472 DC e 1631 DC (Rolandi et *alii*, 2000). These can be found along the slopes laying both in primary and in secondary deposition.

Pyroclastic soil deposits in primary deposition are characterized by the bedding parallel to the bedrock, with a mantling setting. In this case the thickness of the deposit can just reach few meters. Conversely, pyroclastic soils in secondary deposition have been locally reworked by denudation processes and are generally present at the down slope location as a result of erosion processes (rill and gravity) forming alluvial fans thick up to twenty meters. The effect of the erosion process affecting the pyroclastic cover can be interpreted with an empirical relationship between the thickness and the slope angle (De

Vita, 2006). In particular, an increase in slope angle that may occurs upslope determines a decrease of the thickness of the soil deposit due to erosion processes. Thus, a discontinuity can be noted both in the vertical and lateral direction. This influences the hydrogeology of the site and determines a high variability of physical and mechanical soil properties.

### **1.3. THE APPROACH TO DEBRIS SLIDES – DEBRIS FLOWS**

The south eastern sector of Campania region is thoroughly affected by debris flows occurring in volcanic soils. Here the stability of the slopes is a major concern, and this kind of landslides happen with a very high frequency (Guzzetti, 2000). Based on historical database from Guzzetti *et alii*, (1994), De Vita (2000) estimated that the average recurrence time associated to these phenomena is of three years.

These catastrophic events are known from the chronicles since the past century, but strongly interested the scientific community only after the tragic occurrence of “Pizzo d’Alvano”, in 1998. The scientific contributions towards the understanding of the triggering mechanism of these phenomena are based on the well documented cause-effect relationship existing between landslides and rainfalls. The susceptibility of the slope to the landslide is also a relevant aspect that is considered in the literature. Good agreement also exists on the classification of this kind of phenomena as *debris slides-debris flows* (Cruden & Varnes, 1996). These landslides are generally characterized by a complex style: there is an initial *debris slide* of the shallower part of the pyroclastic soil deposit present on the slope and a final *debris flow* where the whole fluid mass is channeled into down slope hollows. There is also an intermediate phase of *debris avalanche* (Hungar *et alii*, 2001), where the instability is extended to a larger portion of the pyroclastic deposit. In this phase the scoured area assumes a typical triangular shape in plane.

The term *debris-flow* indicates a movement of debris and earth whose rheological behavior is similar to a flow due to the high water content and dynamic conditions. This soil-water mixture is characterized by an extremely high velocity estimated to be in the range 5m/s to 15 m/s. Due to the notable portion of water mixed to debris and earth the instable mass can be compared to a viscous fluid more than to a rigid body. As a reference for a preliminary qualitative description of the behavior of this fluid on a sloping surface, the *Bingham's* (Bingham, 1916) model is taken into account. For this kind of materials, friction forces grow inside the mass, between the different layers, as a consequence of the external actions, without any appreciable deformation (these appear only close to the contact with the bedrock). When the shear stress from frictional action equals the *yield strength* large deformations affect the whole mass evolving into a flow. Studying static liquefaction by means of triaxial dead load laboratory tests, Sasitharan *et alii* (1993) found that before static liquefaction of a soil specimen occurs, very little strain happened. It can be speculated that a *debris flow* is triggered after an increase of pore pressure – while the total stresses remain almost constant - due to ground water flowing into the soil. This causes a decrease in effective stresses that in turn determines a decrease in yield strength of the soil. When this latter equals the acting shear stress, failure occurs. Before this point, little strain happened in the soil, while after it, the deformation extends to the entire soil mass.

Several types of triggering mechanism can be distinguished. The first is the one that occurs during the phase of debris-slide. Here the instability is generated by an increase in pore water pressure due to a down slope directed seepage flow. This makes the effective stresses decrease, ultimately resulting in failure. This typically occurs in the zero order basins (Dietrich *et alii*, 1986), or where discontinuities characterize the morphology of the slope. The second triggering mechanism is characteristic of the phase of avalanche. This generally occurs in the middle portion of the slope. Failure occurs under undrained conditions generated by the impact of soil or rocks originally located up slope. During the

flow phase landslides are also generated after scouring and cut of lateral support occurs in the hollows and channels located at the foot of the relief. This is a phenomenon that follows the canalization of the fluid soil masses mobilized upslope.

Following the approach proposed by Corominas (1996), Budetta & De Riso, (2004) analyzed the run out distances, elevation of the sliding area and soil mobilized volumes for the events occurred both in the Sorrento Peninsula (1997) and on the Sarno Mountains. They identified two categories of *debris flows* for the Campania area. For the case of Lattari Mountains, the distances covered by the flows normalized to the elevation of the source area (that is the reach angle) and to the mobilized volume were small compared to the same parameter evaluated for the Sarno Mountains. Thus, the *debris flows* occurred at the Lattari Mountains are characterized by a low mobilization degree, while that of Sarno mountains are characterized by high mobilization degree.

Many aspects that play an important role in triggering a *debris-slide debris-flow* can be identified. These can be subdivided into two main categories: predisposing factors and triggering factors. The first refer to the existing geological condition of the slope prior to the instability. The second are those determining the initiation of the landslide. In the first group it is possible to include the following:

- The geology of the site: the past volcanic activity influenced the stratigraphy of the pyroclastic cover and the mechanical properties of each layer. Related to the depositional characters of the soil, are also the porosity (affecting the permeability of the soil, but also the shear strength) the pore size distribution (affecting mostly the permeability in the non saturated field);
- The slope morphology: the angle of inclination of the slope and the curvature angle, affect both the direction of the groundwater flow and the magnitude of the forces driving the instability. Artificial discontinuities, like road cuts and natural

discontinuities, like vertical rock cliffs, are a source of slope instability (Guadagno *et alii*, 2004);

- - The hydrology: rainfall intensity and duration as well as rain event frequency affect soil moisture content and thus the formation of saturated areas inside the soil. The moisture content is also related to the matrix suction. This represents a surplus of shear strength for the unsaturated soil portions;
- The hydrogeologic conditions: this mostly determines the response of the slope to a rainfall event on which the following in situ stress path depends. At the contact interface of layers with different hydraulic conductivity lateral infiltration and seepage flow are likely to occur. As said, this determines the increase in pore water pressures and thus the decrease in effective stresses on which strength depends.
- Another aspect to take into account is the shallow vegetation covering the slope: several studies (Preston & Crozier, 1999; Selby, 1993) show the importance of a root network as an additional source of cohesion for the soils.
- Among triggering factors, the rainfall intensity in the day of the event and the number of rainy days before the landslide can surely be included. This latter play a fundamental role in triggering the instability as recently demonstrated for the south east Campania area (De Vita, 2000; Celico *et alii*, 2001).

#### **1.4. SUSCEPTIBILITY AND TRIGGERING FACTORS**

As mentioned previously, many are the aspects that can be listed as factor that contribute to make the pyroclastic soils prone to the instability. Some of these are considered and analyzed, for the pyroclastic soils in the study area, in the following paragraphs.

The stratigraphy of the pyroclastic cover at “Monte di Vezzi” is mainly composed by coarse grained pumice layers that are very permeable, that lay on top of fine ashy soils

with low permeability. This configuration allows for the development of saturated areas at the contact interface in response to a rainfall event. The increase in water content in the soil progressively makes the suction decrease. In the mean time, also soil conductivity increases, favoring the development of a down slope directed flow. The result is an increase in pore pressures and the consequent reduction in effective stresses on which shear strength depends. Although the presence of lateral flow was only an assumption not yet experimentally proven in this area, this element is thought to be a fundamental factor in the initiation of the instability, as speculated from most, (Celico *et alii*, 2001; De Vita & Piscopo, 2002; Crosta & Dal Negro, 2003). However, field observations by De Vita *et alii* (2008) for the “Monte di Vezzi” landslide, evidenced some features supporting the hypothesis of down slope directed flow in response to a rainfall event. Three different geological models have been proposed for the description of the stratigraphy characterizing the soils on the slopes of Lattari, Salerno and Sarno Mountains. All of these have as main factor of susceptibility to landslide the abrupt change in permeability between pumice and ashy layers (Celico *et alii*, 2001).

Another predisposing factor is represented both by the primary and secondary porosity that characterize this kind of soils. Pumice deposits show a high secondary porosity due to interconnected voids. This aspect determines a high capacity of water retention (Whitan & Sparks, 1986), that contributes to increase the soil unit weight and in turn the forces driving the instability. Both the pumice and the ashy layers are deposited in a very loose state. Thus they are characterized by a high value of primary porosity. Moreover, the thickness of the whole pyroclastic cover involved in the landslide is not relevant. This means that the confining pressure at the end of the depositional process is very low. Loose soils at low confining pressure show an unstable behavior under undrained or drained-constant-volume conditions. Casagrande (1940) was the first to recognize the role of porosity on the stability of granular soils, introducing the concept of critical void ratio. The steady state concept was than introduced by Pulos (1981). It can be said that a

granular cohesionless soil that shows an unstable behavior is a contractive soil that, due to an increase in pore pressures, reaches the steady state. As the in situ void ratio and confining stress also other factors have to be shown to influence the stability of the soil. These are the initially mobilized friction ( $k_c$ ) and the evolution of the stress path in the field.

Olivares *et alii*, 2003 recognized the susceptibility to liquefaction of granular materials involved in the Cervinara 1999 *debris-flow*. They identified steady state parameters like the critical value of the porosity for laboratory reconstructed samples. However, no estimate are given for a critical value of the in situ void, no estimates are available on the field void ratio. Thus, the necessary but not sufficient condition for *debris slide* to become a *debris flow* is the presence of high water content. The soils also have to be predisposed to fluidization (liquefaction) and, as mentioned, this is solely dependent on physical soil properties (void ratio, and subordinately from grain size, fine content) and influenced mostly from confining pressure, stress state and stress path. The porosity also affects the permeability in the non saturated regime. According to Brooks & Corey model (1966) the unsaturated permeability is a function of the saturated permeability, the matrix suction and the pore size distribution. Areas of the pyroclastic cover where pore size is smaller (likely, the ashy layer) will be characterized by a lower value of the permeability with respect to zones where the pore size is bigger (pumice layer). This happens even though the total porosity is the same. Harr (1977) found that the non homogeneous pore size distribution along the depth caused a change in permeability of one order of magnitude in a soil where the total porosity was found to be constant along the depth.

An element to carefully evaluate is the mineralogical composition of the ashy layer that directly influences the consistency of this soil. Mineralogy also affects the shape of the granular soil elements and ultimately the peak and residual shear strength. Terribile *et alii*, (1996) noted the presence of clay minerals “Allophane” and “Imogolite” for the pedogenized soils of “Pizzo D’Alvano”. Angular shaped grain offer a higher peak

frictional resistance than platy shaped, because of the interlocking effect. This latter aspect seems to be less relevant for what concern the triggering phase, since failures at “Monte di Vezzi” interested the coarse pumice layer. However, a sharp grain shape can have an influence on the following phases of avalanche and flow because it provides the soil with high residual shear strength. Crosta & Dal Negro (2003) noted for the soils of Sarno that the difference between peak and residual friction angle obtained by direct shear tests was of few degrees.

For what concern the morphology of the slope, several are the parameters that can be accounted as susceptibility factors. The morphological discontinuities are referred to as natural cliffs or artificial road cuts and are very likely to affect the stability of the slope. A road cut, as well as a sub vertical cliff live exposed totally or partially the soil profile. Shear strength are reduced because of the lack of lateral confinement, driving stresses acting on weak planes generate the slope failure. Guadagno *et alii* (2004) highlighted the fundamental role played by road cuts and natural slope outcrops in triggering 5-6 May 1998 initial slides. They put in evidence that only 15% of the total initial slides were not linked to a morphological discontinuity.

Also the slope angle has a fundamental role since this directly affects the driving forces. For the *debris flows* occurred in Campania in 1998 it has been reported from several authors that the initial slide took place where slope angles reached values included in the range 35°-40°. Likewise, lateral curvature of the slope, hence the presence of hollows and spurs, have been shown to play a relevant role in influencing groundwater flow convergence and the formation of saturated zones where pore pressures are built up (Anderson & Burt; 1977).

Among the triggering factors one to include is surely represented from earthquakes. The direct correlation between earthquakes and *debris flows* initiation has not been observed yet in this area. However, the cyclic load generated from ground shaking could compact the moist loose soils on the slope, determining a sudden increase in pore water pressure

and ultimately liquefaction. Although earthquakes represent a source of high geological risk in the Campania area they are considered a minor triggering cause with respect to rainfalls.

A well established correlation exists between rain events and landslides initiation. In Campania it has been observed how *debris flow* often occurs at the end of the rainy season, and during or after major rain events. This is mainly due to the high moisture content of the soil during this period, likely very close to saturation. Several analyses on the rainfall events that triggered landslides on the mountains at the south-east border of Campania have been carried out (De Vita, 2000; Celico *et alii*, 2001). This was done with the main aim of defining pluviometric thresholds based on slopes moisture conditions. For the Lattari Mountains it was found that a minimum height of 50 mm of rain, computed daily, is necessary to trigger the instability. This value appeared to be not dependent on previous precipitations (and thus on slopes moisture conditions) if the antecedent rainfall height was of 180 mm or greater. An always increasing rainfall height value is necessary to landslide initiation, as the antecedent rainfall height is less than 180 mm. This shows how the rainfall is an element as well predisposing as triggering the slope instability. In other cases (the Sarno Mountains) it was not possible to define a unique value for the triggering threshold and another correlation was proposed, between rainfall in the day of the event, and homogeneity of the sequence of antecedent rainy days. Here for homogeneous sequences rainfall heights to trigger the landslide are found to be lower than that proposed for Lattari Mountains. Also in this case the study evidenced the importance of the antecedent rainfall heights strictly related to slopes moisture condition.

## **1.5. RESEARCH PLAN**

In an effort to define a complete engineering geological model that suits the areas where the initial debris slide takes place, the geological model of the slope was reconstructed

and back analysis performed. The reconstructed geological model takes into account the main factors of susceptibility to landslide of the slope that were evidenced during field survey and laboratory tests. It is worth to notice that these are mostly the same that also affect other areas of the Campania region like Lattari Mountains or Sarno Mountains, where the catastrophic 1997 and 1998 events took place. The factors that were taken into account are:

- 1) The stratigraphy of the soil at the site. This is obtained by means of visual characterization and laboratory grain size analysis (ASTM D-422). As mentioned previously, soil layering appeared to be one of the fundamental susceptibility factors. At the basal soil interface an increase in pore pressure is likely to occur leading to slope instability.

- 2) The hydraulic properties of the soil that may lead to a more complete understanding of the hydrologic response of the slope to a rainfall event. Even though the hydraulic conductivity is not explicitly involved in the formulation of the model, the inherent anisotropy that depends on the specific layering of the soil plays a fundamental role in triggering the landslide. Based on the stratigraphy at the site, and on experimental evidences in similar settings, the hydrological response of the slope can be summarized as follows: a change in volumetric water content with the time occurs in the pyroclastic cover. This is not uniform but varies along the soil profile differently depending on the location (up slope or down slope) and antecedent soil moisture conditions. A pore pressure increase that travels down slope is generated as a consequence of the infiltration process. This is intended as an initial (up slope) matrix suction decrease (flow in the non saturated area) and eventually, as a seepage flow after saturated area formation (middle of the slope).

Back analysis of the failures is performed using the software SLIDE 5.0 for the evaluation of the strength parameters. Software calculations are then checked by means of spreadsheet, according to the Swedish Circle Method (see chapter 3 for more details) and the Infinite Slope Method. This was performed after the following steps:

a) The evaluation of landslide topography by means of accurate in situ total station theodolite measurements. This allowed for the reconstruction of the scar surface profile and put the basis for the back analysis of the landslide. Moreover, laboratory analyses for the evaluation of the physical parameters were conducted.

b) A discussion on the choice of the appropriate parameters to use as an input for the back analysis. It should be taken into account that some simplification are necessary to come up with a model of the field problem to analyse.

c) Another fundamental aspect to take into account is represented by the stress path that actually occurs in the field, and from the type of failure that the soil experiences. A discussion is done about the possible stress paths occurring in the soil leading to failure. The concept of congruence of the stress state to the actual field physical state is also introduced.

d) Back analysis is actually executed under different hypothesis. The results are: the evaluation of a constant-back calculated value of the shear strength of these soils to use for stability analyses in similar settings; the definition of rain intensity threshold over which the instability is triggered.

## **CHAPTER 2**

## 2.1 SUMMARY OF FIELD MEASURES AND LABORATORY ANALYSES

After the 30 April 2006 landslides occurred at “Monte di Vezzi”, a research study took place to evaluate the landslide susceptibility factors and triggering mechanisms.

During the days following this catastrophic event, several surveys of the site were conducted, allowing for the identification of some general features (Fig. 2.0)

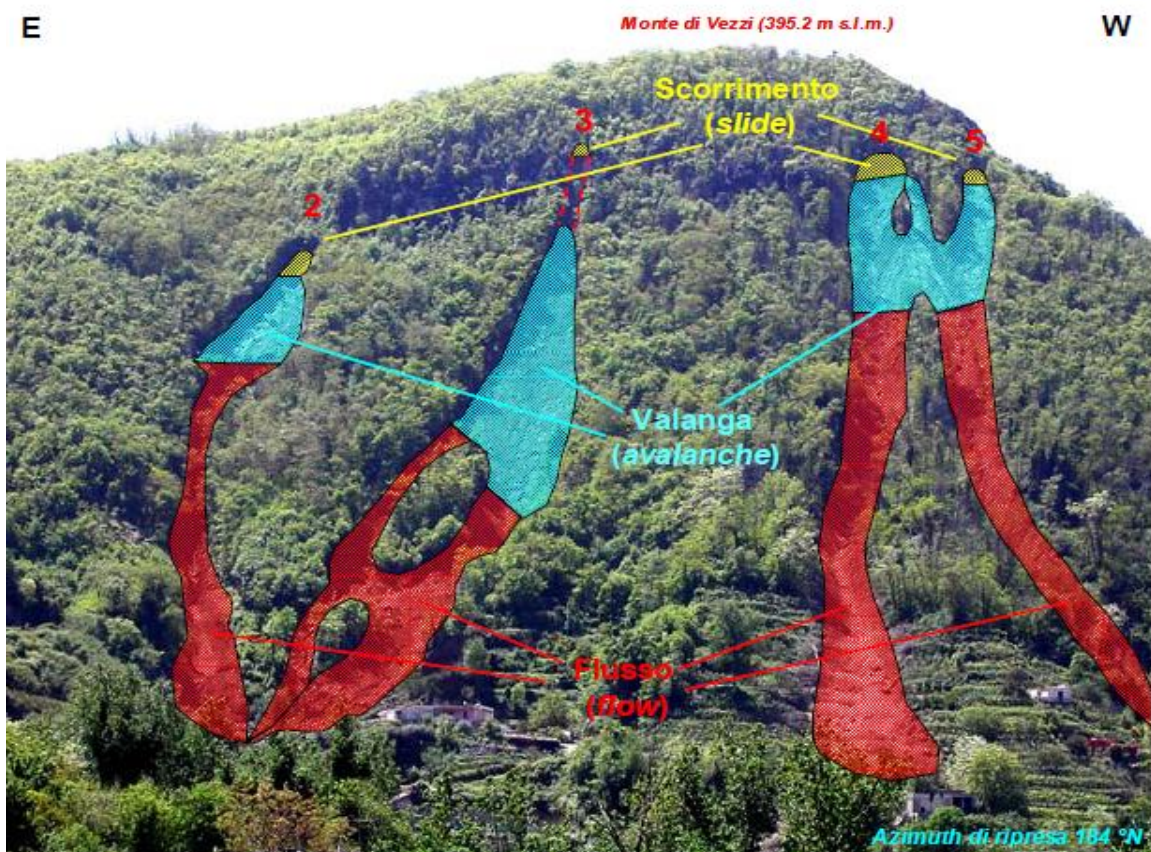


Fig. 2.0: Different phases of the debris slide-debris flow occurred at Monte di Vezzi (from De Vita et al, 2007).

It was possible to assess that the landslide involved the shallow portion of the pyroclastic cover mantling the steep slopes of “Monte di Vezzi”. A preliminary estimate of the mobilized thickness along the median axis of the scar surface is of about one meter. The basal soil that remained in place, exposed after the landslide occurred, was saturated and very soft such deep footprint could be left in the soil during the inspection process.

On the lateral boundary of the scar surface, the mobilized thickness of soil appeared to be much less than one meter. At several locations immediately down slope of the triggering area, there was the evidence of the overtopping of the slid soil mass. This could be interpreted as evidence of soil mass mobilization after undrained loading (Hutchinson & Bhandari, 1971; Sassa, 1985) and trigger of a debris avalanche (Hung *et alii*, 2001) eventually evolving into a channeled flow.

The mobilized soil was very fluid and able to reach distances of the order of magnitude of kilometers.

All the landslides started very close to natural discontinuity such as the widely fractured lava cliff. More in particular it was assessed that three of the five landslides, took place down slope of an outcropping lava cliff while only one was triggered upslope of this cliff. In this latter case the main susceptibility factor is most likely represented by the lack of lateral sustain, that puts the soil mass in a state of cinematic mobility.

The slope angles in the triggering area were very high, and estimated to be included in the range 35-40 degrees.

Several minor rainfalls occurred in the days following the landslide. Subsequent surveys in the triggering area also allowed for the identification of erosion channels on the exposed scar surface, caused by groundwater flows coming to daylight. It was recognized that the seepage channels had their starting point at the interface between the silt and the well graded sand, well visible on the exposed soils scar surface. Therefore it can be speculated that a flow actually aroused at this contact interface, during and after a rain event representing a source of slope instability.

Several field campaigns have been conducted at “Monte di Vezzi” in the aftermath of the landslides and during the following years. The main purposes of these campaigns are:

- To define the stratigraphy of the soil in the triggering area. This was done by visually inspecting the exposed landslide scars, and by means of dynamic penetrometric tests.
- To define the hydraulic characteristics of the soil layers. This was done by means of in situ infiltration tests and laboratory constant head permeability tests on undisturbed samples.
- To define the mechanical properties of the soil layers. This was done by means of in situ dynamic penetrometric tests and by laboratory direct shear tests on undisturbed samples.
- To measure accurately the topography of the landslide scar surfaces. This is the basis for the evaluation of the critical rainfall height by means of back analysis of the stability.

The results of the first field campaign, in which infiltration tests, dynamic penetrometric tests and topography measures were conducted, have been presented in a previous work (De Vita *et alii*, 2007). In the present study, the results of subsequent field and laboratory investigations will be presented.

Bag samples and undisturbed samples were collected at several locations at the crown of the landslides occurred at “Monte di Vezzi”. The undisturbed samples were collected first by means of large cubic-shaped steel boxes, and then by means of an on-purpose designed thick walled steel sampler. In the first case, the samples were tested to evaluate shear strength parameters. In the second case, samples were tested in the laboratory to evaluate soils hydraulic conductivity.

**Bag Samples** – thirteen bag samples were collected and tested in the laboratory for the evaluation of index properties. A summary of the collected samples is presented in table n.1. Sampling was conducted in the triggering area after the excavation of trench to identify the stratigraphy and subsequent evaluation of the thickness of each layer. A schematic of the layering, with corresponding thicknesses is presented in Fig.1a.

Layer (USCS)	Bag Sample		Large Box		Cylindrical	
	n	depth (m)	n	depth (m)	n	depth (m)
SM	7	Several	4	0,4	2	0,4
SW-GW	2		3	1,1	2	1,1
ML	4		3	2,1	2	2,1

**Tab. 1: number of samples collected for each layer and depths of collection.**

In the laboratory, bag samples were prepared according to the ASTM D421 standard and then processed for the evaluation of physical properties such as: Grain size distribution - ASTM D422-63; Specific gravity –ASTM D854-92; Plasticity ASTM D 4318-95. Finally all the soils were classified in accordance to the USCS – ASTM D2487-93. A summary of the results is presented in table 2 while gradation curves are shown in figure 2.2.

**Undisturbed Samples (1)** – the samples were collected as large soil blocks by means of on-purpose-designed cubic thin walled steel boxes. The side of each box is of 12 cm. To collect each sample, a trench was preliminary excavated to reach the specific layer at the desired depth. The following step is to push the box into the soil. To make sampling easier and to minimize sample disturbance, the soil in contact with the external surface of the box was removed as the box was advanced. Once a depth of 12 cm was reached into the layer, the box with the sample were recovered, the box open side leveled and the whole sample sealed. Ten large block samples were collected at several depths and in

different soil layers. A summary of the collected samples is presented in table n.1. The specimens were transported to the laboratory and tested in the direct shear apparatus. From each large box, one “core” sample was obtained. This is in order to minimize the disturbance that affects samples collected from coarse grained soil deposits. Where possible, a second sample was recovered. Samples were tested to obtain peak strength parameters.

**Undisturbed Samples (2)** – the samples were collected by means of an on-purpose-designed steel cylindrical sampler. The internal diameter of the sampler is of about 8 cm. A 16 cm long PVC tube, in which the soil sample will penetrate, is hosted in the hollow of the steel cylinder. The undisturbed samples to test for the evaluation of the soils hydraulic conductivity were collected following the same procedure adopted for the large box samplers: trench excavation; sampler penetration in the soil layer; extrusion after removal of the soil surrounding the sampler. The top half of the sampler can then be unscrewed and removed and the soil sample, penetrated into the PVC tube, can be sealed by means of specially designed caps. These caps will allow for an easy apparatus tubes plug-in during laboratory testing. Since the PVC tubes are transparent, the soil sample collected can be visually inspected to check for the integrity of the soil structure.

Six samples were collected, two for each soil layer. A summary of the collected samples is presented in table n.1. The samples were transported to the laboratory and tested in the constant head permeameter.

In the following, laboratory test result are presented and discussed. In order to define a slope geologic model that is the most possible complete, results from previous investigations are also summarized.

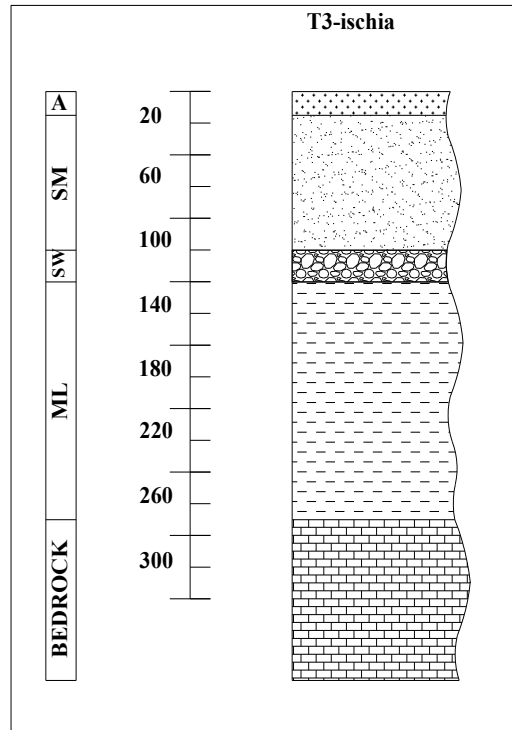


**Fig. 2.1: Typical stratigraphy at “Monte di Vezzi”, Ischia: A, organic soil (Pt); B (B1-Shallow and B2-deep), silty-sand (SM); C1, well graded sand (SW); C2, low plasticity silt (ML) – ASTM D2487; USDA (1998).**

## **2.2 TEST RESULTS AND GEOLOGIC SLOPE MODEL**

In the following paragraphs laboratory test results executed on undisturbed and bag samples are presented. Results from previous laboratory and in situ investigations are also summarized. A comprehensive presentation of these results can be found in De Vita *et alii*, 2007.

### 2.2.1 DISCUSSION OF LABORATORY TEST RESULTS

The first 25cm of soil were recognized in situ as organic soil (Pt) with a large presence of a narrow root network. This layer was not sampled and tested.

The first layer (60 to 80 cm thick) is composed prevalently of sands, with a percentage of fines ranging in the interval 7-15%. The fine is classified as MH-CL. Therefore, these soils (indicated as B in Tab.2) can be identified as SM-SC: “Silty Sand-Clayey sand”.

For the second thin (about 20 cm) layer, both sands and fines content decreased with respect to the previous SM layer, and an increase in gravel content is noted. The fines, where detected, can be identified as ML. The soil layer C1 is classified as GW-SW: “Well Graded Sand with Gravel” or “Well Graded Gravel with Sand”.

It should be noticed that the B layer has a fine content that is relevant with respect to the C1 layer.

The results on samples taken from the third basal layer (C2 in Tab.2), at depth ranging from 1.9 m to 2.3 m, allows to classify this as a ML (PI-LL point plots below the A line): “Silt”, or sometimes as a CL (PI>7 and PI-LL point plots above the A line): “Lean clay”

The void ratio and density estimated for the SM and SW-GW layers, by means of pseudo-undisturbed sampling, confirmed the field observation of granular materials in a very loose arrangement. For SM this parameter is  $e=1.86$  with  $G_{s_{av}}=2.56$ ; for SW-GW it is  $e=2.04$  to and  $G_s=2.55$ ; for C2 it is  $e=0.96$  to  $1.15$  and  $G_s=2.54$ .

From table 2 it is evident that besides the high secondary porosity that contributes to increase the value of the void ratio, some degree of disturbance has affected the measures, leading in some cases to a wide range of variability. Further field measures are necessary for SM and SW-GW layers, for a more refined estimate of such an important parameter that has been recognized to play a central role in phenomena like liquefaction of coarse granular materials.

The highest depth of sample collection is around 2.0 m. Therefore, the stratigraphy was completed based on several penetrometric tests that have been previously conducted at the site.

layer	fine (%)	LL (%)	PI (%)	fine class	sand (%)	gravel (%)	Cu & Cc	soil class	Gs	e
B	15	35.5	12.4	ML-CL	45	40	66 - 5.2	SM-SC	2.48	1.86
	12	36.2	15.9	CL-ML	62	26	25 - 6.5	SC-SM	2.67	
	7	39.5	17.4	CL-ML	50	53	12 - 2.8	SC-SM	2.52	
C1	8	29.9	4.8	ML	36	56	43 - 1.76	GW w/ sand	2.5	2.04
	0	-	-	-	54	46	6 - 1.28	SW w/ gravel	2.61	
	0.5	-	-	-	45.5	54	6.1 - 1.10	GW w/ sand	2.55	
C2	73	39.8	11.9	ML	22	4	10 72	ML w/sand	2.5	0.96 to 1.15
	76	-	-	-	20	8	10 72	ML w/sand	2.63	
	53	34.8	3.1	ML	30	17	12	ML sandy	2.68	
	78	40.8	5.8	ML	17	5	6 71	ML w/sand	2.46	
	73	34.7	10	ML-CL	22	4	12 98	ML w/sand	2.56	
	48	36	13	CL-ML	44	8		ML w/sand	2.42	

**Tab. 2: Summary of laboratory index properties test results on bag samples according to ASTM D2487**

Undisturbed soil samples were collected for the determination of shear strength parameters. The samples were collected from the large boxes and CD direct shear tests were conducted (ASTM D-3080-90). The coarse grained soil samples recovered at depth of 0.4 m and 1.1 m were saturated for several hours under the chosen consolidation pressure and then sheared at a strain rate of 0.12 mm/hr. The fine grained soil samples recovered at higher depths were saturated over night and then sheared at a strain rate of 0.08 mm/hr. All the samples recovered from shallow depths (0.4 m) showed a contracting behavior upon shearing. Dilatant behavior was noted in some case for samples collected at higher depths (see appendixes). Displacement–shear strength curves and displacement-vertical stress curves are shown in appendix 2.

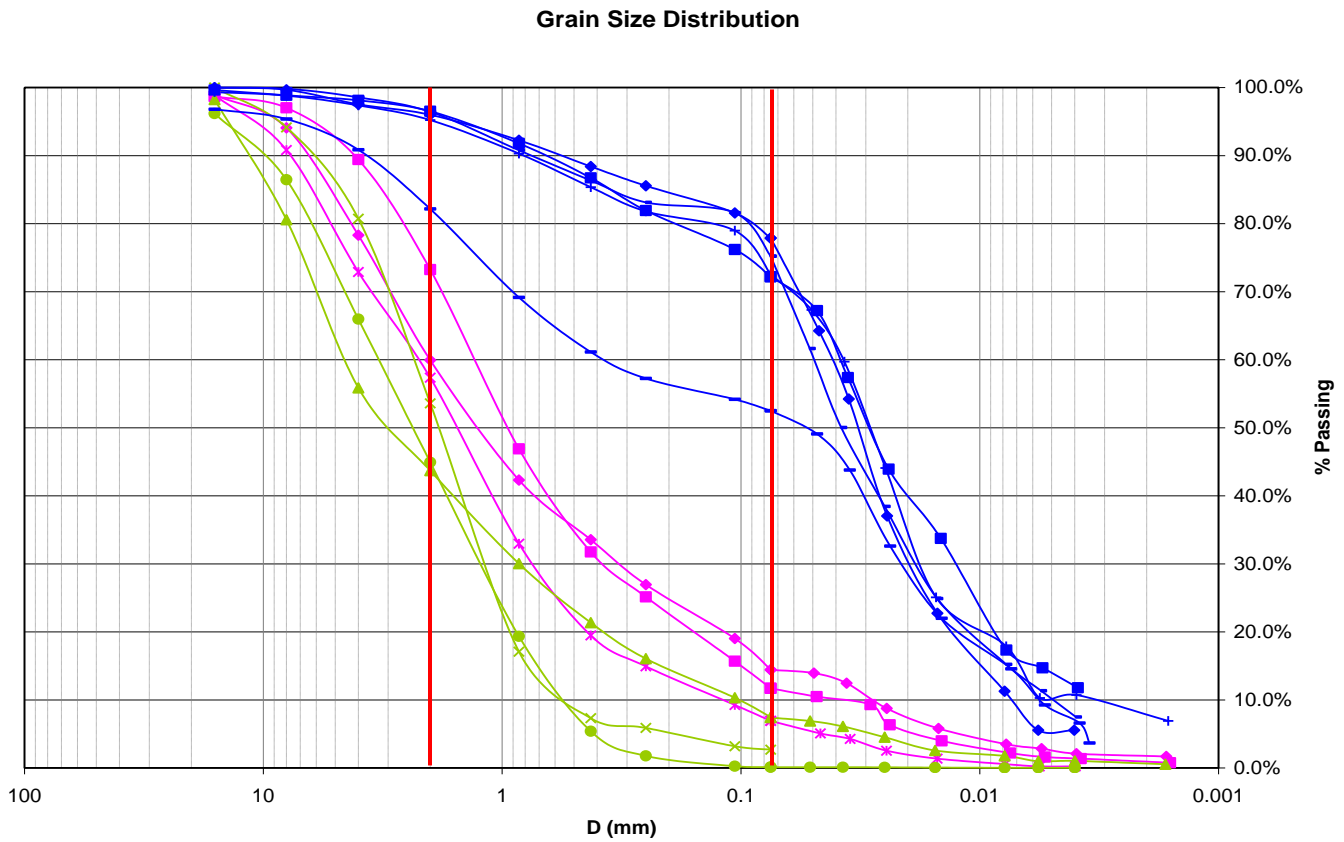


**Fig.2.2: grain size distribution curves: SM; SW-GW; ML**

A comprehensive normal stress-shear stress plot and shear strength versus depth plot are also presented in this appendix. All test results are summarized in table n. 3 and in figure 2.3.

Layer (USCS)	$\gamma_m$ (kN/m <sup>3</sup> )	$\phi'$ (deg)	$c'$ (kPa)
SM	16	36,9	5,8
SM	18.0	37,2	11,1
ML	17.5	27,9	29,4

**Tab. 3: Summary of laboratory CD Shear test results on undisturbed samples. Peak shear strength parameters.**

The material in situ appeared to be cohesionless, except for the basal soil that showed some inherent cohesion. However, it can be seen that test results show some cohesion also in the case of the first two layers. A possible explanation could be the following: the undisturbed soil samples were tested in a 6 cm- side shear frame. The maximum diameter of the soil being tested in such a frame is 6 mm (ASTM D3080-90). The soil actually tested had particle size (30 to 45% in weight) considerably higher than this maximum threshold. This might have induced some additional soil cohesion.

Undisturbed soil samples were collected for the evaluation of the permeability of the soil. The samples in PVC tubes were tested in a constant head permeameter. The coarse grained soil samples recovered at depth of 0.4m and 1.1m were tested under a constant head of 13 cm and 23 cm respectively. The fine grained soil samples recovered at 2.1 m were tested at a  $\Delta h$  of 85 cm. Estimates of permeability are obtained by means of the following equation, that is based on flow rate definition and on Darcy's Law (energy losses in the connecting tubes are neglected):

$$k = \frac{Qh}{\pi R^2 \Delta H}$$

Where:  $k$  is the hydraulic transmissivity,  $Q$  the flow rate,  $h$  the height of the sample,  $R$  the radius of the sample,  $\Delta H$ , the difference in height between top of the sample and reservoir headwater. Once saturation was achieved for each sample keeping  $\Delta H$  constant, measurements of  $Q$  were taken by evaluating the flown in volume of water for each specimen over a fixed amount of time. All test results are summarized in table n. 4.

Layer	depth (m)	k (cm/sec)
B	0.4	1.00E-02
B	1.1	1.37E-04
C2	2.1	2.31E-05

**Tab. 4: Summary of laboratory permeability tests on undisturbed samples.**

Constant head conditions are not actually occurring in situ during rain water infiltration. However, constant head permeability tests allowed putting in evidence one key susceptibility factor. The permeability of the soil decreases with depth by one to two orders of magnitude. This will likely lead to the formation of a seepage flow at the coarse grained-fine grained contact interface. The laboratory tests results are in good agreement with the infiltration tests performed in situ.

#### **2.2.2 OVERVIEW OF PREVIOUS WORK: IN SITU PERMEABILITY AND DYNAMIC PENETROMETRIC TESTS**

Dynamic penetrometric tests were conducted both on the crown and on the lateral boundaries of the scar surfaces. These tests were executed by means of a light penetrometer with conic tip (apex angle of 40 degrees) and ram of 10 kg in weight. The blow count was recorded for each 10 cm advance of the tip. A typical test result is shown in figure 2.4a. It can be noted that there is a net decrease in the dynamic soil resistance at the interface between the upper layers and the basal fine layer. The soils dynamic resistance was estimated by means of the “Dutch formula”. The dynamic resistance of the upper loose soils (well graded sand to silty sand) was reckoned to be almost one fourth of that of the underlying fine grained layer (low plasticity silt). The results of these tests gave a contribution to identifying the features of those layers located at depth not reached

by the trench excavations, and also added information useful refine the geologic model of the slope.

Infiltration tests were also performed at the site in order to estimate the hydraulic properties of the layers involved in the landslides. The test was performed by means of the Amoozegar permeameter (Amoozegar, 1989), that allows for keeping a constant hydraulic head above the borehole. The flow rate from the reservoir towards the borehole is recorded versus the time. Knowing the flow rate and the geometry of the borehole, the  $k_{sat}$  is calculated by means of Darcy's law.

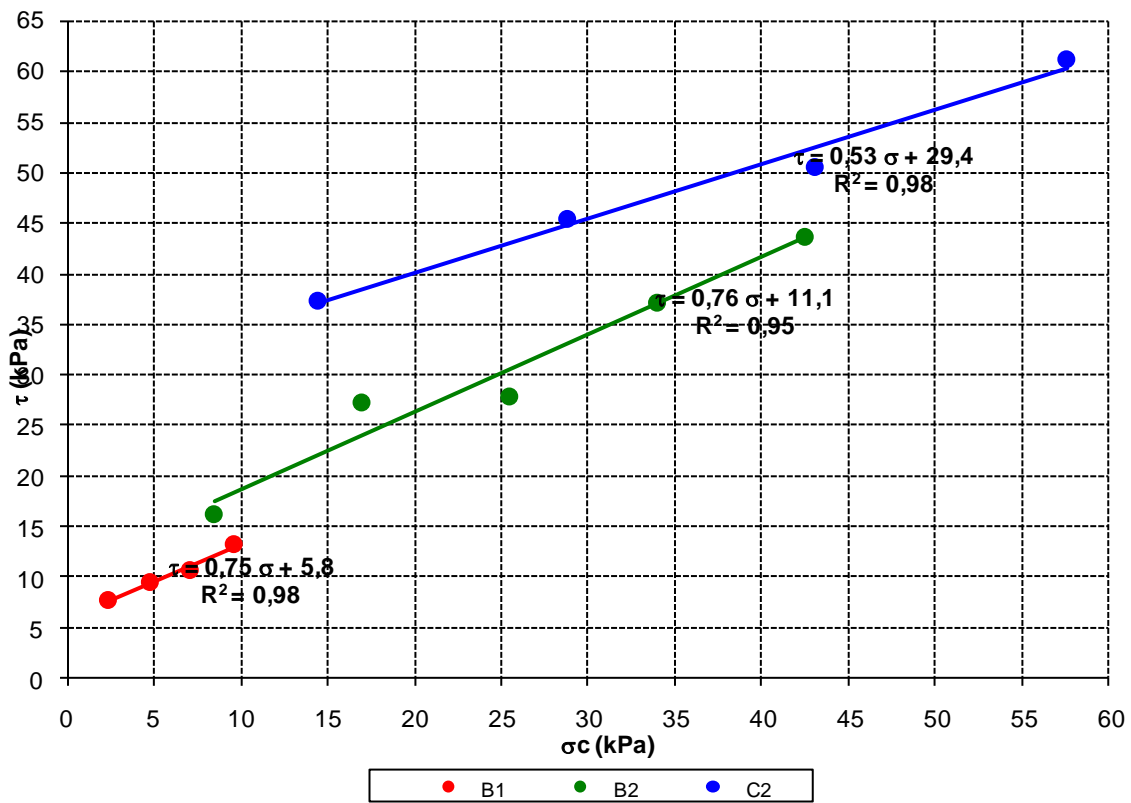


**Fig. 2.3: Direct shear test results (peak shear strength parameters).**

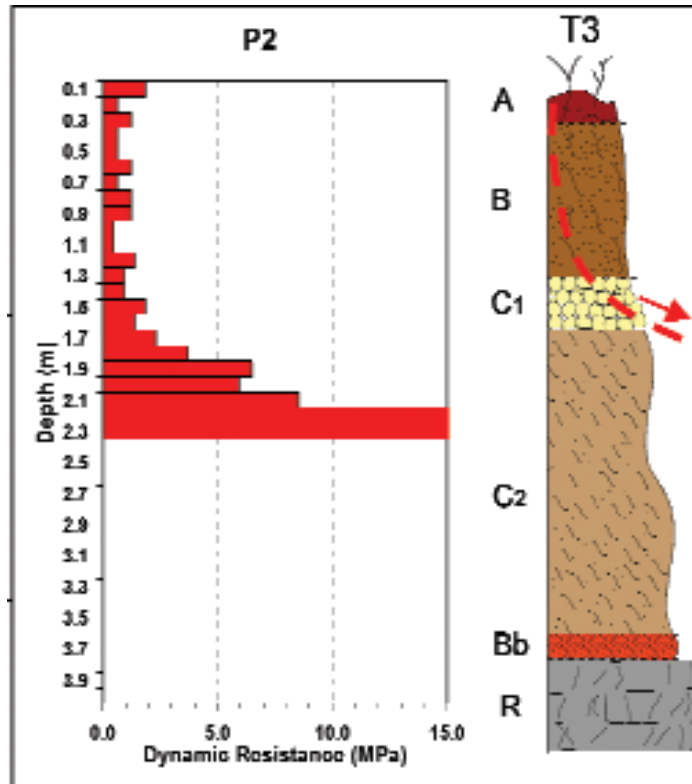


**Fig. 2.4a: Typical penetrometric test result and in situ soil stratigraphy (from De Vita *et alii*, 2007).**

The test has been conducted over prolonged time in order to reduce the unsaturated flow effects that take place at the beginning of the test in the soil. For the upper layer (C1-well graded sand to SM-silty sand) the saturation was almost immediately achieved and the value of the saturated permeability resulted  $k_{sat}=10^{-2}$  cm/s. The saturation was reached in a relatively longer time when the deeper layer was tested (C2-low plasticity silt) and the value of the saturated permeability resulted  $k_{sat}=10^{-5}$  cm/s. Results of the infiltration tests are presented in figure 2.4b.

### 2.2.3 GEOLOGIC MODEL OF THE SLOPE

The field surveys and laboratory tests allowed for the definition of the engineering geological model of the slope that takes into account the main factors of susceptibility to landslide. These were recognized to be the followings:

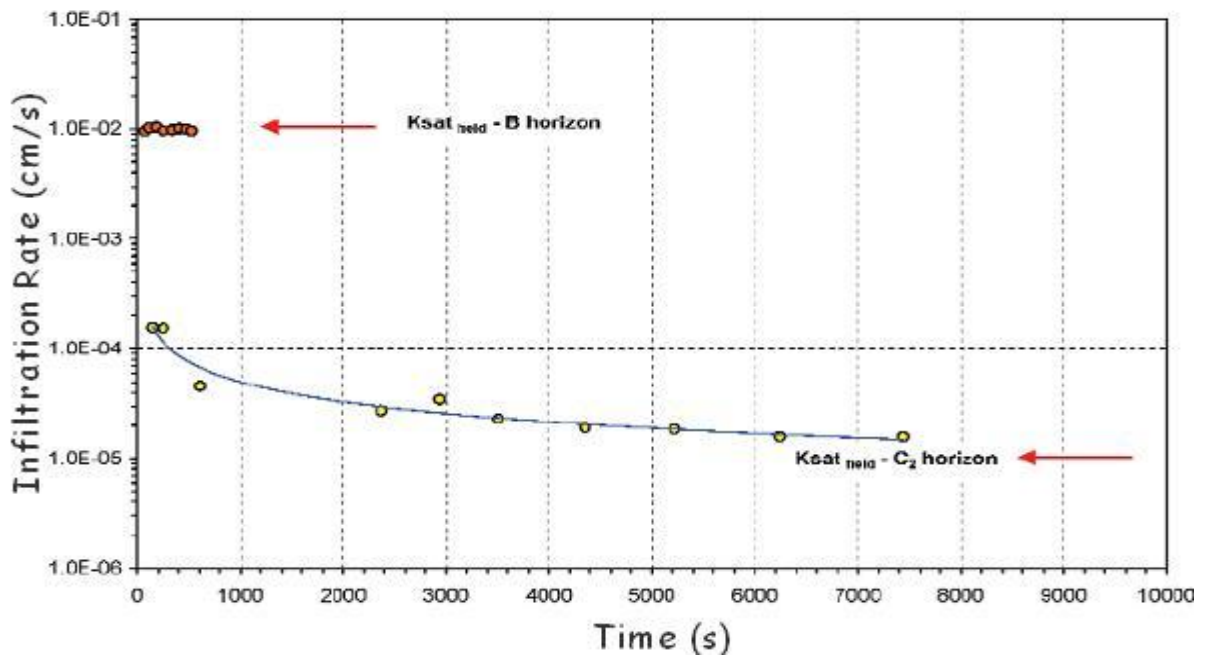


**Fig.2.4b: In situ infiltration test results (from De Vita *et alii*, 2007).**

- The layering of the soils on the slope and the hydraulic discontinuity in the vertical direction as a consequence of the particular stratification. Here, besides the first few centimeters of organic soil (Pt), the coarse and permeable well graded sand to silty sand (SW-SM) stratum lays above the relatively compacted and low plasticity silt (ML), with low permeability. This represents a hydraulic discontinuity where saturated zones are likely to form, or seepage flow could arise. Both are source of positive pore pressure that can ultimately trigger the landslide.

- The low density (high void ratio) of the soil, especially in the first meter of thickness. Casagrande A. (1940) recognized this factor to be fundamental for slope stability. Kramer & Seed, (1988) put in evidence that this parameter affects the susceptibility to liquefaction under static loading, therefore the lower the density of the soil, the higher its susceptibility to liquefaction. Kramer & Seed, (1988) also stated that dense soils do not liquefy enhancing the fact that the low density of the soil in place is a necessary (but not sufficient) condition for static liquefaction.
- The slope angle and the natural morphological discontinuities played a key role in predisposing the slope to the instability. The results of topographic measurements performed on the slopes of “Monte di Vezzi” are presented in the following sections and will constitute the basis for the back analysis of the failures.

### **2.3 PROPOSED MECHANISM OF FAILURE**

In the previous section, field and laboratory tests have been discussed. These were to evaluate the physical properties of the soil and hydraulic and mechanical behavior of the pyroclastic cover in its entirety. Thus, the purpose of this investigation was to define the soil susceptibility to slide. Based on these factors, one step further could be that of defining a model describing the mechanism leading to failure. In the following section, possible scenarios describing the hydraulic response of the slope to a rainfall event are proposed. Also, the evolution of the stress path in the soil is evaluated as a consequence of the hydraulic slope response. It appears clear at this point that a thorough study of these kind of phenomena cannot neglect neither of these two aspects: the hydraulics and the mechanics.

### 2.3.1 HYDRAULIC SLOPE RESPONSE

Campbell (1975) proposed for the Santa Monica Mountains debris flows a mechanism of failure that was based on a particular configuration where a permeable soil was laying on the top of relatively impermeable bedrock. The reduction of permeability with the depth turned out to be a source of slope instability.

Based on field observations a similar failure modality was proposed by Celico & Guadagno (1998) for the pyroclastic flows that involved the slopes of the mountains at the south eastern boundary of the Campania Plain especially during the late nineties. In this case a critical aspect was the alternation of coarse grained and fine grained-less permeable soils. The same geologic model appeared to be suitable for the "Monte di Vezzi" debris flows as well (De Vita *et alii*, 2007). Here the different nature of the bedrock, with respect to the Sarno Mountains case, didn't seem to play a fundamental role for what concern the triggering of the instability.

The hydrologic response of the slope is strictly linked to the initiation of flow failures. In the models previously mentioned, it is outlined the cause-effect relationship existing between the slope response to a rainfall event and the initiation of the instability. In Campbell's model the pore pressures are due to water table rising mainly as a consequence of rainwater infiltration. When a rainfall event happens, the infiltration of water in the bulk, along the vertical direction, was shown not to be the only relevant seepage component. As infiltration goes on, saturated areas form where a decrease in soil permeability is registered, and subsequent transversal seepage flow also arises. This leads to an increase of pore pressures and, later on, to failure. Vertical and transversal seepage flow take place according to either the non saturated or to the saturated permeability (also depending on antecedent moisture conditions (Johnson & Sitar, 1990) of the soil). The permeability can be expressed by means of the Brooks & Corey (1966) model, as a function of the pore size distribution, of the matrix suction and of the saturated

transmissivity. The formation of saturated zones have been documented in many studies related to colluvial or layered soils, where abrupt change in permeability verifies.

The topography has a strong control on the formation of saturated zones (Anderson & Brut, 1977) since most of the times gravity drives the ground water flows. Saturated zones have been shown not to be uniform on the slope but dislocated on the slope at several elevations. In some cases these may be disconnected as they are bordered by the non saturated areas where the non saturated permeability regulates the flux (Harr, 1977); or may be connected by an underground network of micro pipes (Tanaka *et alii*, 1988). This latter may explains the rapid slope response to the storm that happens in some cases. The fact that the saturated zones are isolated or partially connected allows speculating that positive pore pressure may arise in the soil also for rainfall intensities that are less than the saturated permeability of the soil. This is because the parameter controlling the seepage is the permeability in the non saturated regime that characterizes the areas of the slope bordering the saturated regions and keeping them separated.

Harr (1977) has given a contribution in defining the hydrologic response of the slope, in terms of direction of the flow during and after a rainfall event. This was done for a study area that has hydro-geological features very similar to those of the pyroclastic cover of the slopes of “Monte di Vezzi”, object of this study. The sub-horizontal flow is a consequence of the change in permeability along the depth (vertical). The direction of the flow is related to its magnitude that in turn depends on rainfall intensity. More in particular, during the storm, the vertical component (infiltration) is relevant and is comparable to the flow in the direction parallel to the slope. Thus the total flow direction will result from the sum of these two components and will have an inclination greater than the slope angle (flow directed into the slope). After the storm the infiltration is negligible with respect to the lateral flow component. This latter is approximated with the total flow component. From a mechanics standpoint, the results from Harr can be interpreted as follows: the infiltration component provides stabilization to the slope, but

flows are more intense during the storm. On the other side, the stabilizing component is negligible, but flows are less intense, after the storm.

Similar results were found by Anderson & Sitar (1995) that evidenced the presence of saturated zones rapidly forming high on the slope and moving down slope as pulses (transient flow) with a velocity of 0.05 m/s. Johnson & Sitar (1990) put in evidence the fundamental role played from the antecedent slope moisture conditions prior to a rainfall event, in the process leading to pore pressures built up. Similar rain event may or may not push the slope close to critical stability conditions. This is based on antecedent moisture conditions. The response of a dry slope to a rain storm is that of a shallow nearly saturated area formation, with eventually pore pressures built up, upslope. Here the infiltration of rain water to deeper strata is contrasted since this is controlled by unsaturated hydraulic conductivity. Down slope there are similar conditions, but a higher decrease in matrix suction is registered for more deep layers. This is the evidence of lateral infiltration becoming relevant down slope (this is likely due to both flow convergence from lateral sources and seepage from upslope).

For what concerns wet slopes the configuration is almost analogous to the one previously described, but with significant differences in terms of pore pressures: high water content is verified in the soil upslope, but no pore pressures can arise due to the high value of soil permeability (whom value is very close to that of saturated conditions). Here all the infiltrated water is discharged down slope. Down slope, at shallower depths a slight increase in positive pore pressures is registered being the soil saturated due to rain water infiltration; at increasing depth significant pore pressures can be registered due to water flowing from upslope and to infiltration. This means that, the closer is the soil to saturation, the higher the will be permeability of the soil and the faster the discharge. Therefore, the pore pressure pulse will be propagating down slope with higher velocity.

Although the results from Harr's and Johnson and Sitar's works are site specific, several aspects can be found out that also match other authors works. Thus, conceptual models

obtained from these works can be accounted as a guide for critical slope conditions assessment. Qualitative water content, suction and factor of safety profiles are shown in figure 2.5a, 2.5b, 2.5c and 2.5d.

- A: Down slope; initially wet

This profile shows a condition where the permeability can reach saturated values at the contact interface with the less permeable layer. Discharge of water from the up slope soil portion will lead to the formation of saturated areas down slope. This will happen in the deeper layers of the soil profile where positive values of pore pressures are achieved. This condition is critical for the stability of the slope, since surface forces (seepage forces) are relevant.

- B: Up slope; initially dry

In this profile the shallower strata rapidly reaches relatively high water contents, that make the matrix suction drop down with a consequent increase in soils hydraulic conductivity. Lateral flow can be predominant, mostly due to the lower conductivity of the middle-deep portion of the soil profile. The thickness of the soil subject to transversal infiltration may however increase due to the minor vertical infiltration component.

- C: Up slope; initially wet

The same thing can be said for this profile: here the water content along the depth is almost constant. For the up slope profile body forces are predominant (gravity) and the relatively impermeable medium is crossed mainly in the vertical direction. Chances of a slight lateral infiltration component due to the higher water content in the lower portion of the soil profile. However, the lateral flow still happens in the non saturated regime.

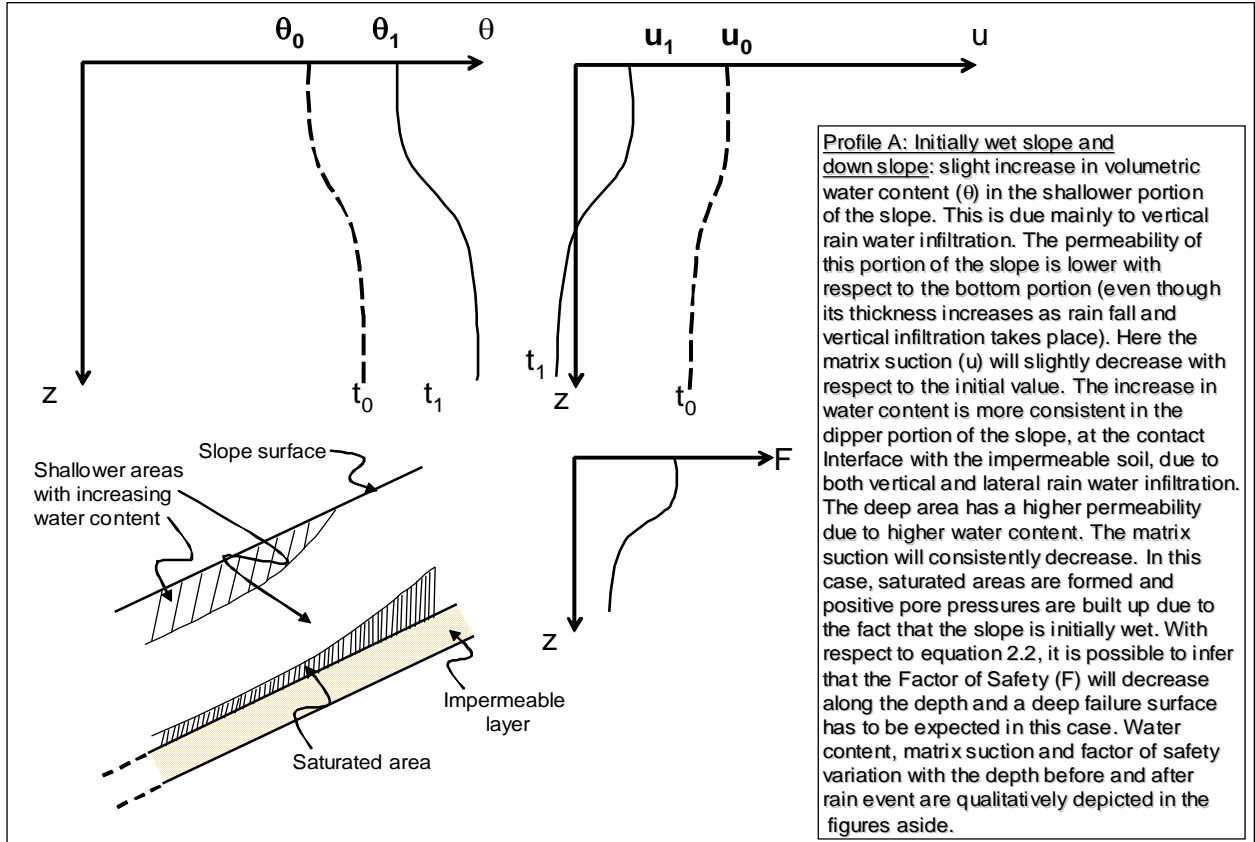


**Fig. 2.5a: Water content, matrix suction and factor of safety versus depth-Initially wet slope; down slope.**

- D: Down slope; initially dry

This profile shows a situation where rain water infiltration is coupled with unsaturated transversal flow coming from upslope. There are no major changes in the water content with the depth, being this latter slightly higher for the deeper layers.

For what concern the factor of safety, it is well known that this parameter decreases with depth in cohesive soils. This can be easily shown with an infinite slope approach and by characterizing the strength of the soil by means of effective stresses parameters.

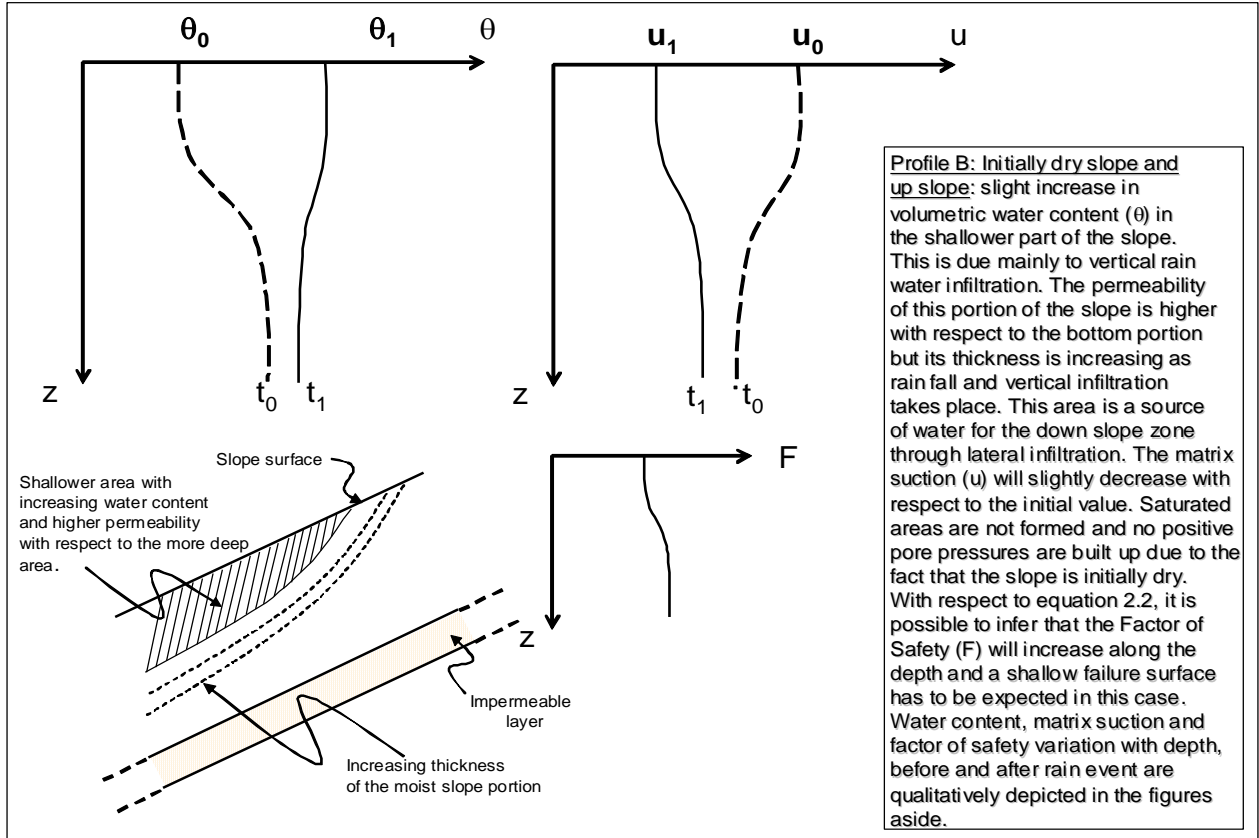


**Fig. 2.5b: Water content, matrix suction and factor of safety versus depth-Initially dry slope; up slope.**

The factor of safety can be expressed as (Duncan and Wright, 2005-modified):

$$(1) \quad F = \frac{c'l}{w \times \sin \delta} + \frac{\tan \phi'}{\tan \delta} + \frac{\tan \phi'}{\tan \delta} \left( \frac{\gamma_w h_w}{\gamma_m (h - h_w) + \gamma_{sat} h_w} \right)$$

where: F= factor of safety; c' and  $\phi'$ = effective stresses parameters;  $\delta$  slope angle;  $\gamma_w$ ,  $\gamma_m$ ,  $\gamma_{sat}$ = water, moist and saturated unit weights;  $h_w$ , h= thickness of the saturated soil portion and thickness of the cover; w= average weight of the soil; l= length of the considered portion of slope of weight w.

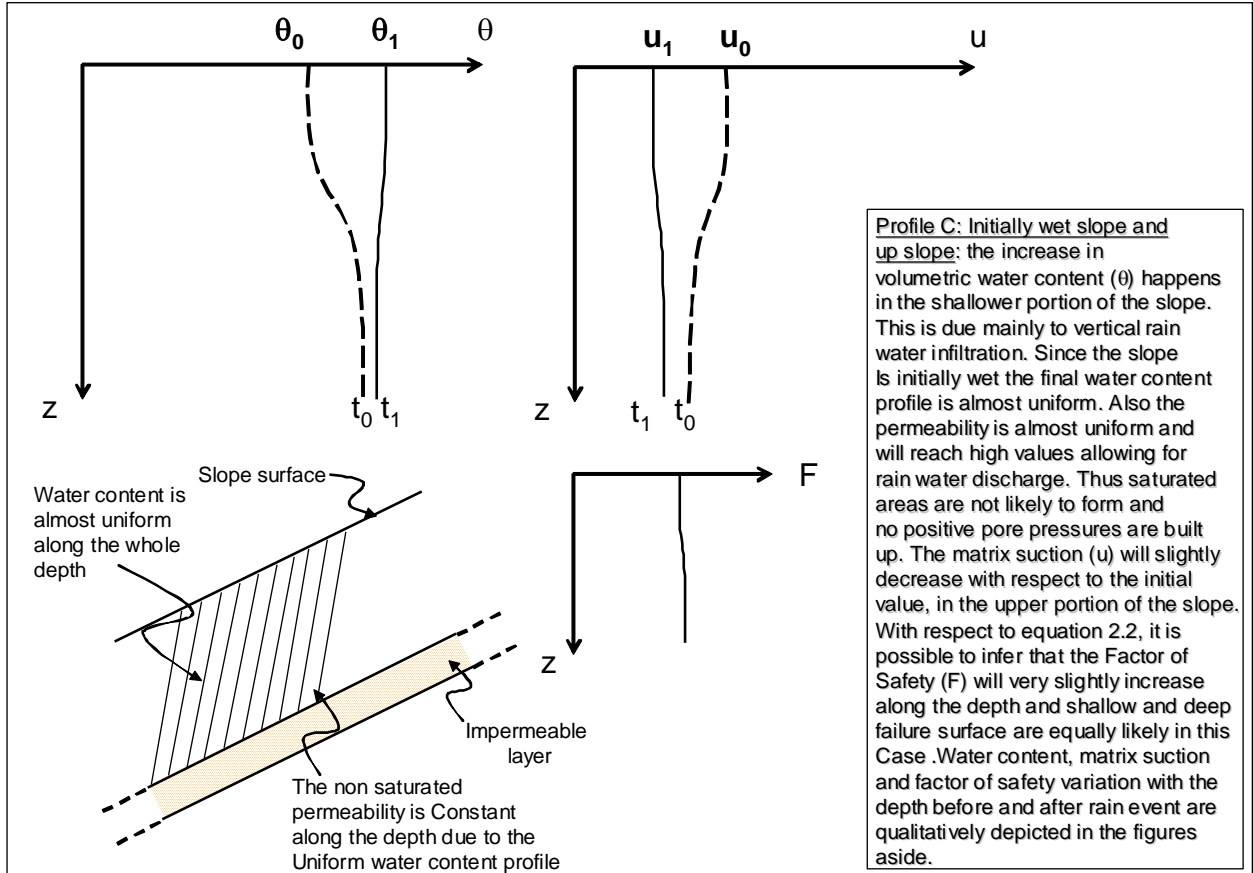


**Fig. 2.5c: water content, matrix suction and factor of safety versus depth-Initially wet slope; up slope.**

Pyroclastic soils are cohesionless soils and the only alternative source of cohesion is represented from matrix suction. This is when root derived cohesion is neglected. Matrix suction appears in non saturated soils. It is caused by inter granular water and its ultimate effect is that of an apparent cohesion of the entire soil matrix.

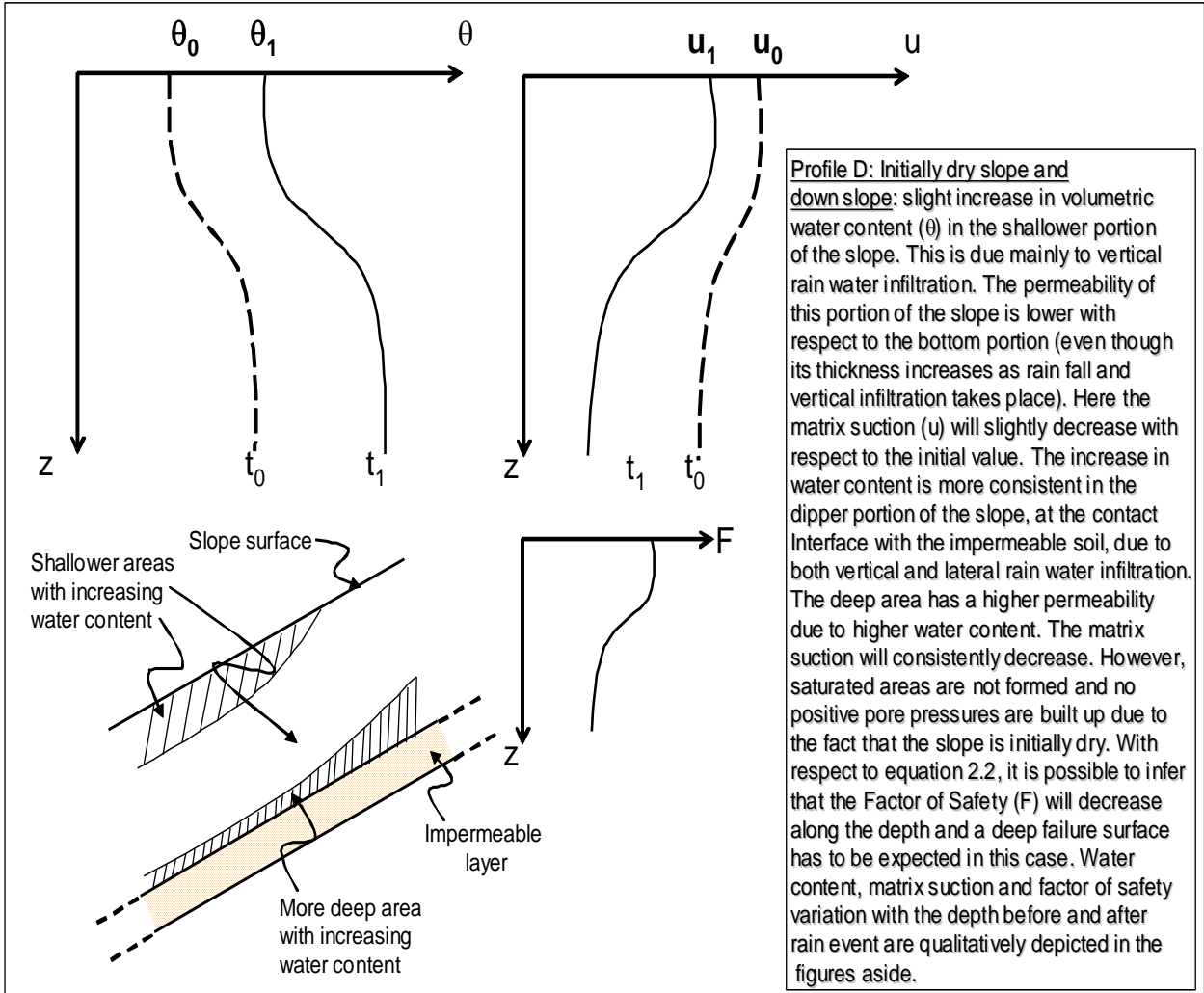


**Fig. 2.5d: water content, matrix suction and factor of safety versus depth-Initially dry slope; down slope.**

If matrix suction is taken into account, the first and third term cannot co-exist ( $h_w=0$ ) in the factor of safety equation. This latter will become

$$(2) \quad F = \frac{c'l}{w \times \sin \delta} + \frac{\tan \phi'}{\tan \delta}$$

and  $c'$  = matrix suction in this specific case.

One question that arises is: in a medium where matrix suction is developed, how does the factor of safety change along the depth? And likewise, should one be concerned about shallow failure surfaces or deep failure surfaces? The answer to these questions may be helpful in defining the approach to the analysis of the stability of the slope. To put some more light on this topic, water content profiles should be considered (such those defined in fig. 2.5). Matrix suction in fact depends on water content along the depth. For profiles A and D the water content increases along the depth. The matrix suction variation will be inversely proportional to the water content change along the depth. The factor of safety will decrease along the depth. It has to be noted that profile A includes a saturated basal flow and thus, saturated abrupt change in factor of safety diagram slope should happen at a certain depth. This latter coincides with the thickness of the saturated soil portion. For profile B and C the water content decreases along the depth. Matrix suction will increase and so will the factor of safety.

It can be said that for case A and D, deep failure surfaces are less safe (even though in case C the water content, matrix suction and consequently the factor of safety could be almost uniform along the depth). Conversely, shallower surfaces are less safe in case of profiles B and C.

Each one of the previously presented schemes is equally likely to happen, and all of those conditions should be taken into account. However, in this work only the first configuration is considered. This is for two main reasons: the first is that the failure surface at the site appeared to be deep, located at the contact interface with the impermeable boundary. The second is that the quantity of water in the soil in place, after failure was very abundant. This suggested that saturated zones were formed in the bulk at the contact interface triggering the instability.

The response of the slope to a rainfall event is represented by the formation of saturated zones and of a down slope directed flow. The rapidity with which pore pressures are built

up is related to the interconnection of saturated areas. The direction of the flow is related to layering, rainfall intensity and topography of the site.

These elements can help in understanding the failure mechanism and defining a model for the analysis.

### **2.3.2 FIELD STRESS PATH**

The stress state change is a consequence of the hydraulic response of the slope and can be qualitatively described throughout several phases.

Since the magnitude of  $\sigma'_1$  and  $\sigma'_3$  is not known, the starting point of the stress path in the p-q plane can be defined by means the Lowe's hypothesis (Lowe, 1966). Lowe assumed that there is no principal stresses rotation between initial state and failure. This is a reasonable assumption for slopes with inclination greater than 25 degrees (Anderson & Sitar, 1995). In this case the slope should be very close to instability. This hypothesis allows for the evaluation of the initial Mohr's circle and of the starting point of the stress path. However, if the average inclination of the failure plane is known, a trial and error procedure could be used for the evaluation of the starting point of the stress path, by means of the pole method.

It is worth to notice that the inclination  $\beta$  of the consolidation line is fixed, and the starting point of the field stress path depends on moisture content  $\theta_w$  (saturation degree  $S = \theta_w / e$ ), for a soil with a given specific (Gs) gravity and void ratio (e) (Fig.n.2.6a). If S increases the initial point will move to the right on the p-q plane, and vice versa.

The degree of saturation affects the negative pore pressure that develops in the soil. The lower the water content, the higher the suction. This also means that a generic soil element on the failure surface will be subjected to a higher confining pressure ( $p'$ ) as a result of body forces (overburden pressure) and suction itself. The lower the saturation degree, the higher the amount of water that will be necessary to generate positive pore

pressures to trigger the instability. Similar evaluations are also reported in Johnson and Sitar (1990). Thus, if the moisture content decreases, there will be two components determining the stress path onto the p-q plane. One is the negative pore pressure or matrix suction, and the second is that due to the change in moist unit weight. This latter component is directed upward on the p-q plane, but is not vertical as it can be seen in figure 2.6c. Likewise, when the moisture content increases due to the rain water infiltration process previously described, the stress path will have a first component that is the decreasing matrix suction (in the unsaturated regime) or an increasing pore pressure (when saturated zones are formed). A second component is due to the increase in moist unit weight. This component is directed downward on the p-q plane, but is not vertical as it can be seen in figure 2.6c. The components due to the variation in pore pressure are horizontal vectors on the p-q plane (in the same direction and in the opposite direction of the axes p, respectively).

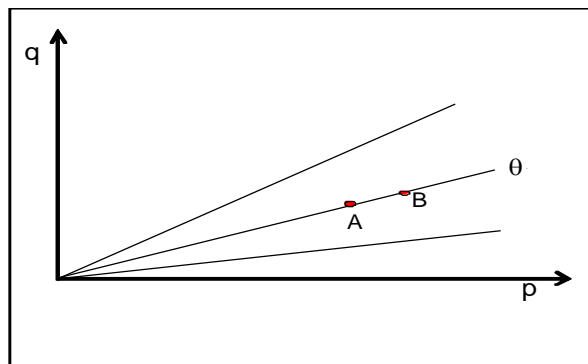


**Fig. 2.6a: Variation of the starting point of the stress path on the  $k_0$  line depending on moisture content (saturation degree).**

If the whole column of soil involved in the instability would turn saturated, there would be a huge decrease in effective stress state due to buoyancy effect. More likely, saturation take place just for the bottom part of the soil. The buoyancy effect only occurs for the

portion of soil at the contact interface with the impermeable soil (likely, few centimetres over 1 to 1.15 m of soil thickness). If the components of the stress path due to change in moist unit weight are neglected, the field stress path can be represented by a horizontal line (fig.n.2.3d). It is also worth to notice the following fact: when the evolution of the stress state is approximated with a horizontal vector, it is assumed that no rotation of principal stresses takes place. Therefore, there is no adjunct of external load. This means that the shear stress on the failure plane remains constant, while the effective normal stress on the failure plane decreases. Thus failure happens because of a decrease in frictional resistance and not for an increase of shear stress on the failure plane.

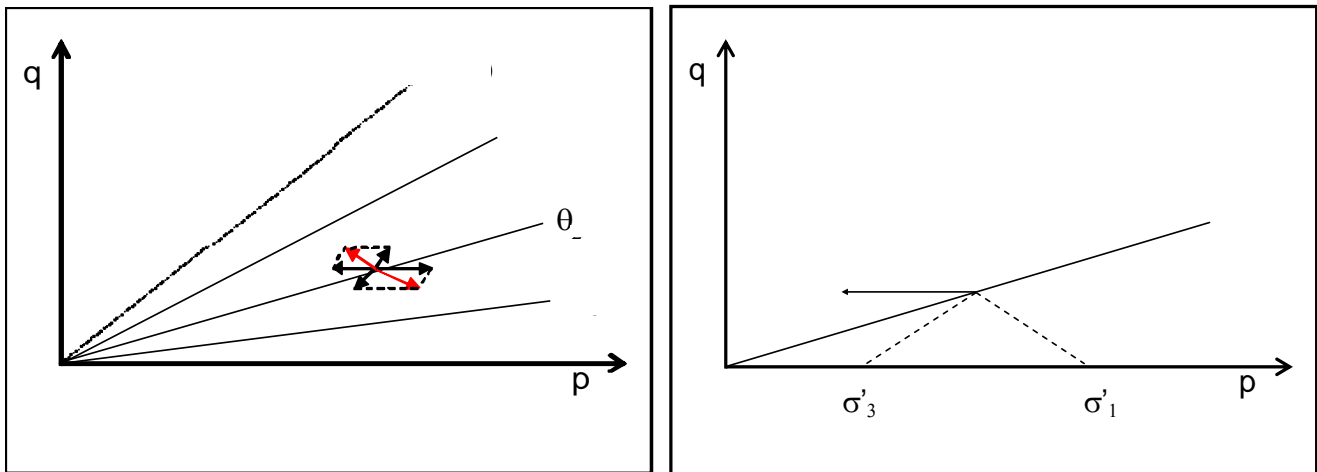


**Fig. 2.7b and c: Stress path components and horizontal stress path assumed.**

The mechanism of failure can be outlined as follows: the particular arrangement of the layers (that is schematized in the geologic model) is favorable to the formation of saturated zones. Due to the decrease in permeability at the contact interface coarse-fine soil, and to rain water infiltration, a seepage flow arises in the direction parallel to the slope. This is source of positive pore pressures ultimately triggering the landslide.

Campbell's hypothesis was that the destabilization of the slope happened just because of vertical rainwater infiltration. Several authors have shown with their researches that the transversal infiltration component is relevant. The pore pressure increase leads to a decrease in the mean effective stress ( $p'$ ) on the failure plane that in turn results in a decrease in shear strength. In the hypothesis of horizontal stress path, the soil is failed because the actual in situ shear stress (that is not significantly changing between the beginning of rainwater infiltration and failure) is matched from the decreasing shear strength: from  $\sigma'_{t1} \tan \phi'$  to  $\sigma'_{t2} \tan \phi'$ , with  $\sigma'_{t2} < \sigma'_{t1}$  due to increasing pore pressures. The change in stress state due to external loading that would mobilize other frictional components (under drained conditions) other than mineral-to-mineral friction is not verified in this case. It should be finally noted that this conceptual model of the mechanism of failure, is based on the geologic model of the slope (defined in the previous sections, that takes into account susceptibility factors), on the hydrologic response of the slope to a rainfall event, (identified as the main triggering factor); on the evolution of the stress state in the soil as a consequence of pore pressure increase due to vertical infiltration and to lateral seepage flow.

#### **2.4. FAILURE AND COLLAPSE OF GRANULAR MATERIALS**

In this section, a distinction is made between two modes of soil rupture: failure and collapse. These will both be defined for granular materials like the pyroclastic silty sand and well graded sand at "Monte di Vezzi", Ischia. Failure occurs when the internal friction of soil is totally mobilized due to an external solicitation. Conversely, collapse occurs when the internal friction of the soil is not fully mobilized. While failure is a more common concept in geotechnical engineering, collapse is less treated and an insight of the main concept can be appropriate. After analyzing large scale slides in granular materials,

Sladen *et alii*, (1985), introduced the concept of collapse surface. This surface can be defined in the 3D space mean confining stress (p)-mean deviator stress (q)-void ratio (e) and its position depends on the density of the soil. Collapse of the soil will occur when the soil stress path hits this collapse surface. The intersection of the collapse surface with the p-q plane can be represented as a straight line. This line is obtained according to Sladen *et alii* (1985), by connecting the peak and the residual strength point of the effective stress path that occurs in the soil once it is sheared under no volume change conditions. Other authors (Ishihara *et alii*, 1993, and Alarcon-Guzman *et alii*, 1988) identify the collapse surface with the post peak portion of the same effective stress path. As said, the vertical position of the collapse surface depends on the void ratio of the soil. Sasitharan *et alii* (1993), showed that the same collapse surface could be obtained by means of an undrained stress path and of a drained-constant-volume stress path. Therefore, they concluded that the collapse surface represents a state boundary. The collapse surface position on the p-q plane will be the higher, the higher the density (the lower the void ratio) of the soil.

When failure of a soil occurs an external solicitation is applied. Deformation of the initial soil structure is induced and the internal friction is mobilized. Several components can contribute to the internal friction, depending on the soils initial density: mineral-to-mineral; particle rearrangement; dilatancy (Rowe, 1962). After large deformations, a flow structure is achieved (Casagrande, 1940) and the soil is at the critical state.

Collapse or static liquefaction occurs after an internal solicitation. The pore pressure slowly rises due to a seepage flow taking place in the soil. In this case, no change in soil structure occurs and no additional friction is mobilized as a consequence of the pore pressure increase. Sasitharan *et alii* (1993), conducted a series of dead load tests on reconstructed samples at different void ratios. They noted that the soil collapses once the constant-deviator-stress (CDS) stress path, hit the collapse surface defined for the sample. As mentioned this surface is given by the post peak portion of the effective stress path

obtained during condition of no volume change of the sample with a given density. Once the CDS stress path touches the collapse surface, the soil goes to the critical state. They also noted that, before collapse occurred, the deformation of the soil sample was close to zero and the mobilized friction angle was included in the range 14-18 degrees.

Kramer & Seed (), investigated the static liquefaction resistance of fine Sacramento River sand. They looked at the effect of confining pressure, pre-shear stress state and relative density. They concluded that the increase in confining stress and an increase in soil density result in a static liquefaction resistance increase. Conversely, the pre existing shear increase results in a drastic decrease in static liquefaction resistance. Pre existing shear will occur in sloping soils where artificial or natural cuts are present. This determines the lack of lateral support. These discontinuities were recognized as one of the main landslide susceptibility factors in the 1998 Sarno debris-flow (Guadagno *et alii*, 2004).

The steady state and the critical state can be considered to be the same, for the purposes of this manuscript (Sladen *et alii*, 1985). The steady state of deformation is defined as the state at which the soil continuously deforms at constant normal effective stress, constant shear strength, constant volume and constant velocity (Pulos, 1981). At this stage soils are modeled to react with residual strength parameters. The steady state will always occur whether the soil collapses or is failed, while the peak, and peak friction angle, depend on the type of stress path.

Based on what discussed so far, it can be said that failure is a non equilibrated behavior where the stress state in the material, induced from an external solicitation, is not supported by the soil strength. On the other hand, collapse is a non congruent behavior where the stress state induced by the external actions could be supported by the soil strength, but that actual stress state cannot exist because of the high void ratio of the soil. The collapse surface (or state boundary) delimitate a region of points representing non

congruent stress states, for a given void ratio. For all those point, a limit equilibrium analysis is meaningless.

#### **2.4.1. MODEL OF SOIL FAILURE FOR “MONTE DI VEZZI” LANDSLIDE**

Based on what just explained, the stress parameters to model the soil depend on the stress path. Also the consolidation pressure can play an important role as it will be explained later on. To choose the stress parameters for the stability analysis, several stress paths can be identified. In the following, a cluster of stress paths will be discussed, together with the associated strength parameters. The stress path shown in figure 2.7 is typical of soils being sheared in triaxial compression under consolidated drained conditions. In this case, volume change is allowed and friction is fully mobilized. The stress parameter associated to this stress path is the result of several components and is the peak friction angle. This occurs once an external solicitation is applied and there is the chance of volume change (compression or extension).

The stress path presented in figure 2.8 is typical of soils being sheared in triaxial compression under undrained or drained-constant-volume conditions. This stress path is assumed to describe the stress state change during the phase of debris-avalanche, when the soil is destabilized due to soil masses slid up slope. For the purpose of analyzing the behavior of granular soil during the initial debris slide, the undrained or the drained-constant-volume stress path will be considered for the definition of a collapse surface.

The stress path depicted in figure 2.9 models the stress change due to seepage flow occurring in the soil. A detailed description of this stress path is found in 2.3.2. This stress path is typical of those cases where the pore pressure is slowly rising under drained conditions. It can be speculated that two main cases can be distinguished: one where the soil in situ is subject to high confining pressures and the second where the in situ

confining pressure is low. In the first case the horizontal stress path will travel towards the boundary surface as a consequence of the increase in pore pressure. Collapse will occur once the constant-deviator-stress stress path hits the boundary surface.

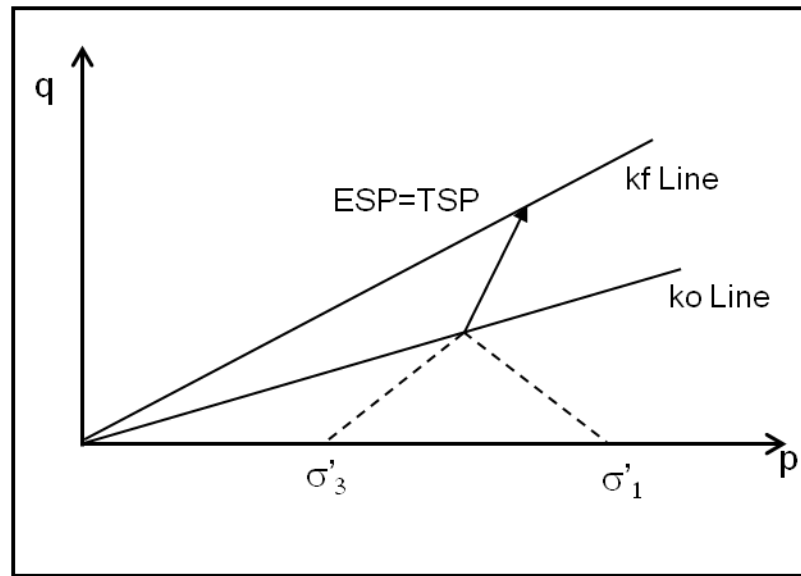


**Fig. 2.7: CD stress path: it is assumed to occur due to an external solicitation. Soil reacts with the peak friction angle. The  $k_0$ -line passes through the top of the Mohr's circle representing the soil stress state after consolidation. The  $k_f$ -line passes through the top of the Mohr's circle representing the soil stress state at failure, when peak deviator stress is achieved. The effective stress path (ESP) is the line going through the top points of the effective stress Mohr's circles representing the stress state between consolidation and failure. The total stress path (TSP) is the line going through the top points of the total stress Mohr's circles representing the stress state between consolidation and failure.**

Similarly, at lower confining stresses, the constant-deviator-stress stress path will travel towards the steady state line and the soil will fail once the stress path hits this line.

When failure occurs it is not clear which is the parameter to use to model the strength of the soil, since it is demonstrated that the ultimate strength is not mobilized (Sasitharan *et alii*, 1993). A limit equilibrium stability analysis seems to be not appropriate in this case. In the second case the soil goes to the steady state and it is reasonable to model the soil strength with the residual friction angle.

To approach the stability analysis of a slope that is subject to the initial debris slide triggered after intense rain fall, two main steps should be taken.

1. What type of failure is expected
2. What are the parameters to model the strength of the soil

Among all the stress paths discussed previously, the more appropriate to describe the initial debris slide is deemed to be the third one, in case of low confining pressures.

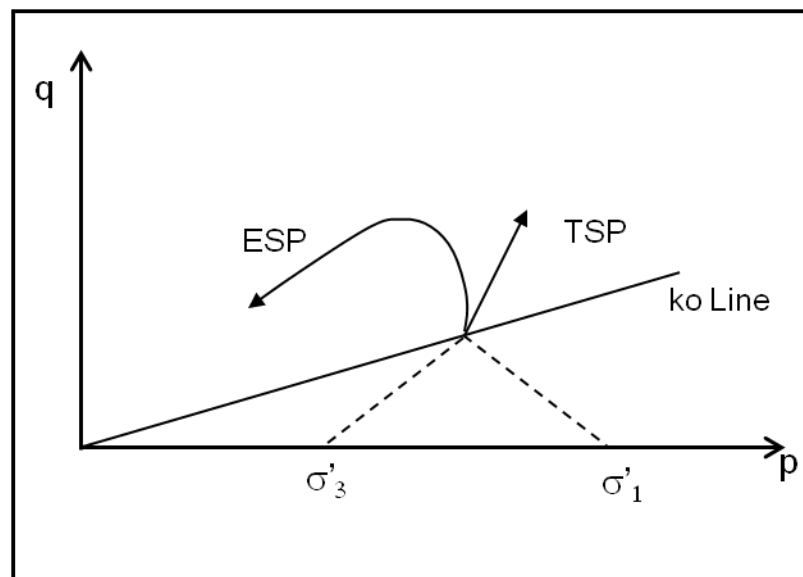


**Fig. 2.8: CU stress path: it is assumed to occur due to an external solicitation. The effective stress path (ESP) defines the collapse surface**

Therefore, the strength parameters to model the soil are assumed as

$$c' = 0 \text{ and } \phi' = \phi'_{\text{residual}}$$

A limit equilibrium stability analysis seems also to be appropriate since the soil experiences failure rather than collapse.

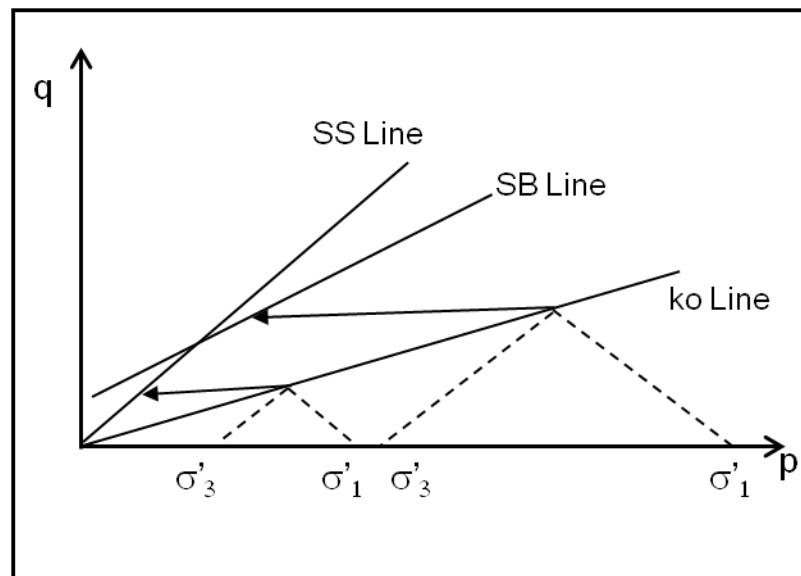
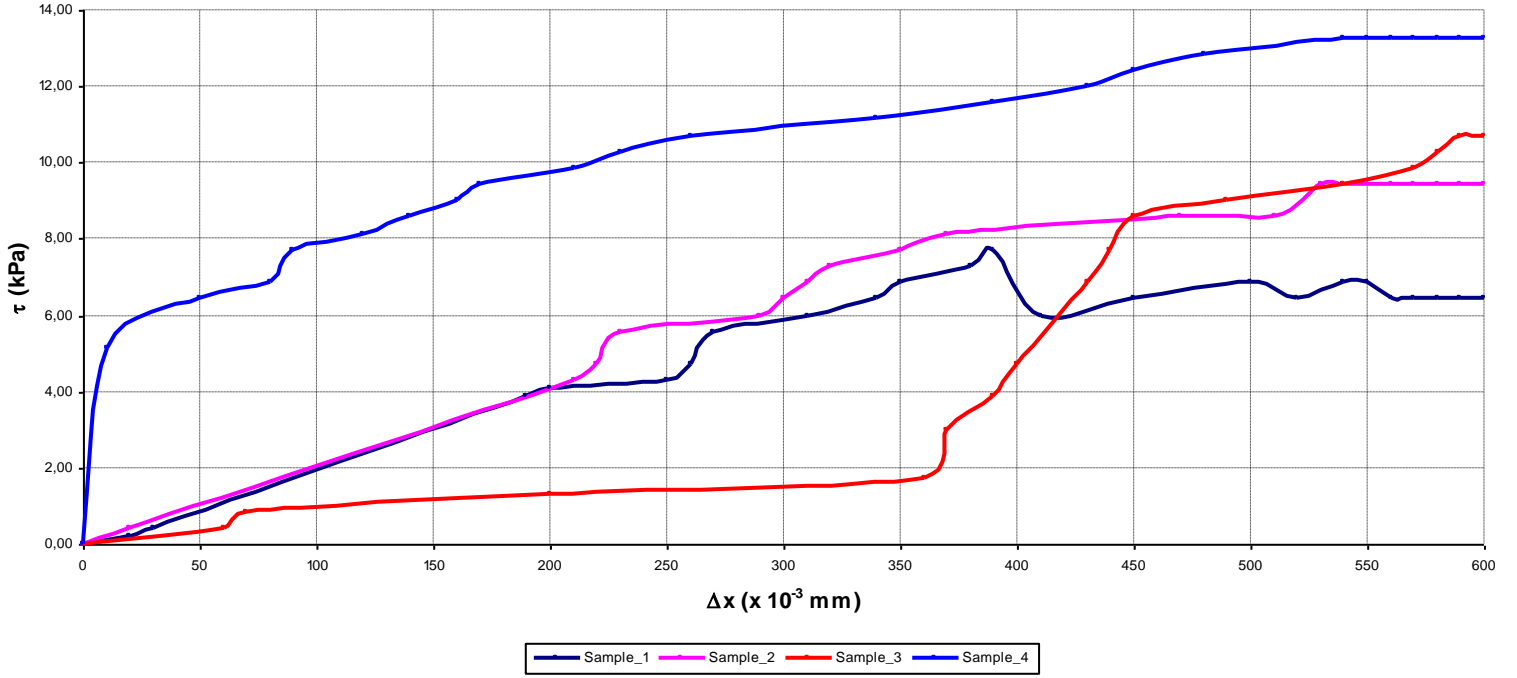


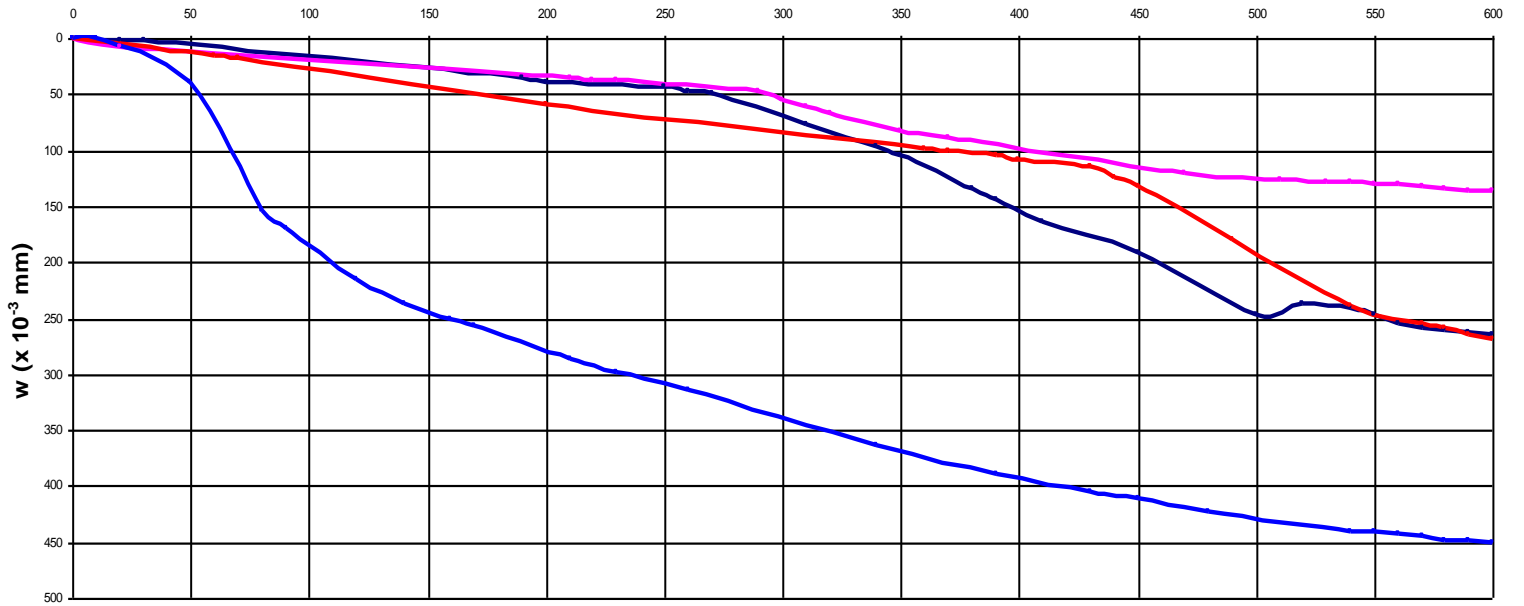
**Fig. 2.9: CDS stress path: it is assumed to occur due to an internal solicitation. The effective stress path (ESP) hits the collapse surface at high confining pressures or the steady state line at lower confining pressures. The steady state line (SS) passes through the top of the Mohr's circle representing the soil stress state at the steady state. The state boundary (SB) is assumed to have the significance defined in Sasitharan et al (1993).**

## APPENDIX TO CHAPTER II

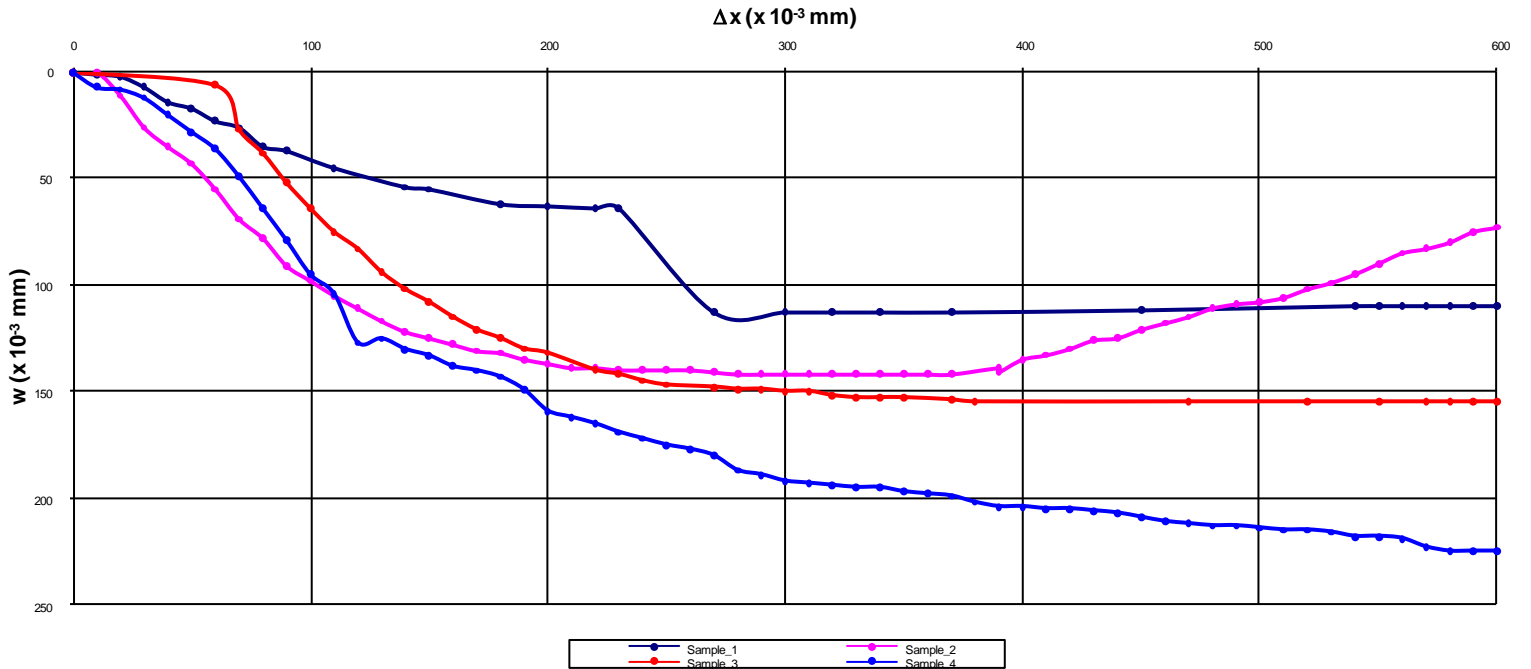
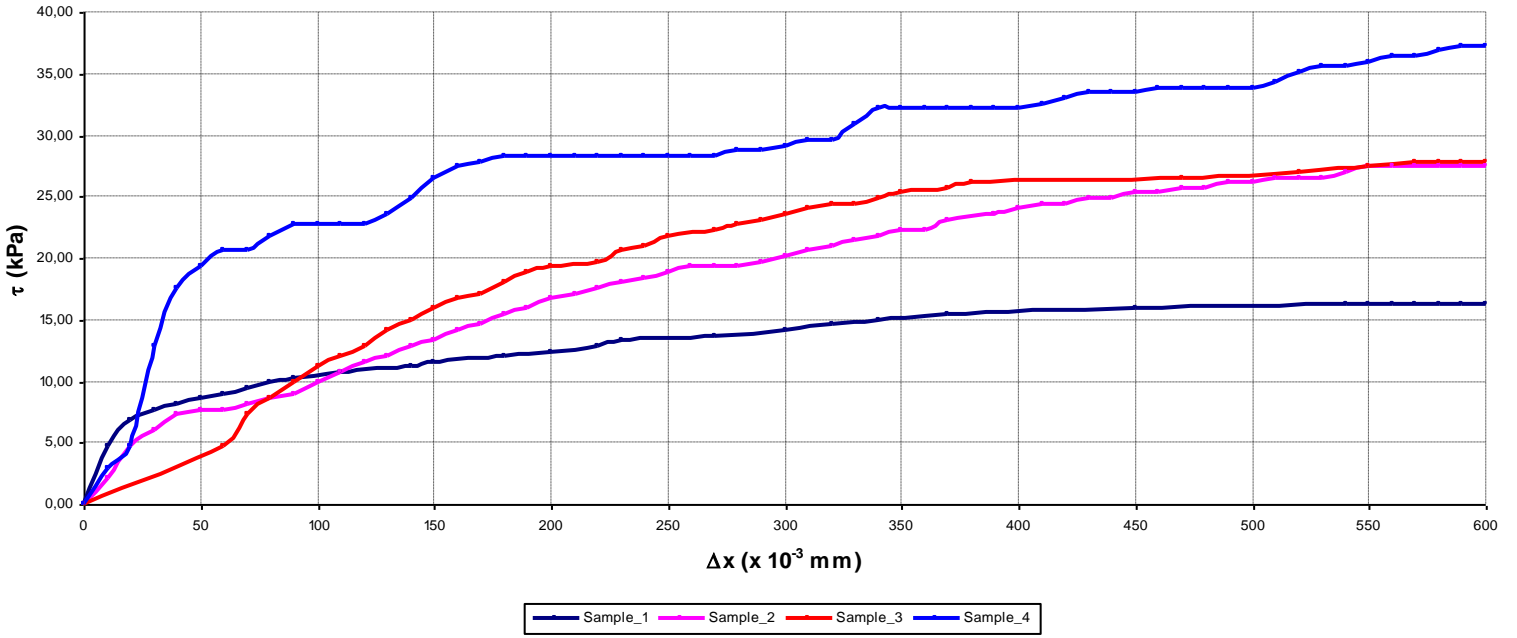
Depth=0.4 m - SM



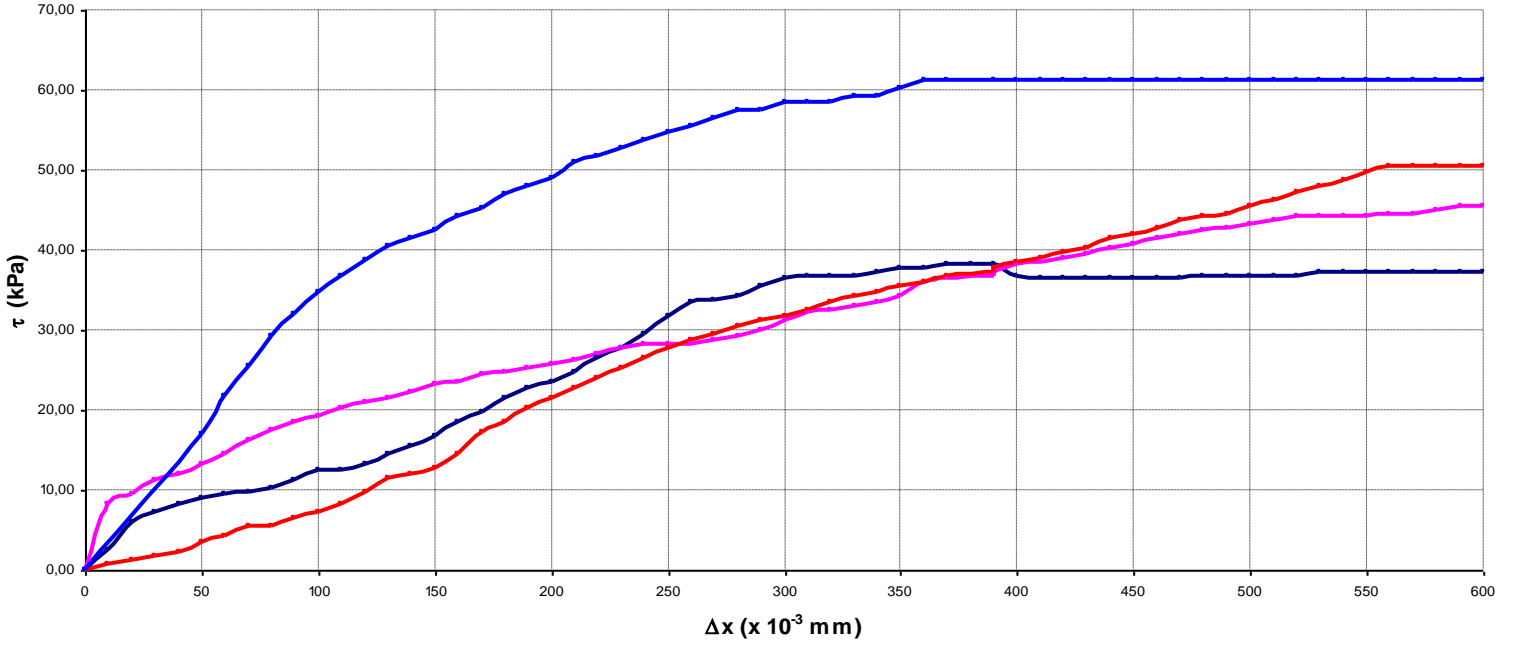
Δx (10<sup>-3</sup> mm)



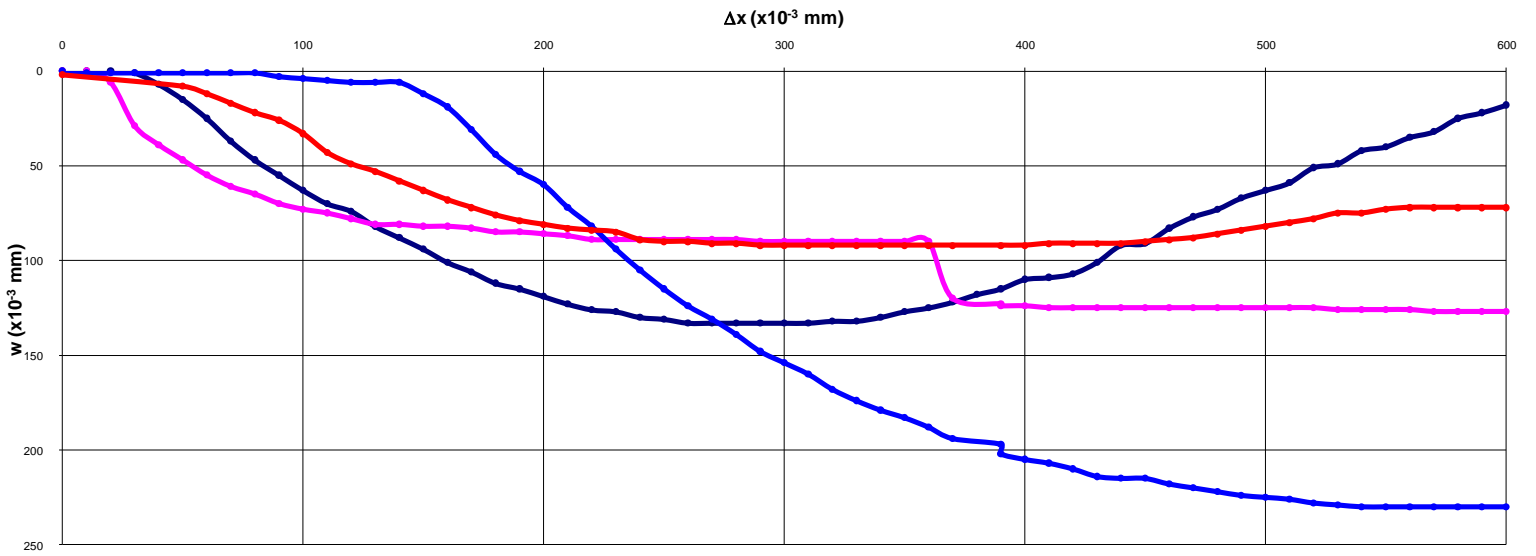
Depth=1.1 m - SW-GW



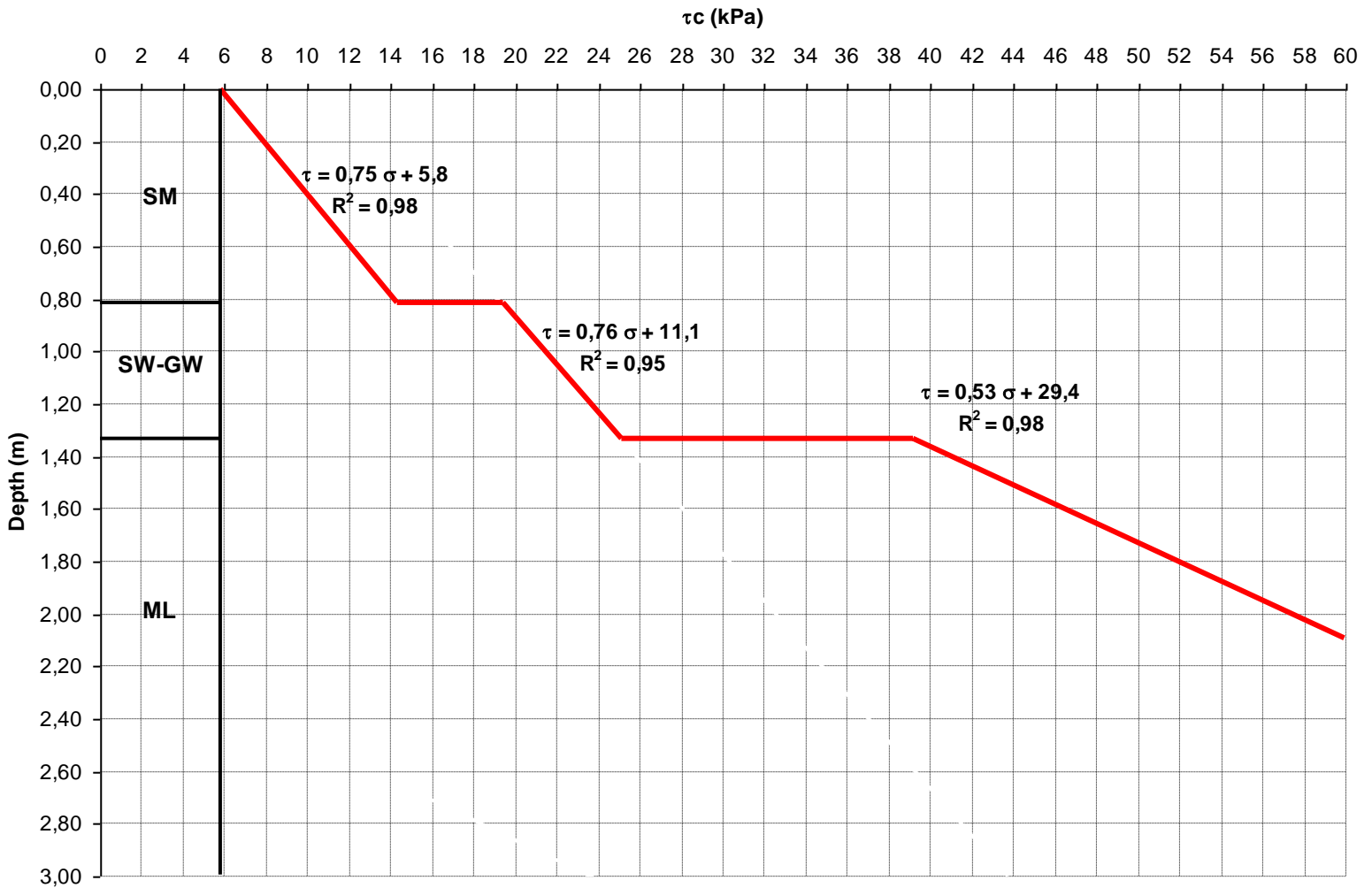
Depth=2.1 m - ML

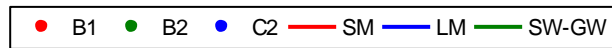
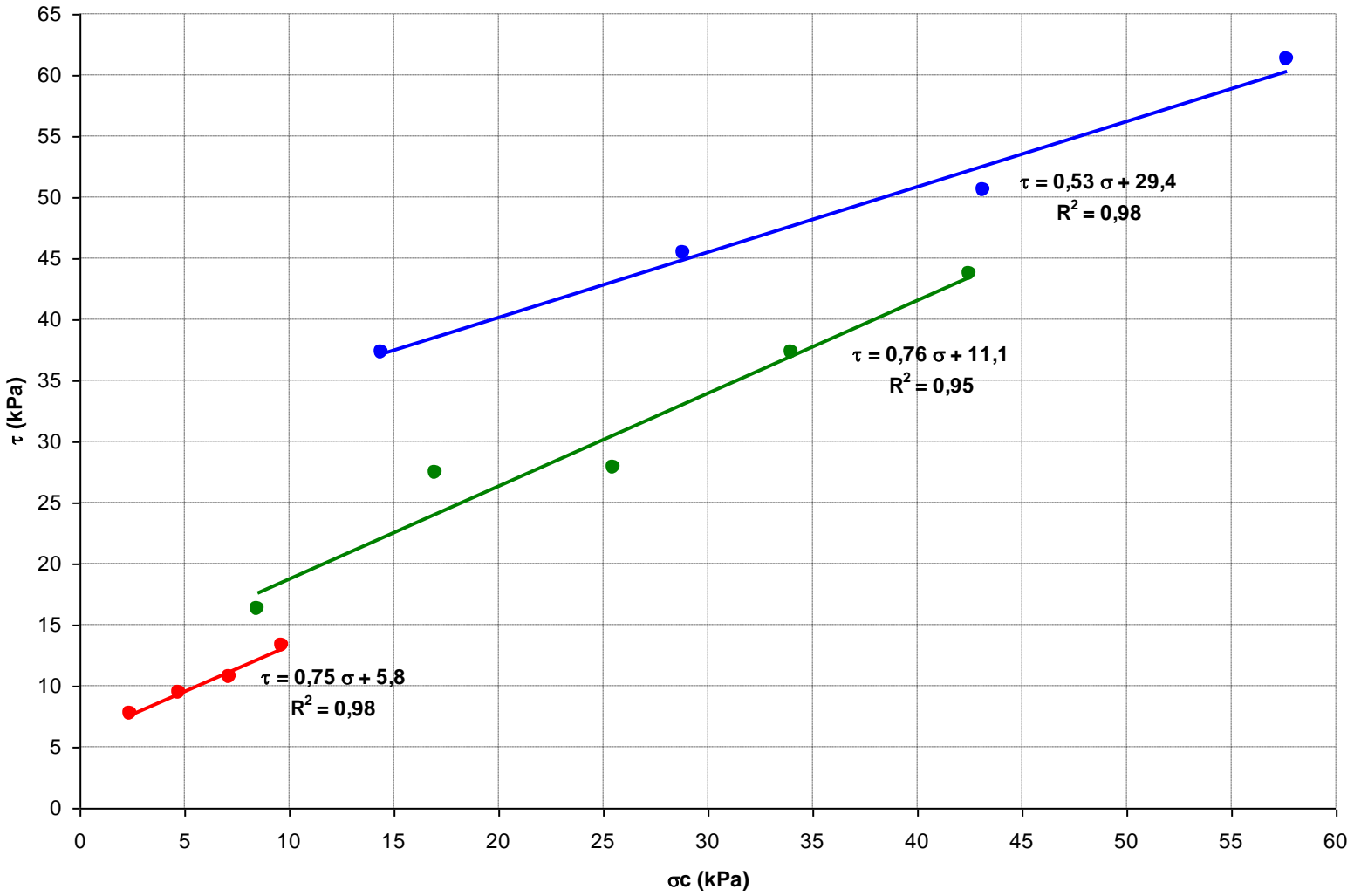


Sample\_1 Sample\_2 Sample\_3 Sample\_4



Sample\_1 Sample\_2  
Sample\_3 Sample\_4





## **CHAPTER 3**

### 3.1. MEASUREMENTS OF THE SCAR TOPOGRAPHY

The evaluation of the landslide scar geometry appears to be fundamental if a detailed analysis of the triggering landslide mechanism has to be conducted. For this purpose, the available topographic charts are not enough accurate. Therefore, total station theodolite measurements of the scar topography were taken for the landslides n. 2, 4 and 5, at “Monte di Vezzi” (figure 3.1). This allowed for the reconstruction of one axial profile and of three transversal profiles for each one of the landslides.

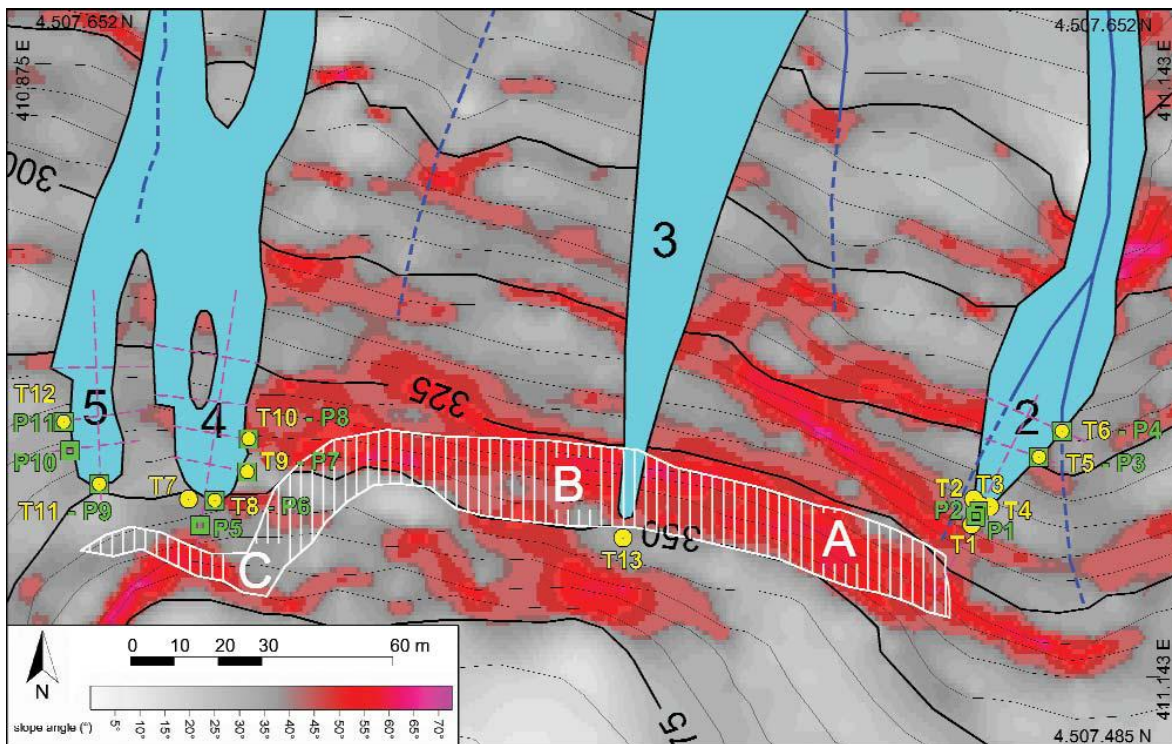


**Fig. 3.1: Landslide perimeter, numeration and in situ test location (from De Vita et alii, 2007)**

The topographic surveys turned out to be fundamental for the evaluation of the mechanism triggering the landslides. Moreover, coupling the transversal and the axial scar profiles also allowed for an estimate of the total volume of soil involved in the instability, and thus for the evaluation of the mobility of the landslide (Corominas, 1996; Budetta & De Riso, 2004).

All the measurements taken were processed in AutoCAD and profiles of the landslide scar were obtained. Based on these measurements, it was recognized that a circular geometry was best fitting the scar surface profiles. These circles are tangent to the basal low plasticity silt layer. A summary of the geometric features of the failure surface is given in table 3.1 (see also fig.3.2.). Reconstructed slope profiles are also obtained and are presented in the appendix B.

Landslide n.	$\beta$	R	$\theta$	$h_{av}$
2	36	16,75	50	1,39
4	38	16,73	53	1,32
5	39	16,75	35	0,65

**Tab. 3.1: Summary of landslide geometry:  $\beta$ =slope angle; R=failure surface radius;  $\theta$ =apex angle;  $h_{av}$ = average thickness (along y-direction; see fig. 3.5) of the pyroclastic cover.**

### 3.2. BACK ANALYSIS OF THE FAILED SLOPES

The limit equilibrium analysis is usually executed to evaluate the stability of a slope. By means of this approach, only the forces acting on the soil masses and the soil resistances are taken into account. The factor of safety of the slope is defined as the shear stress over the strength required for equilibrium. With the limit equilibrium methods the soil is modeled as brittle. This means no deformations until failure and after failure,

deformations not dependent on the stresses: that is the soil reaches the steady state after failure. The slope stability analysis is performed by means of a slice method. In all of the slice methods, the shear strength is assumed to act in the center of the base of each slice. The weight of the slice is represented as vector acting in the center of gravity of the slice. Surface interactions between slices act on the lateral boundary (when considered) and can have different inclination depending on the adopted method of analysis. The choice of the most appropriate method and the advantages of one method with respect to another is beyond the scopes of this document. The model used for the back analysis is illustrated schematically in figure 3.2. When a slope failure occurs, back analysis can be used to estimate an unknown parameter. The reliability of this estimate mostly depends on the accuracy with which known parameters are evaluated. The back analysis of a slope failure is usually done assuming the condition of limiting equilibrium for which the factor of safety is equal to unity (Duncan and Wright, 2005). Since only one equation for the factor of safety is available, the back analysis allows for the evaluation of only one parameter included in the factor of safety formula.

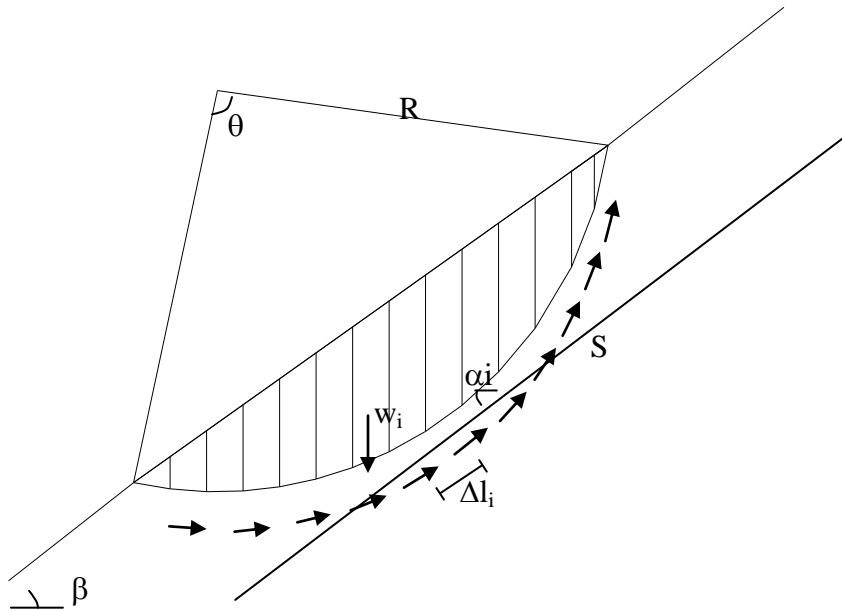


**Fig. 3.2: Slope model assumed in the back analysis.**

Mostly after the last tragic events of Sarno, 1998, several descriptions of the landslide triggering mechanism in the Campania region have been proposed. Whereas there is a good agreement inside the local scientific community on the geologic model of the slope, one point appears to be source of controversy: is the landslide triggered because of the formation of saturated zone on the slope? Or the combination of very high slope angles and decrease in matrix suction, without soil saturation, is enough to start the instability? Back analysis could be used to answer these questions.

As said, the back analysis only allows for the evaluation of one parameter among those included in the equation of the factor of safety. The back analysis executed in terms of effective stresses could be used to verify the hypothesis of saturated zones formation. Usually, no reliable estimate or in situ measurements of the pore pressure triggering the instability are available. Therefore, the back analysis will allow evaluating the critical pore

pressure that developed at failure. This happens once appropriate effective strength parameters are input in the expression of the factor of safety. The critical pore pressure, together with a model describing the hydrologic response of the slope, would be relevant for the definition of hydrologic threshold.

To investigate the hypothesis of failure happening before saturation is reached, the back analysis in terms of total stresses seems to be more appropriate. The shear resistance, to use for future stability analyses in similar settings, is the estimated parameter. In this case it is assumed that:

$$(3.1) \quad S=c+\sigma \tan \phi,$$

and  $S$  constant along the whole length of the critical circle. Assuming  $S$  as constant is a way to overcome the problem of having two unknowns in the equation of the factor of safety (the cohesion and the friction angle). The assumption of constant shear strength can be furthermore justified. Soil slices such those closer to the ends of the shear surface have a greater cohesion component than the frictional one. This is for the shear surface being shallower and the shear stress on the failure plane is not relevant. On the other hand, these slices are likely to have lower water content and thus a more relevant matrix suction component. The opposite happens for the slices in the central part of the landslide body. The shear surface is deeper and the water content is higher leading to a frictional component relevant with respect to matrix suction.

### **3.2.1. BACK ANALYSIS IN THE HYPOTHESIS OF UNSATURATED SOILS**

The back analysis in terms of total stresses parameters, was performed using of the computer program SLIDE 5.0. The 2D model was drawn in Autocad after processing the data obtained from field measurements of the scar surface in the sliding area, and then

imported in SLIDE 5.0. The pre existing slope topography was approximated by a straight line passing through the vertex of the landslide top crown. A three layers geologic model was developed in accordance with the field observations at the landslide scar: the first silty sand layer (SM), than the well graded sandy layer (SW-SM) and finally, the low plasticity silt layer (ML). Field measurements also allowed for an estimate of the total apparent thickness of the coarse strata ranging in the interval 0.95-2.10 m. The unit weight used in the analysis and saturation conditions assumed were as follows:  $\gamma$  (SM-unsaturated) = 16 kN/m<sup>3</sup>;  $\gamma$  (SW-GW-unsaturated) = 18.5 kN/m<sup>3</sup>;  $\gamma$  (ML-saturated) = 17.5 kN/m<sup>3</sup>. The method used in the analysis was Spencer's method. Circular geometry of the sliding surface was the work hypothesis. The number of slices in which each circle was divided during software iterations was set equal to 50. The circular surfaces imported in SLIDE 5.0 have radius of about 16.75m. The analyses were performed by fixing from time to time the strength property of the two upper layers (SM and SW-GW), and run the software until the factor of safety for the measured scar surface equaled one. When this occurred, the fixed value was chosen as the back calculated constant shear strength of the soil. Calculations were also performed according to the Infinite Slope model. The factor of safety equals the shear strength over the stresses required for equilibrium. The shear strength was obtained after setting the factor of safety equal to one. More in particular, the parameter  $S/\gamma h$  is evaluated for each landslide:

$$(3.2) \quad F = \frac{S}{w \sin \beta}, F = 1, w = \gamma \times h \cos \beta$$

being  $S$  the constant shear strength of the soil to estimate,  $h$  the average apparent thickness of the pyroclastic cover,  $\beta$  the slope angle and  $\gamma$  the average unit weight. Rearranging the (3.2) it results:

$$(3.3) \quad \frac{S}{\gamma h} = \frac{\sin 2\beta}{2}$$

The average soil unit weight is evaluated as:

$$(3.4) \quad \gamma = \frac{h(SM)}{h_{tot}} \gamma(SM) + \frac{h(SW)}{h_{tot}} \gamma(SW)$$

Results from this model are compared to those obtained from the software calculations and are shown in table 3.2.

### **3.2.1.1. DISCUSSION OF RESULTS**

The back calculated constant shear strength according to the Spencer's method results as: 8.30 kPa (landslide n.2 - 2.00 m apparent thickness); 7.5 kPa (n.4 – 2.10 m); 4.0 kPa (n.5- 0.95 m). If the ratio of the shear strength to the  $\gamma h$  of the pyroclastic cover in the sliding area is considered, values of 0.237, 0.210 and 0.255 are found. According to the infinite slope approach, the back calculated constant shear strength results as 15.40, 12.37 and 6.86 kPa, for the three landslides respectively. Normalized strength lead to the following values of  $S/\gamma h=0.476$ ,  $S/\gamma h=0.486$ ,  $S/\gamma h=0.489$  respectively. The infinite slope model is the most conservative approach that can be taken for factor of safety evaluation. This is for end effects are not taken into account with this model. In terms of back analysis, the former conclusion is inverted: shear strength calculated by means of an infinite slope approach are unconservative.

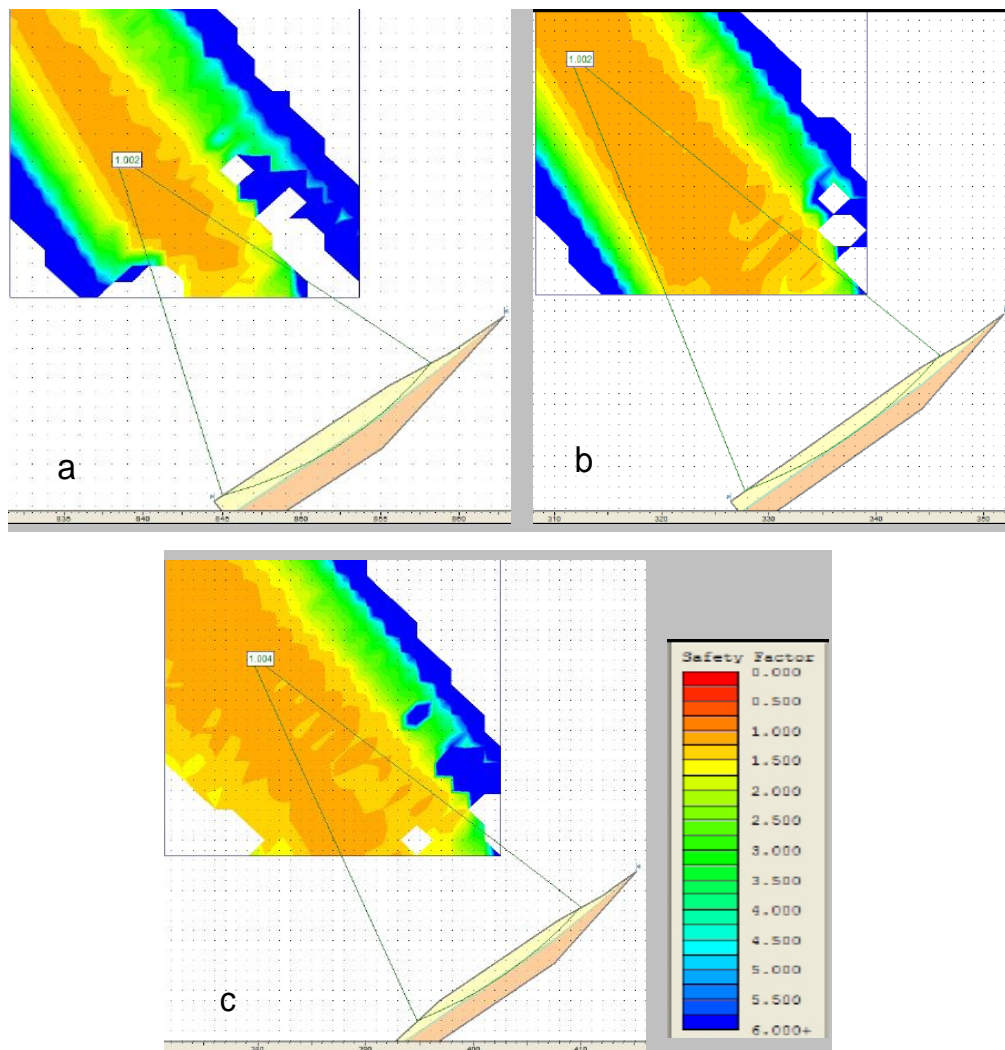


**Fig. 3.3: Results obtained from Spencer's Method on landslide n.2.**

Values of the  $S/\gamma h$  ratio calculated by means of the infinite slope model are only dependent on the slope angle. These resulted to be greater (up to 40%) than the same values back calculated by means of the computer model and actual landslide geometry. Similar evaluations can be also found in Duncan & Stark (1992) where back analysis was used for the evaluation of effective cohesion for the soils of the Orinda formation, close to

the San Francisco Bay. Considering a finite slope for the analysis (e.g. rotational slide on a long slope) allows for including end effect that result in a more accurate estimate of the shear strength. Although the data base is restricted, for future stability analyses in similar settings, where the same hypotheses of this study are satisfied, the suggested value of the ratio of the constant shear strength to the average  $\gamma h$  of the pyroclastic cover should be included in the range 0.21 – 0.25.

Land slide n	$\beta$ (deg)	$\gamma_{av}$ (kPa/m)	$h_{app}$ (m)	SPENCER'S		INFINITE SLOPE		$\Delta$ (%)
				S (kPa)	S/ $\gamma h$	S (kPa)	S/ $\gamma h$	
2	36	17,5	2,0	8,30	0,237	15,40	0,476	200
4	38	17,0	2,10	7,50	0,210	12,37	0,485	230
5	38	16,5	0,95	4,00	0,255	6,86	0,489	191

**Tab. 3.2: Summary back analysis results: Spencer's and Infinite Slope method.**

In both the analysis performed the real and apparent pyroclastic soil thicknesses are related as:

$$(3.5) \quad h_r = h_a \times \cos\beta$$

in reality this is not true since the thickness of the soil cover will be less than the theoretical value. The thickness of the soil is related to the slope angle since the latter is driving the major erosion processes: high slope angle will allow for a smaller thickness of the cover. De Vita *et alii* (2006) found an empirical relationship linking these two parameters, for the Sarno Mountains area, based on resistivity measurements of the thickness of the pyroclastic cover of a sample slope. However, in the performed analyses, results are normalized to the apparent thickness and to the unit weight of the soil. Therefore, the error affecting the soil apparent thickness and unit weight estimate, influence both the infinite slope and the Spencer's method results in the same way. Thus,

the unconservative estimate done with one method with respect to the other only depends on whether or not the end effects are taken into account. Therefore, evaluating accurately the scar topography, also in the case of shallow landslides has a significant impact on the evaluation of the back calculated constant shear strength of the soil?

### **3.2.2. BACK ANALYSIS IN THE HYPOTHESIS OF SATURATED AREA FORMATION**

The back analysis of the failed slopes has been executed in the hypothesis of saturated area formation at the interface between the well graded sand and the low plasticity silt. More in particular, two cases have been taken into account. In the first case, the stability analysis is executed using the peak effective friction angle and effective cohesion of the soil. These parameters were calculated by means of CD-direct shear test on undisturbed samples. Results of the tests are presented in the previous chapter (2.2.1).

In the second case the back analysis is executed assuming residual strength parameters. This assumption is supported by the discussion presented in the previous chapter (2.4.1) and is re called in the following (3.2.2). Residual strength parameters are assumed for all the three landslides analyzed. These are specified in the following.

The aim of the back analysis is to evaluate the thickness of the saturated area in which the seepage flow occurs. The thickness necessary in to trigger the landslide is the critical rainfall height. For this purpose, the use of the software slide 5.0 seems to be not suitable and Spreadsheet calculations are executed. The stability analysis is approached by means of the Bishop modified method (Bishop, 1955).

This method satisfies the moment equilibrium of the entire soil mass and the equilibrium of the forces acting on the slices, in the vertical direction. Forces acting between slices are assumed to be horizontal. Although this is not a complete method, very good

approximations are obtained, being the differences with more accurate methods (e.g. Spencer's Method) minimal. Bishop's equation is written as:

$$(3.6) \quad F = \frac{\sum \left[ \frac{c' \Delta l \cos \alpha_i + (W_i - u_i \Delta l \cos \alpha_i) \tan \phi'}{\cos \alpha_i + (\sin \alpha_i \tan \phi' / F)} \right]}{\sum w_i \sin \alpha_i}$$

Where  $F$  is the factor of safety;  $c'$ , the peak effective cohesion (equal to zero in case of residual strength parameters);  $\phi'$ , the peak (residual) effective friction angle;  $\alpha_i$ , the inclination of each slice;  $W_i$ , the total weight of each slice;  $u_i$ , the pore pressure in the center of the slice;  $\Delta l_i$ , the length of the base of the slice.

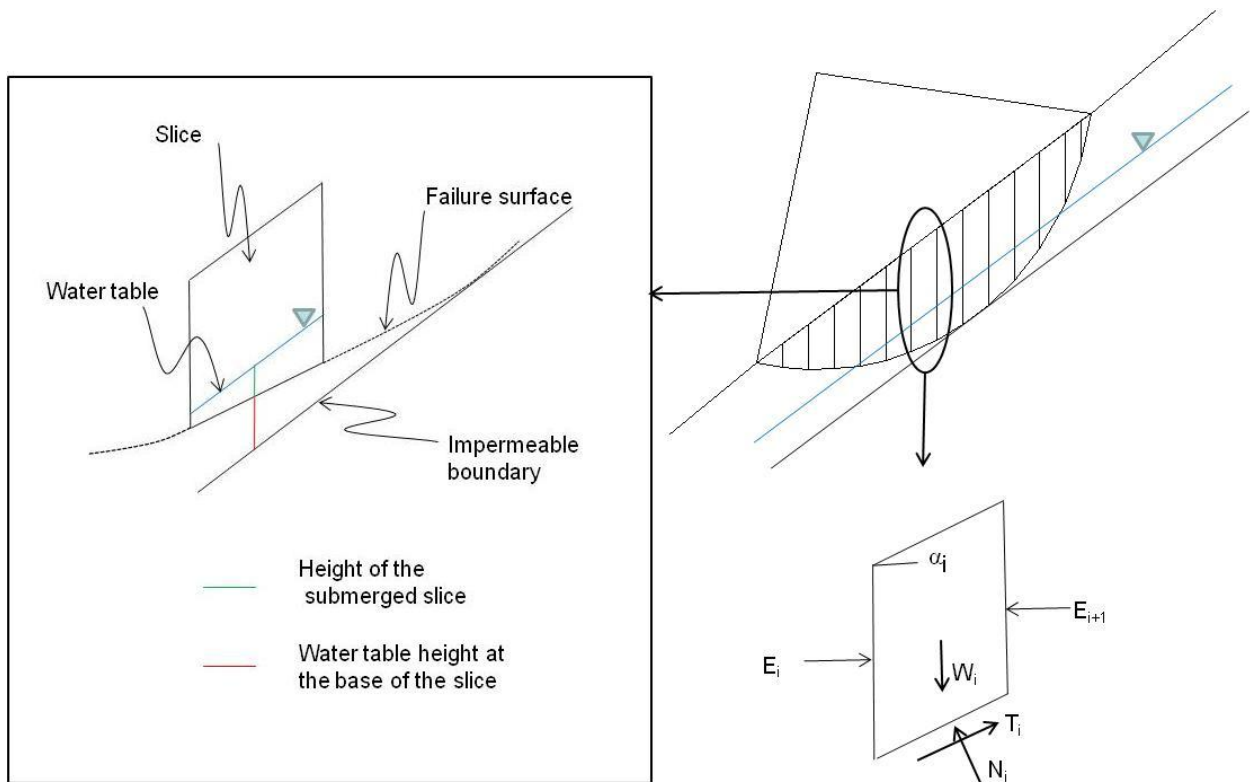


**Fig. 3.4: Subdivision in slices of the slid soil mass and forces acting on the slices.**

With reference to figure 3.4, calculations are performed as follows:

1. The vertical height (H) of the water table, representing the steady seepage flow, is fixed.
2. Given the landslide geometry and strength parameters (peak or residual), total unit weight and pore pressure in the center of the slice are calculated as:

$$(3.7) \quad W_i = \{[\gamma_m \times (h_i - H)] + (\gamma_{sat} \times H)\} \times b_i$$

$$(3.8) \quad u_i = \gamma_w \times h_{pi} \text{ (submerged slices)}$$

$$(3.9) \quad u_i = 0 \text{ (non submerged slices)}$$

Where:  $h_i$ , the average height of the slice;  $b_i$ , the width of the slice;  $\gamma_m$ , the moist unit weight of the soil;  $\gamma_{sat}$ , the saturated unit weight of the soil;  $\gamma_w$ , the unit weight of the water.  $u_i=0$ , for non submerged slopes;  $h_{pi}$  is the piezometric height measured in the center of the slice. This is given by  $h'_i \cos^2\alpha_i$ , being  $h'_i$  the height of the water table at the base of the slice (see fig. 3.4).

3. Factor of safety is fixed for the right hand of the Bishop's equation and trial and error is executed until the calculated F converges to the fixed value.
4. The critical height ( $h_{CRba}$ ) is found when F equals to one.

A summary of the results of spreadsheet calculations is presented in the following paragraphs. The entire set of calculations, and the profiles of the slopes used for the stability analysis, is presented in the appendix to this chapter.

### 3.2.2.1. BACK ANALYSIS USING PEAK PARAMETERS TO MODEL THE SHEAR STRENGTH OF THE SOIL: SUMMARY OF CALCULATIONS

The back analysis of the three landslides at “Monte di Vezzi” has been performed using the results from measurements of the scar topography and the peak effective friction angle and peak effective cohesion. The results of direct shear tests on undisturbed samples to obtain peak shear strength parameters are summarized in table 3 of the previous chapter. Although the basal layer has been sampled and tested, it is assumed not to be interested by the initial debris slide. The results obtained from the back analysis are summarized in the following table 3.3.

landslide n.	Apparent thickness (m)	slope (deg)	$h_{CRba}$ (m)-vertical	FS
2	2	36	2	1.31
4	2.1	38	2.1	1.37
5	0.95	38	0.85	1

**Tab. 3.3: Summary back analysis results obtained using peak friction angle and cohesion.**

It can be seen that using peak shear strength parameters, the factor of safety will be well above one in case of landslide 2 and 4, for the whole soil thickness saturated. The limit equilibrium is reached only in case of landslide 5, for a saturated soil thickness of 0.85 meters.

### 3.2.2.2. SHEAR STRENGTH OF THE SOIL INVOLVED IN THE INITIAL DEBRIS-SLIDE

The shear strength of soils is commonly defined by means of Coulomb's law (Coulomb, 1773). The material resists to an external solicitation by mobilizing both frictional and cohesive resistance. The general form of Coulomb's Law is:

$$(3.10) \quad S = c + \sigma_f \tan \phi$$

It is accepted that effective stress control the strength of granular materials. Thus, the normal stress on the failure plane is expressed by means of Terzaghi's principle of effective stresses (1942) as:

$$(3.11) \quad \sigma'_f = \sigma - u$$

and  $c$  and  $\tan \phi$  in equation 3.10 become the effective stresses parameters  $c'$  and  $\tan \phi'$ . Shear strength expressed in terms of effective stress parameters (and thus, in effective stresses analyses) is advised any time pore pressures can be evaluated reliably (Bishop & Bjerrum, 1960). This mostly happens when drained conditions (CD) verify in the field. Shear strength expressed in terms of total stress parameters (in total stresses analyses) has to be used any time undrained condition verify in the field (CU). It is fundamental for a correct analysis, that the assumptions on drainage conditions match the actual drainage conditions verified in the field.

The stability analysis for an initial debris-slide can be conducted using effective stress parameters. The pore pressure in this case are not shear induced but are due to the seepage taking place after the rain water infiltration process. Assumption of drained conditions during the initial debris-slide seems to be reasonable. The process of rain

water infiltration leading to decrease in matrix suction and to down slope directed flow and pore pressures built is assumed to be relatively slow.

The effective stress parameters also have to be estimated and used consistently, taking into account stress paths that happen in the field. In their paper on the shear and compressibility characteristics of granular materials under drained conditions, Lee and Seed (1967) pointed out that dense sand expand under shearing provoked in triaxial compression tests showing a brittle behavior. High friction angles are expected in this case (e.g. 40 deg). Conversely, loose sands compress under shearing provoked in triaxial compression tests, with a ductile behavior evidenced in the  $\sigma_d$ - $\varepsilon$  plot. Lower values of friction angle are obtained in this latter case (e.g. 30 deg). There will be a value of the void ratio, as Casagrande (1940) first pointed out, at which shear will happen with no change in volume. This is the critical void ratio and the soil at this point will be at the steady state (Pulos, 1981). The friction angle of the soil in this case is the residual or the steady state friction angle. Dense sands reach the steady state after a peak of resistance at relatively low deformations while loose sands will get to the steady state without reaching a peak, at large deformations. Rowe (1962) defined frictional components of the shear strength of granular materials as a function of porosity. He pointed out that loose sands (high porosity) will react with an angle of shearing resistance that has two components: the mineral-to-mineral and the particle rearrangement. As porosity decreases, granular soils start to dilate during triaxial compression and this result in higher friction angles. Thus, dilatancy as well as particle rearrangement will appear for sands under triaxial compression depending on their porosity. Taylor (1948) speculated that the increase in resistance (high friction angles) was due to the greater amount of energy that has to be spent in order to fail under compression dense, dilatant sand.

In case of drained loading condition, the stress state on the failure plane changes continuously until failure. Failure occurs when the shear stress on the failure plane exceeds the shear strength. Because of the consistent deformation that takes place in the

soil during these processes where an external load is applied, the soil can develop additional shear strength due to particle rearrangement or dilatancy effects (peak strength). This will occur depending on the density of the soil in situ. However, as described in the previous section, and as also defined from other authors (Sassa, 1985), the stress state evolution of the soil prior to a debris flow trigger, can be represented by a horizontal stress path. In this case no external load is applied and the shear stress on the failure plane does not change throughout the whole evolution of the stress path until failure. Two main differences can be identified with respect to the case where an external load is applied:

1. Failure occurs because of a reduction of the effective stresses on the failure plane and not because of an increase in shear stress on the failure plane that overcomes the shear resistance of the soil. Thus, if the ratio of the mean shear stress on the failure plane ( $q'$ ) to the mean effective stresses on the failure plane ( $p'$ ) is defined, failure occurs because of a decrease in  $p'$  while  $q'$  remains constant and the  $q'/p'$  ratio reaches a critical value.
2. For the initial debris slide, it can be assumed that no deformation occur until failure is reached. Thus, it is unlikely that particle rearrangement and dilatancy, that are sources of strength due to deformations, will occur. Therefore, the angle of repose could be more appropriate to describe the shear strength of granular soils during initial slide. Since a sliding mass on a slope composed of granular elements will stop when the residual friction angle will balance the gravity actions, the angle of repose could be set equal to the residual friction angle, with little conservatism.

Granular materials are usually considered cohesionless. However, source of cohesion are represented both from root networks and from matrix suction or from some degree of cementation between grains.

### 3.2.2.3. BACK ANALYSIS USING RESIDUAL PARAMETERS TO MODEL THE SHEAR STRENGTH OF THE SOIL: SUMMARY OF CALCULATIONS

The back analysis of the three landslides at “Monte di Vezzi” has been performed using the measured scar topography and the residual effective friction angle. Cohesion is assumed to be zero. Friction angle is assumed equal to the slope angle.

landslide n.	thickness (m)	slope (deg)	$h_{CRba}$ (cm)	FS	h/H
2	2	36	0.35	1.00	0.175
4	2.1	38	0.4	1.03	0.190
5	0.95	38	0.15	0.96	0.158

**Tab. 3.4: Summary back analysis results obtained using adopted values of residual friction angle and no cohesion.**

It can be seen that using residual shear strength parameters, the limit equilibrium is reached in all the cases and the height (measured along the vertical direction) of the saturated soil has very reasonable values included in the range 15 cm to 40 cm.

As expected, the critical height of the saturated zone is directly proportional to the (apparent) thickness of the soil cover. It is also reasonable to expect that the height of saturated zone be inversely proportional to the slope angle, even though this is only evidenced comparing landslide n.2 and n.5, and not n.2 and n.4. In this latter case

however, the angle increase effect likely is zeroed of by the greater thickness of the pyroclastic cover.

### **3.3. PLUVIOMETRIC THRESHOLD BASED ON BACK ANALYSIS**

The critical height of the seepage flow necessary to trigger the initial debris slide has been calculated for landslides n.2, n.4 and n.5 at “Monte di Vezzi”, by means of back analysis. Based on these data a value of the critical rainfall intensity can be obtained. A model is needed to translate the critical seepage flow height into the critical rainfall intensity. A two dimensional model is assumed as shown in figure 3.5. A control volume of the seepage flow is considered and the continuity equation is applied to this volume. The x-axis is assumed parallel to the slope. At the generic abscissa  $x$ , the flow into the lateral surface (h per unit width) is  $q_x$ . The outgoing flow through the same lateral surface of the sample volume, at abscissa  $x+dx$ , is  $q_{x+dx}$ . The rain water infiltration is assumed to occur in the vertical direction. The incoming flow generated by the infiltration is  $q_I \cos \beta$  and occurs along the y direction (by definition the flow is perpendicular to the slope sub grade).

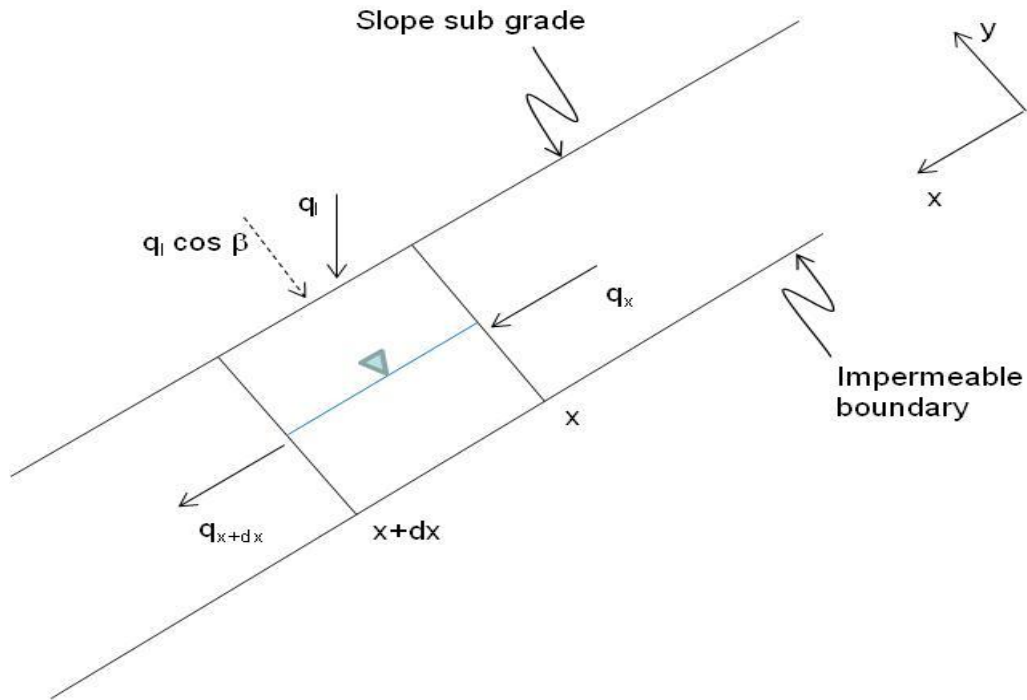


**Fig. 3.5: Two-dimensional model assumed to compute the continuity equation.**

Water loss due to evapo-transpiration is neglected. According to the studies of Johnson and Sitar, (1990) and Harr, (1977), and as also explained in chapter 2, it can be assumed that this scenario will occur upslope, for an already wet slope, once the seepage flow takes place. Assuming positive incoming flow, the continuity equation can be written as:

$$(3.12) \quad q_x - q_{x+dx} + q_l = \left( \frac{\partial h}{\partial t} \right) \cdot dx \cdot n \cdot 1$$

$$(3.13) \quad q_x - q_x - \frac{\delta q_x}{\delta x} + I \cdot dx \cdot \cos \beta \cdot 1 = \left( \frac{\partial h}{\partial t} \right) \cdot dx \cdot n \cdot 1$$

$$(3.14) \quad - \frac{\delta}{\delta x} (k_x i \cdot h \cdot 1) \cdot dx + I \cdot dx \cdot \cos \beta \cdot 1 = \left( \frac{\partial h}{\partial t} \right) \cdot dx \cdot n \cdot 1$$

being  $k_x$  the permeability along the x direction;  $i$ , the flow gradient;  $I$ , the rainfall intensity;  $n$  the porosity. It is assumed that  $k_x$  is constant. This is a reasonable assumption if it is restricted to a small area, such that where the initial debris-slide was triggered. Therefore, in the continuity equation, the term:

$$(3.15) \quad (k_x i \cdot h \cdot 1)$$

is constant and its derivative in the x direction is zero. Thus, the continuity equation becomes:

$$(3.16) \quad I \cdot dx \cdot \cos \beta \cdot 1 = \left( \frac{\partial h}{\partial t} \right) \cdot dx \cdot n \cdot 1$$

$$(3.17) \quad I \cdot \cos \beta = \left( \frac{\partial h}{\partial t} \right) \cdot n$$

Integrating equation 3.17, it results:

$$(3.18) \quad I \cdot t_R \cdot \cos \beta = (h_{CR} - h_{IN}) \cdot n$$

Where  $t_R$  is the rainfall duration,  $\beta$  is the slope angle,  $h_{CR}$  is the critical height and  $h_{IN}$  is the initial seepage flow height. If the soil close to the impervious basal layer is not saturated, the  $h_{IN}$  is zero. Thus, neglecting this quantity will lead to a conservative estimate of the rainfall intensity. Conversely, if the soil close to the impervious boundary is saturated and some flow has arisen, as it could occur during rain events close to each other,  $h_{IN}$  is greater than zero. However, this latter case is very difficult to model, since direct measures of the flow in the soil would be necessary and the  $h_{IN}$  can be set equal to zero. Therefore, the critical height obtained from the simplified form of the continuity

equation is assumed to be the height of the seepage flow to trigger the instability in case of moist soil, close to saturation (for which matrix suction approaches zero), but in which no seepage flow has taken place yet. The continuity equation can be re written as:

$$(3.19) \quad I \cdot t_R \cdot \cos \beta = h_{CR} \cdot n$$

Being  $t_R$  the duration of the rain fall event. The quantity  $h_{CRba}$  is the flow height, computed along the vertical direction, calculated by means of back analysis. The height component along the y-axis is:

$$(3.20) \quad h_{CRba} \cos \beta$$

And substituting in the previous equation it results

$$(3.21) \quad I \cdot t_R = h_{CRba} \cdot n$$

The critical rainfall intensity that triggers the initial debris-slide can be calculated as:

$$(3.22) \quad I_{CR} = \frac{h_{CRba} \cdot n}{t_R}$$

A rainfall intensity threshold for the Ischia 2006 landslides could be obtained by means of equation 3.22, knowing  $h_{CRba}$  from back analysis and assuming different time durations of the rainfall event. The result is shown in the plot in figure 3.6.

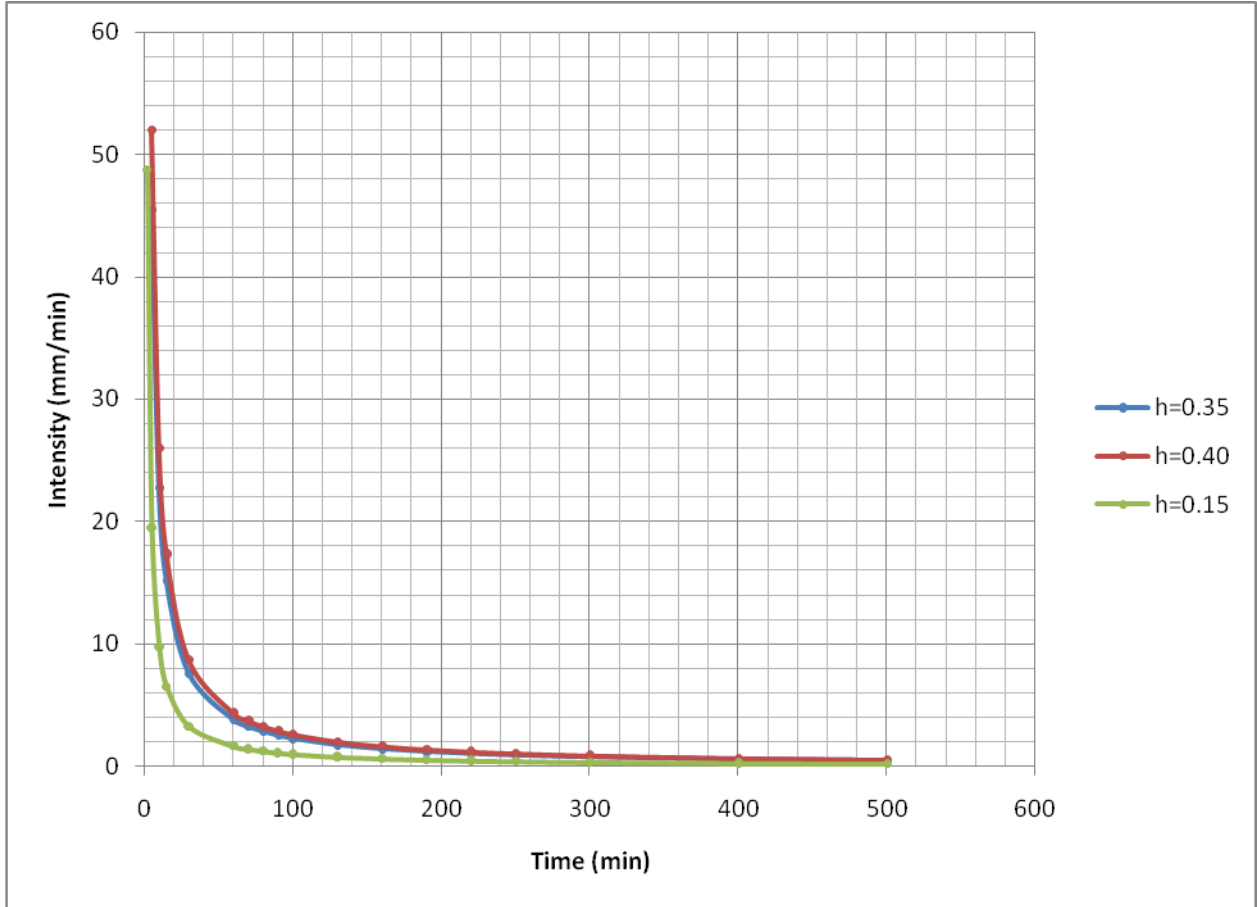


**Fig. 3.6: Back calculated rainfall intensity thresholds.**

### 3.4. DISCUSSION OF RESULTS AND CONCLUSIONS

The “Monte di Vezzi”, Ischia, 2006 debris-slide was an event of small magnitude, compared to others occurred in the Campania region during the last decades, although it had as well tragic consequences. However, the study of this occurrence allowed for the

definition of a template that, in the opinion of the writer, should be considered when analyzing initial debris-slides. Some conclusions that can be drawn from this study are:

- Debris-slides are punctual phenomena and their study implies detailed analyses at the slope scale. These analyses have to be aimed to define the geologic model of the slope, and therefore, to identify the slopes factors of susceptibility to slide. The geologic model helps to understand the response of the slope during rainfall events and to describe and further analyze the triggering mechanism. Detailed topographic measures are necessary to overcome the low definition of the available topographic maps.
- Based on the assumed in situ stress path, the debris-slide back analysis has been conducted modeling the soil with residual shear strength parameters. Results from the back analysis show that a considerable height of the saturated zone is necessary to trigger the instability. For the “Monte di Vezzi” 2006 debris-slide this is estimated in the range 15 to 40 cm. This result strengthens the hypothesis of failure happening after the occurrence of a seepage flow, rather than a reduction of the matrix suction with no saturated area formation.
- In the case of the “Monte di Vezzi” landslide, scar surface topographic measurements have been the base for back analysis. These allowed recognizing the circular shape of the failure surface and to conduct a more refined limit equilibrium analysis.
- Back analysis executed in terms of total stresses shows that the shear strength of the soil, normalized to the factor  $\gamma H$  (H thickness of the soil cover) is included in the range 0.210 – 0.255. This parameter is greatly over estimate

if the infinite slope model is used instead of the more refined Spencer Method for the back analysis calculations.

- Back analysis executed in terms of effective stresses allowed for the evaluation of the critical heights of the saturated zone. This in turn allowed for the evaluation of critical rainfall intensities and the definition of pluviometric threshold for the study area. The threshold rain fall intensity is presented in figure 3.6.
- Pluviometric thresholds are linked to the slope inclination, thickness of the pyroclastic cover and in situ porosity of the soil. Whereas for high slope angle values, slope angle influence can be neglected, the influence of the thickness of the cover is relevant and plays a fundamental role in defining rainfall heights threshold. For the Ischia 2006 landslide it has been found that the thickness of the saturated zone, normalized to the thickness of the pyroclastic cover, is included in the range 0.16 to 0.19.

**APPENDIX TO CHAPTER III**

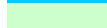
Land Slide 2 - Peak Strength Parameters - Bishop Modified Method - H=0.25 m

strip	b <sub>i</sub> (m)	α <sub>i</sub> (deg)	sin α <sub>i</sub>	cos α <sub>i</sub>	h <sub>i</sub> (m)	A <sub>i</sub> (m <sup>2</sup> )	Δl <sub>i</sub> (m)
1	0.88	12	0.208	0.978	0.23	0.202	0.90
2	0.88	15	0.259	0.966	0.66	0.581	0.91
3	0.88	18	0.309	0.951	1.04	0.915	0.93
4	0.88	22	0.375	0.927	1.37	1.206	0.95
5	0.88	25	0.423	0.906	1.63	1.434	0.97
6	0.88	28	0.469	0.883	1.83	1.610	1.00
7	0.88	32	0.530	0.848	1.96	1.725	1.04
8	0.88	35	0.574	0.819	2.02	1.778	1.07
9	0.88	39	0.629	0.777	1.99	1.751	1.13
10	0.88	43	0.682	0.731	1.86	1.637	1.20
11	1.32	48	0.743	0.669	1.77	2.336	1.97
12	0.44	52	0.788	0.616	1.35	0.594	0.71
13	0.93	58	0.848	0.530	0.50	0.465	1.75

γm(kPa/m)	γ (kPa/m)	tg φ'	φ'	β	cos β	H(m)
20.000	16.000	0.727	36.0	36	0.81	0.250

w <sub>i</sub> (kN/m)	C <sub>i</sub> (kPa)	h'p <sub>i</sub> (m)	hp <sub>i</sub> (m)	u <sub>i</sub> (kPa)	w <sub>i</sub> sin α <sub>i</sub>	c <sub>i</sub> Δl <sub>i</sub> cos α <sub>i</sub>	(w <sub>i</sub> - u <sub>i</sub> Δl <sub>i</sub> cos α <sub>i</sub> )tan φ'
3.238	5.5	0	0	0.00	0.673	4.840	2.353
9.293	5.5	0	0	0.00	2.405	4.840	6.752
14.643	5.5	0	0	0.00	4.525	4.840	10.639
19.290	11	0	0	0.00	7.226	9.680	14.015
22.950	11	0	0	0.00	9.699	9.680	16.674
26.646	11	0.079	0.052	0.51	12.510	9.680	19.035
28.477	11	0.208	0.136	1.34	15.090	9.680	19.836
29.322	11	0.264	0.173	1.70	16.818	9.680	20.220
28.899	11	0.239	0.156	1.53	18.187	9.680	20.015
27.069	11	0.101	0.066	0.65	18.461	9.680	19.252
37.382	11	0	0	0.00	27.781	14.520	27.160
9.504	5.5	0	0	0.00	7.489	2.420	6.905
7.440	5.5	0	0	0.00	6.309	5.115	5.405

NUM	DEN	F
6.82	0.67	
10.92	2.41	
14.53	4.52	
22.24	7.23	1.97
24.81	9.70	
27.19	12.51	
28.29	15.09	F
29.01	16.82	
29.42	18.19	
29.44	18.46	
44.19	27.78	
10.29	7.49	
12.48	6.31	
<b>289.64</b>	<b>147.17</b>	<b>1.97</b>

 Submerged slices  
 Trial Value of F

Land Slide 2 - Peak Strength Parameters - Bishop Modified Method - H=0.85 m

strip	b <sub>i</sub> (m)	α <sub>i</sub> (deg)	sin α <sub>i</sub>	cos α <sub>i</sub>	h <sub>i</sub> (m)	A <sub>i</sub> (mq)	Δl <sub>i</sub> (m)
1	0.88	12	0.208	0.978	0.23	0.202	0.90
2	0.88	15	0.259	0.966	0.66	0.581	0.91
3	0.88	18	0.309	0.951	1.04	0.915	0.93
4	0.88	22	0.375	0.927	1.37	1.206	0.95
5	0.88	25	0.423	0.906	1.63	1.434	0.97
6	0.88	28	0.469	0.883	1.83	1.610	1.00
7	0.88	32	0.530	0.848	1.96	1.725	1.04
8	0.88	35	0.574	0.819	2.02	1.778	1.07
9	0.88	39	0.629	0.777	1.99	1.751	1.13
10	0.88	43	0.682	0.731	1.86	1.637	1.20
11	1.32	48	0.743	0.669	1.77	2.336	1.97
12	0.44	52	0.788	0.616	1.35	0.594	0.71
13	0.93	58	0.848	0.530	0.50	0.465	1.75

γm(kPa/m)	γ (kPa/m)	tg φ'	φ'	β	cos β	H(m)
20.000	16.000	0.727	36.0	35	0.82	0.850

w <sub>i</sub> (kN/m)	C <sub>i</sub> (kPa)	h'p <sub>i</sub> (m)	hp <sub>i</sub> (m)	u <sub>i</sub> (kPa)	w <sub>i</sub> sin α <sub>i</sub>	c <sub>i</sub> Δl <sub>i</sub> cos α <sub>i</sub>	(w <sub>i</sub> - u <sub>i</sub> Δl <sub>i</sub> cos α <sub>i</sub> )tan φ'
3.238	5.5	0	0	0.00	0.673	4.840	2.353
9.293	5.5	0	0	0.00	2.405	4.840	6.752
14.643	5.5	0	0	0.00	4.525	4.840	10.639
22.282	11	0.205	0.138	1.35	8.347	9.680	15.326
25.942	11	0.469	0.315	3.09	10.964	9.680	16.874
28.758	11	0.669	0.449	4.40	13.501	9.680	18.079
30.589	11	0.795	0.533	5.23	16.210	9.680	18.878
31.434	11	0.858	0.576	5.65	18.030	9.680	19.227
31.011	11	0.824	0.553	5.42	19.516	9.680	19.063
29.181	11	0.69	0.463	4.54	19.901	9.680	18.297
41.870	11	0.429	0.288	2.82	31.116	14.520	27.712
9.504	5.5	0	0	0.00	7.489	2.420	6.905
7.440	5.5	0	0	0.00	6.309	5.115	5.405

NUM	DEN	
6.76	0.67	
10.81	2.41	
14.35	4.52	<b>F</b>
23.11	8.35	1.76
24.57	10.96	
25.78	13.50	
26.77	16.21	<b>F</b>
27.38	18.03	
27.72	19.52	
27.62	19.90	
43.27	31.12	
9.91	7.49	
11.96	6.31	
<b>280.01</b>	<b>158.99</b>	<b>1.76</b>

Submerged slices/to change  
Trial Value of F

Land Slide 2 - Peak Strength Parameters - Bishop Modified Method - H=2.00 m

strip	b <sub>i</sub> (m)	α <sub>i</sub> (deg)	sin α <sub>i</sub>	cos α <sub>i</sub>	h <sub>i</sub> (m)	A <sub>i</sub> (mq)	Δ <sub>i</sub> (m)
1	0.88	12	0.208	0.978	0.23	0.202	0.90
2	0.88	15	0.259	0.966	0.66	0.581	0.91
3	0.88	18	0.309	0.951	1.04	0.915	0.93
4	0.88	22	0.375	0.927	1.37	1.206	0.95
5	0.88	25	0.423	0.906	1.63	1.434	0.97
6	0.88	28	0.469	0.883	1.83	1.610	1.00
7	0.88	32	0.530	0.848	1.96	1.725	1.04
8	0.88	35	0.574	0.819	2.02	1.778	1.07
9	0.88	39	0.629	0.777	1.99	1.751	1.13
10	0.88	43	0.682	0.731	1.86	1.637	1.20
11	1.32	48	0.743	0.669	1.77	2.336	1.97
12	0.44	52	0.788	0.616	1.35	0.594	0.71
13	0.93	58	0.848	0.530	0.50	0.465	1.75

γm(kPa/m)	γ (kPa/m)	tg φ'	φ'	β	cos β	H(m)
20.000	16.000	0.727	36.0	35	0.82	2.000

w <sub>i</sub> (kN/m)	C <sub>i</sub> (kPa)	h' <sub>p<sub>i</sub></sub> (m)	h <sub>p<sub>i</sub></sub> (m)	u <sub>i</sub> (kPa)	w <sub>i</sub> sin α <sub>i</sub>	c <sub>i</sub> Δ <sub>i</sub> cos α <sub>i</sub>	(w <sub>i</sub> - u <sub>i</sub> Δ <sub>i</sub> cos α <sub>i</sub> )tan φ'
10.278	5.5	0.23	0.154	1.51	2.137	4.840	6.500
16.333	5.5	0.66	0.443	4.34	4.227	4.840	9.089
21.683	5.5	1.04	0.698	6.85	6.700	4.840	11.377
26.330	11	1.37	0.919	9.02	9.863	9.680	13.364
29.990	11	1.63	1.094	10.73	12.674	9.680	14.929
32.806	11	1.83	1.228	12.05	15.402	9.680	16.133
34.637	11	1.96	1.315	12.90	18.355	9.680	16.916
35.482	11	2.02	1.355	13.30	20.351	9.680	17.277
35.059	11	1.99	1.335	13.10	22.063	9.680	17.097
33.229	11	1.86	1.248	12.24	22.662	9.680	16.314
47.942	11	1.77	1.188	11.65	35.628	14.520	23.658
13.024	5.5	1.35	0.906	8.89	10.263	2.420	6.622
14.880	5.5	0.50	0.336	3.29	12.619	5.115	8.587

NUM	DEN	
10.37	2.14	
12.55	4.23	
14.45	6.70	<b>F</b>
20.30	9.86	1.31
21.57	12.67	
22.58	15.40	
23.29	18.35	<b>F</b>
23.70	20.35	1.31
23.78	22.06	
23.43	22.66	
35.31	35.63	
8.59	10.26	
13.70	12.62	
<b>253.62</b>	<b>192.95</b>	

Submerged slices/to change  
Trial Value of F

Land Slide 4 - Peak Strength Parameters - Bishop Modified Method - H=0.25 m

strip	b <sub>i</sub> (m)	α <sub>i</sub> (deg)	sin α <sub>i</sub>	cos α <sub>i</sub>	h <sub>i</sub> (m)	A <sub>i</sub> (m <sup>2</sup> )	Δl <sub>i</sub> (m)
1	0.93	10	0.174	0.985	0.24	0.223	0.94
2	0.93	14	0.242	0.970	0.69	0.642	0.96
3	0.74	17	0.292	0.956	1.02	0.755	0.77
4	1.12	20	0.342	0.940	1.43	1.602	1.19
5	0.93	24	0.407	0.914	1.70	1.581	1.02
6	0.93	24	0.407	0.914	1.94	1.804	1.02
7	0.93	31	0.515	0.857	2.10	1.953	1.08
8	0.93	37	0.602	0.799	2.12	1.972	1.16
9	0.93	39	0.629	0.777	2.05	1.907	1.20
10	0.93	43	0.682	0.731	1.89	1.758	1.27
11	1.29	48	0.743	0.669	1.60	2.064	1.93
12	0.58	53	0.799	0.602	1.05	0.609	0.96
13	0.93	58	0.848	0.530	0.46	0.428	1.75

γm(kPa/m)	γ (kPa/m)	tg φ'	φ'	β	cos β	H(m)
20.000	16.000	0.727	36.0	35	0.82	0.250

w <sub>i</sub> (kN/m)	C <sub>i</sub> (kPa)	h' <sub>p<sub>i</sub></sub> (m)	hp <sub>i</sub> (m)	u <sub>i</sub> (kPa)	w <sub>i</sub> sin α <sub>i</sub>	c <sub>i</sub> Δl <sub>i</sub> cos α <sub>i</sub>	(w <sub>i</sub> - u <sub>i</sub> Δl <sub>i</sub> cos α <sub>i</sub> )tan φ'
3.571	5.5	0	0	0.00	0.620	5.115	2.595
10.267	5.5	0	0	0.00	2.484	5.115	7.460
12.077	5.5	0	0	0.00	3.531	4.070	8.774
25.626	11	0	0	0.00	8.764	12.320	18.618
25.296	11	0	0	0.00	10.289	10.230	18.379
28.867	11	0	0	0.00	11.741	10.230	20.973
32.178	11	0.386	0.259	2.54	16.573	10.230	21.662
32.476	11	0.404	0.271	2.66	19.544	10.230	21.798
31.434	11	0.327	0.219	2.15	19.782	10.230	21.384
28.123	11	0	0	0.00	19.180	10.230	20.433
33.024	11	0	0	0.00	24.542	14.190	23.993
9.744	5.5	0	0	0.00	7.782	3.190	7.079
6.845	5.5	0	0	0.00	5.805	5.115	4.973

NUM	DEN	
7.37	0.62	
11.90	2.48	
12.11	3.53	<b>F</b>
29.15	8.76	2.04
27.03	10.29	
29.48	11.74	
30.65	16.57	<b>F</b>
31.62	19.54	2.04
31.57	19.78	
31.47	19.18	
40.89	24.54	
11.59	7.78	
12.13	5.80	
<b>306.95</b>	<b>150.64</b>	

Submerged slices/to change  
Trial Value of F

Land Slide 4 - Peak Strength Parameters - Bishop Modified Method - H=0.85 m

strip	b <sub>i</sub> (m)	α <sub>i</sub> (deg)	sin α <sub>i</sub>	cos α <sub>i</sub>	h <sub>i</sub> (m)	A <sub>i</sub> (mq)	Δl <sub>i</sub> (m)
1	0.93	10	0.174	0.985	0.24	0.223	0.94
2	0.93	14	0.242	0.970	0.69	0.642	0.96
3	0.74	17	0.292	0.956	1.02	0.755	0.77
4	1.12	20	0.342	0.940	1.43	1.602	1.19
5	0.93	24	0.407	0.914	1.70	1.581	1.02
6	0.93	24	0.407	0.914	1.94	1.804	1.02
7	0.93	31	0.515	0.857	2.10	1.953	1.08
8	0.93	37	0.602	0.799	2.12	1.972	1.16
9	0.93	39	0.629	0.777	2.05	1.907	1.20
10	0.93	43	0.682	0.731	1.89	1.758	1.27
11	1.29	48	0.743	0.669	1.60	2.064	1.93
12	0.58	53	0.799	0.602	1.05	0.609	0.96
13	0.93	58	0.848	0.530	0.46	0.428	1.75

γ <sub>m</sub> (kPa/m)	γ (kPa/m)	tg φ'	φ'	β	cos β	H(m)
20.000	16.000	0.727	36.0	35	0.82	0.850

w <sub>i</sub> (kN/m)	C <sub>i</sub> (kPa)	h' <sub>p<sub>i</sub></sub> (m)	h <sub>p<sub>i</sub></sub> (m)	u <sub>i</sub> (kPa)	w <sub>i</sub> sin α <sub>i</sub>	c <sub>i</sub> Δl <sub>i</sub> cos α <sub>i</sub>	(w <sub>i</sub> - u <sub>i</sub> Δl <sub>i</sub> cos α <sub>i</sub> )tan φ'
3.571	5.5	0	0	0.00	0.620	5.115	2.595
10.267	5.5	0	0	0.00	2.484	5.115	7.460
12.077	5.5	0	0	0.00	3.531	4.070	8.774
29.434	11	0.225	0.151	1.48	10.067	12.320	20.180
28.458	11	0.518	0.348	3.41	11.575	10.230	18.372
32.029	11	0.732	0.491	4.82	13.027	10.230	20.015
34.410	11	0.905	0.607	5.96	17.722	10.230	20.975
34.708	11	0.926	0.621	6.10	20.888	10.230	21.098
33.666	11	0.844	0.566	5.56	21.187	10.230	20.706
31.285	11	0.692	0.464	4.56	21.336	10.230	19.652
37.410	11	0.392	0.263	2.58	27.801	14.190	24.762
9.744	5.5	0	0	0.00	7.782	3.190	7.079
6.845	5.5	0	0	0.00	5.805	5.115	4.973

NUM	DEN	
7.31	0.62	
11.79	2.48	
11.97	3.53	<b>F</b>
30.20	10.07	1.82
26.58	11.57	
28.11	13.03	
29.36	17.72	<b>F</b>
30.16	20.89	
30.08	21.19	
29.77	21.34	
40.33	27.80	
11.15	7.78	
11.62	5.80	
<b>298.44</b>	<b>163.82</b>	<b>1.82</b>

Submerged slices/to change  
Trial Value of F

Land Slide 4 - Peak Strength Parameters - Bishop Modified Method - H=2.10 m

strip	b <sub>i</sub> (m)	α <sub>i</sub> (deg)	sin α <sub>i</sub>	cos α <sub>i</sub>	h <sub>i</sub> (m)	A <sub>i</sub> (mq)	Δl <sub>i</sub> (m)
1	0.93	10	0.174	0.985	0.24	0.223	0.94
2	0.93	14	0.242	0.970	0.69	0.642	0.96
3	0.74	17	0.292	0.956	1.02	0.755	0.77
4	1.12	20	0.342	0.940	1.43	1.602	1.19
5	0.93	24	0.407	0.914	1.70	1.581	1.02
6	0.93	24	0.407	0.914	1.94	1.804	1.02
7	0.93	31	0.515	0.857	2.10	1.953	1.08
8	0.93	37	0.602	0.799	2.12	1.972	1.16
9	0.93	39	0.629	0.777	2.05	1.907	1.20
10	0.93	43	0.682	0.731	1.89	1.758	1.27
11	1.29	48	0.743	0.669	1.60	2.064	1.93
12	0.58	53	0.799	0.602	1.05	0.609	0.96
13	0.93	58	0.848	0.530	0.46	0.428	1.75

γ <sub>m</sub> (kPa/m)	γ (kPa/m)	tg φ'	φ'	β	cos β	H(m)
20.000	16.000	0.727	36.0	35	0.82	2.100

w <sub>i</sub> (kN/m)	C <sub>i</sub> (kPa)	h' <sub>p<sub>i</sub></sub> (m)	h <sub>p<sub>i</sub></sub> (m)	u <sub>i</sub> (kPa)	w <sub>i</sub> sin α <sub>i</sub>	c <sub>i</sub> Δl <sub>i</sub> cos α <sub>i</sub>	(w <sub>i</sub> - u <sub>i</sub> Δl <sub>i</sub> cos α <sub>i</sub> )tan φ'
11.383	5.5	0.24	0.161	1.58	1.977	5.115	7.203
18.079	5.5	0.69	0.463	4.54	4.374	5.115	10.066
18.293	5.5	1.02	0.684	6.71	5.348	4.070	9.681
35.034	11	1.43	0.960	9.41	11.982	12.320	17.794
33.108	11	1.70	1.141	11.19	13.466	10.230	16.493
36.679	11	1.94	1.302	12.77	14.919	10.230	18.020
39.060	11	2.10	1.409	13.82	20.117	10.230	19.038
39.358	11	2.12	1.423	13.96	23.686	10.230	19.166
38.316	11	2.05	1.376	13.49	24.113	10.230	18.720
35.935	11	1.89	1.268	12.44	24.508	10.230	17.702
43.860	11	1.60	1.074	10.53	32.594	14.190	21.995
14.616	5.5	1.05	0.705	6.91	11.673	3.190	7.707
14.657	5.5	0.46	0.309	3.03	12.430	5.115	8.603

NUM	DEN	
11.44	1.98	
13.82	4.37	
12.37	5.35	<b>F</b>
26.86	11.98	1.37
23.66	13.47	
25.02	14.92	
25.89	20.12	<b>F</b>
26.30	23.69	1.37
26.06	24.11	
25.55	24.51	
34.03	32.59	
10.63	11.67	
14.00	12.43	
<b>275.64</b>	<b>201.19</b>	

Submerged slices/to change  
Trial Value of F

Land Slide 5 - Peak Strength Parameters - Bishop Modified Method - H=0.25 m

strip	b <sub>i</sub> (m)	α <sub>i</sub> (deg)	sin α <sub>i</sub>	cos α <sub>i</sub>	h <sub>i</sub> (m)	A <sub>i</sub> (m <sup>2</sup> )	Δl <sub>i</sub> (m)
1	0.57	26	0.438	0.899	0.10	0.057	0.63
2	0.60	25	0.423	0.906	0.33	0.198	0.66
3	0.60	27	0.454	0.891	0.52	0.312	0.67
4	0.44	29	0.485	0.875	0.66	0.290	0.50
5	0.75	31	0.515	0.857	0.74	0.555	0.87
6	0.60	34	0.559	0.829	0.91	0.546	0.72
7	0.60	37	0.602	0.799	0.96	0.576	0.75
8	0.60	39	0.629	0.777	0.98	0.588	0.77
9	0.60	42	0.669	0.743	0.94	0.564	0.81
10	0.76	47	0.731	0.682	0.76	0.578	1.11
11	0.43	46	0.719	0.695	0.62	0.267	0.62
12	0.60	51	0.777	0.629	0.50	0.300	0.95
13	0.60	54	0.809	0.588	0.19	0.114	1.02

γ <sub>m</sub> (kPa/m)	γ (kPa/m)	tg φ'	φ'	β	cos β	H(m)
20.000	16.000	0.727	36.0	39	0.78	0.250

w <sub>i</sub> (kN/m)	C <sub>i</sub> (kPa)	h' <sub>pi</sub> (m)	h <sub>pi</sub> (m)	u <sub>i</sub> (kPa)	w <sub>i</sub> sin α <sub>i</sub>	c <sub>i</sub> Δl <sub>i</sub> cos α <sub>i</sub>	(w <sub>i</sub> - u <sub>i</sub> Δl <sub>i</sub> cos α <sub>i</sub> )tan φ'
0.912	5.5	0	0	0.00	0.400	3.135	0.663
3.168	5.5	0	0	0.00	1.339	3.300	2.302
4.992	5.5	0	0	0.00	2.266	3.300	3.627
4.646	5.5	0	0	0.00	2.253	2.420	3.376
9.630	5.5	0.096	0.058	0.57	4.960	4.125	6.687
9.336	5.5	0.186	0.112	1.10	5.221	3.300	6.303
9.816	5.5	0.242	0.146	1.43	5.907	3.300	6.507
10.008	5.5	0.250	0.151	1.48	6.298	3.300	6.626
9.624	5.5	0.221	0.133	1.31	6.440	3.300	6.421
10.002	5.5	0.095	0.057	0.56	7.315	4.180	6.956
4.266	5.5	0	0	0.00	3.068	2.365	3.099
4.800	5.5	0	0	0.00	3.730	3.300	3.487
1.824	5.5	0	0	0.00	1.476	3.300	1.325

NUM	DEN	
3.58	0.40	
5.27	1.34	
6.54	2.27	<b>F</b>
5.50	2.25	1.97
10.33	4.96	
9.28	5.22	
9.61	5.91	<b>F</b>
9.83	6.30	
9.82	6.44	
11.70	7.31	
5.69	3.07	
7.41	3.73	
5.22	1.48	
<b>99.79</b>	<b>50.67</b>	<b>1.97</b>

Submerged slices/to change  
Trial Value of F

Land Slide 2 - Residual Strength Parameters - Bishop Modified Method - H=0.25 m

strip	b <sub>i</sub> (m)	α <sub>i</sub> (deg)	sin α <sub>i</sub>	cos α <sub>i</sub>	h <sub>i</sub> (m)	A <sub>i</sub> (m <sup>2</sup> )	Δl <sub>i</sub> (m)
1	0.88	12	0.208	0.978	0.23	0.202	0.90
2	0.88	15	0.259	0.966	0.66	0.581	0.91
3	0.88	18	0.309	0.951	1.04	0.915	0.93
4	0.88	22	0.375	0.927	1.37	1.206	0.95
5	0.88	25	0.423	0.906	1.63	1.434	0.97
6	0.88	28	0.469	0.883	1.83	1.610	1.00
7	0.88	32	0.530	0.848	1.96	1.725	1.04
8	0.88	35	0.574	0.819	2.02	1.778	1.07
9	0.88	39	0.629	0.777	1.99	1.751	1.13
10	0.88	43	0.682	0.731	1.86	1.637	1.20
11	1.32	48	0.743	0.669	1.77	2.336	1.97
12	0.44	52	0.788	0.616	1.35	0.594	0.71
13	0.93	58	0.848	0.530	0.50	0.465	1.75

γm(kPa/m)	γ (kPa/m)	tg φ'	φ'	β	cos β	H(m)
20.000	16.000	0.700	35.0	36	0.81	0.250

w <sub>i</sub> (kN/m)	C <sub>i</sub> (kPa)	h' <sub>p<sub>i</sub></sub> (m)	h <sub>p<sub>i</sub></sub> (m)	u <sub>i</sub> (kPa)	w <sub>i</sub> sin α <sub>i</sub>	c <sub>i</sub> Δl <sub>i</sub> cos α <sub>i</sub>	(w <sub>i</sub> - u <sub>i</sub> Δl <sub>i</sub> cos α <sub>i</sub> )tan φ'
3.238	0	0	0	0.00	0.673	0.000	2.268
9.293	0	0	0	0.00	2.405	0.000	6.507
14.643	0	0	0	0.00	4.525	0.000	10.253
19.290	0	0	0	0.00	7.226	0.000	13.507
22.950	0	0	0	0.00	9.699	0.000	16.070
26.646	0	0.079	0.052	0.51	12.510	0.000	18.345
28.477	0	0.208	0.136	1.34	15.090	0.000	19.117
29.322	0	0.264	0.173	1.70	16.818	0.000	19.487
28.899	0	0.239	0.156	1.53	18.187	0.000	19.290
27.069	0	0.101	0.066	0.65	18.461	0.000	18.554
37.382	0	0	0	0.00	27.781	0.000	26.175
9.504	0	0	0	0.00	7.489	0.000	6.655
7.440	0	0	0	0.00	6.309	0.000	5.210

NUM	DEN	
2.03	0.67	
5.71	2.41	
8.85	4.52	<b>F</b>
11.45	7.23	1.04
13.49	9.70	
15.30	12.51	
15.87	15.09	<b>F</b>
16.17	16.82	<b>1.04</b>
16.06	18.19	
15.58	18.46	
22.38	27.78	
5.81	7.49	
4.73	6.31	
<b>153.43</b>	<b>147.17</b>	

Submerged slices/to change  
Trial Value of F

Land Slide 2 - Residual Strength Parameters - Bishop Modified Method - H=0.30 m

strip	b <sub>i</sub> (m)	α <sub>i</sub> (deg)	sin α <sub>i</sub>	cos α <sub>i</sub>	h <sub>i</sub> (m)	A <sub>i</sub> (m <sup>2</sup> )	Δl <sub>i</sub> (m)
1	0.88	12	0.208	0.978	0.23	0.202	0.90
2	0.88	15	0.259	0.966	0.66	0.581	0.91
3	0.88	18	0.309	0.951	1.04	0.915	0.93
4	0.88	22	0.375	0.927	1.37	1.206	0.95
5	0.75	25	0.423	0.906	1.58	1.185	0.83
6	1.09	28	0.469	0.883	1.78	1.940	1.23
7	0.88	32	0.530	0.848	1.96	1.725	1.04
8	0.88	35	0.574	0.819	2.02	1.778	1.07
9	0.88	39	0.629	0.777	1.99	1.751	1.13
10	1.01	43	0.682	0.731	1.90	1.919	1.38
11	1.20	48	0.743	0.669	1.81	2.172	1.79
12	0.44	52	0.788	0.616	1.35	0.594	0.71
13	0.93	58	0.848	0.530	0.50	0.465	1.75

γm(kPa/m)	γ (kPa/m)	tg φ'	φ'	β	cos β	H(m)
20.000	16.000	0.700	35.0	36	0.81	0.300

w <sub>i</sub> (kN/m)	C <sub>i</sub> (kPa)	h' <sub>p<sub>i</sub></sub> (m)	hp <sub>i</sub> (m)	u <sub>i</sub> (kPa)	w <sub>i</sub> sin α <sub>i</sub>	c <sub>i</sub> Δl <sub>i</sub> cos α <sub>i</sub>	(w <sub>i</sub> - u <sub>i</sub> Δl <sub>i</sub> cos α <sub>i</sub> )tan φ'
3.238	0	0	0	0.00	0.673	0.000	2.268
9.293	0	0	0	0.00	2.405	0.000	6.507
14.643	0	0	0	0.00	4.525	0.000	10.253
19.290	0	0	0	0.00	7.226	0.000	13.507
18.960	0	0	0	0.00	8.013	0.000	13.276
32.351	0	0.12	0.079	0.77	15.188	0.000	22.064
28.653	0	0.257	0.168	1.65	15.184	0.000	19.046
29.498	0	0.306	0.200	1.96	16.919	0.000	19.444
29.075	0	0.276	0.181	1.77	18.298	0.000	19.267
31.916	0	0.135	0.088	0.87	21.767	0.000	21.735
34.752	0	0	0	0.00	25.826	0.000	24.334
9.504	0	0	0	0.00	7.489	0.000	6.655
7.440	0	0	0	0.00	6.309	0.000	5.210

NUM	DEN	
2.03	0.67	
5.70	2.41	
8.83	4.52	<b>F</b>
11.43	7.23	1.03
11.12	8.01	
18.35	15.19	
15.76	15.18	<b>F</b>
16.08	16.92	
15.99	18.30	
18.19	21.77	
20.72	25.83	
5.78	7.49	
4.71	6.31	
<b>154.69</b>	<b>149.82</b>	<b>1.03</b>

Submerged slices/to change  
Trial Value of F

Land Slide 4 - Residual Strength Parameters - Bishop Modified Method - H=0.25 m

strip	bi (m)	$\alpha_i$ (deg)	$\sin \alpha_i$	$\cos \alpha_i$	hi (m)	Ai (mq)	$\Delta li$ (m)
1	0.93	10	0.174	0.985	0.24	0.223	0.94
2	0.93	14	0.242	0.970	0.69	0.642	0.96
3	0.74	17	0.292	0.956	1.02	0.755	0.77
4	1.12	20	0.342	0.940	1.43	1.602	1.19
5	0.93	24	0.407	0.914	1.70	1.581	1.02
6	0.93	24	0.407	0.914	1.94	1.804	1.02
7	0.93	31	0.515	0.857	2.10	1.953	1.08
8	0.93	37	0.602	0.799	2.12	1.972	1.16
9	0.93	39	0.629	0.777	2.05	1.907	1.20
10	0.93	43	0.682	0.731	1.89	1.758	1.27
11	1.29	48	0.743	0.669	1.60	2.064	1.93
12	0.58	53	0.799	0.602	1.05	0.609	0.96
13	0.93	58	0.848	0.530	0.46	0.428	1.75

$\gamma_m$ (kPa/m)	$\gamma$ (kPa/m)	T	$\tan \phi'$	$\phi'$	$\beta$	$\cos \beta$	H(m)
20.000	16.000	2.810	0.700	35.0	35	0.82	0.250

wi (kN/m)	Ci (kPa)	h'pi(m)	hpi(m)	ui (kPa)	wi sin $\alpha_i$	ci $\Delta li$ cos $\alpha_i$	$(wi - ui \Delta li \cos \alpha_i) \tan \phi'$
3.571	0	0	0	0.00	0.620	0.000	2.501
10.267	0	0	0	0.00	2.484	0.000	7.189
12.077	0	0	0	0.00	3.531	0.000	8.456
25.626	0	0	0	0.00	8.764	0.000	17.943
25.296	0	0	0	0.00	10.289	0.000	17.712
28.867	0	0	0	0.00	11.741	0.000	20.213
32.178	0	0.386	0.259	2.54	16.573	0.000	20.877
32.476	0	0.404	0.271	2.66	19.544	0.000	21.008
31.434	0	0.327	0.219	2.15	19.782	0.000	20.609
28.123	0	0	0	0.00	19.180	0.000	19.692
33.024	0	0	0	0.00	24.542	0.000	23.124
9.744	0	0	0	0.00	7.782	0.000	6.823
6.845	0	0	0	0.00	5.805	0.000	4.793

NUM	DEN	
2.28	0.62	
6.39	2.48	
7.39	3.53	F
15.48	8.76	1.09
15.08	10.29	
17.21	11.74	
17.57	16.57	F
17.72	19.54	1.09
17.44	19.78	
16.84	19.18	
20.17	24.54	
6.12	7.78	
4.46	5.80	
<b>164.14</b>	<b>150.64</b>	

Submerged slices  
 Trial Value of F

Land Slide 4 - Residual Strength Parameters - Bishop Modified Method - H=0.35 m

strip	bi (m)	$\alpha_i$ (deg)	$\sin \alpha_i$	$\cos \alpha_i$	hi (m)	Ai (mq)	$\Delta li$ (m)
1	0.93	10	0.174	0.985	0.24	0.223	0.94
2	0.93	14	0.242	0.970	0.69	0.642	0.96
3	0.74	17	0.292	0.956	1.02	0.755	0.77
4	1.12	20	0.342	0.940	1.43	1.602	1.19
5	0.93	24	0.407	0.914	1.70	1.581	1.02
6	0.93	24	0.407	0.914	1.94	1.804	1.02
7	0.93	31	0.515	0.857	2.10	1.953	1.08
8	0.93	37	0.602	0.799	2.12	1.972	1.16
9	0.93	39	0.629	0.777	2.05	1.907	1.20
10	0.93	43	0.682	0.731	1.89	1.758	1.27
11	1.29	48	0.743	0.669	1.60	2.064	1.93
12	0.58	53	0.799	0.602	1.05	0.609	0.96
13	0.93	58	0.848	0.530	0.46	0.428	1.75

$\gamma_m$ (kPa/m)	$\gamma$ (kPa/m)	$\tan \phi'$	$\phi'$	$\beta$	$\cos \beta$	H(m)
20.000	16.000	0.700	35.0	35	0.82	0.350

wi (kN/m)	Ci (kPa)	h'pi(m)	hpi(m)	ui (kPa)	wi sin $\alpha_i$	ci $\Delta li$ cos $\alpha_i$	(wi - ui $\Delta li$ cos $\alpha_i$ )tan $\phi'$
3.571	0	0	0	0.00	0.620	0.000	2.501
10.267	0	0	0	0.00	2.484	0.000	7.189
12.077	0	0	0	0.00	3.531	0.000	8.456
25.626	0	0	0	0.00	8.764	0.000	17.943
25.296	0	0	0	0.00	10.289	0.000	17.712
30.169	0	0.213	0.143	1.40	12.271	0.000	20.212
32.550	0	0.386	0.259	2.54	16.764	0.000	21.137
32.848	0	0.404	0.271	2.66	19.768	0.000	21.268
31.806	0	0.327	0.219	2.15	20.016	0.000	20.869
29.425	0	0.173	0.116	1.14	20.068	0.000	19.862
33.024	0	0	0	0.00	24.542	0.000	23.124
9.744	0	0	0	0.00	7.782	0.000	6.823
6.845	0	0	0	0.00	5.805	0.000	4.793

NUM	DEN	
2.28	0.62	
6.37	2.48	
7.37	3.53	<b>F</b>
15.42	8.76	1.07
15.01	10.29	
17.13	12.27	
17.70	16.76	<b>F</b>
17.84	19.77	1.07
17.55	20.02	
16.87	20.07	
20.01	24.54	
6.07	7.78	
4.42	5.80	
<b>164.04</b>	<b>152.70</b>	

Submerged slices  
 Trial Value of F

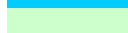
Land Slide 4 - Residual Strength Parameters - Bishop Modified Method - H=0.70 m

strip	bi (m)	$\alpha_i$ (deg)	$\sin \alpha_i$	$\cos \alpha_i$	hi (m)	Ai (mq)	$\Delta li$ (m)
1	0.93	10	0.174	0.985	0.24	0.223	0.94
2	0.93	14	0.242	0.970	0.69	0.642	0.96
3	0.74	17	0.292	0.956	1.02	0.755	0.77
4	1.12	20	0.342	0.940	1.43	1.602	1.19
5	0.93	24	0.407	0.914	1.70	1.581	1.02
6	0.93	24	0.407	0.914	1.94	1.804	1.02
7	0.93	31	0.515	0.857	2.10	1.953	1.08
8	0.93	37	0.602	0.799	2.12	1.972	1.16
9	0.93	39	0.629	0.777	2.05	1.907	1.20
10	0.93	43	0.682	0.731	1.89	1.758	1.27
11	1.29	48	0.743	0.669	1.60	2.064	1.93
12	0.58	53	0.799	0.602	1.05	0.609	0.96
13	0.93	58	0.848	0.530	0.46	0.428	1.75

$\gamma_m$ (kPa/m)	$\gamma$ (kPa/m)	T	$\tan \phi'$	$\phi'$	$\beta$	$\cos \beta$	H(m)
20.000	16.000	2.810	0.700	35.0	35	0.82	0.700

wi (kN/m)	Ci (kPa)	h'pi(m)	hpi(m)	ui (kPa)	wi sin $\alpha_i$	ci $\Delta li$ cos $\alpha_i$	$(wi - ui \Delta li \cos \alpha_i) \tan \phi'$
3.571	0	0	0	0.00	0.620	0.000	2.501
10.267	0	0	0	0.00	2.484	0.000	7.189
12.077	0	0	0	0.00	3.531	0.000	8.456
28.762	0	0.235	0.158	1.55	9.837	0.000	18.926
27.900	0	0.518	0.348	3.41	11.348	0.000	17.315
31.471	0	0.732	0.491	4.82	12.800	0.000	18.899
33.852	0	0.905	0.607	5.96	17.435	0.000	19.824
34.150	0	0.926	0.621	6.10	20.552	0.000	19.942
33.108	0	0.844	0.566	5.56	20.836	0.000	19.565
30.727	0	0.692	0.464	4.56	20.956	0.000	18.549
36.636	0	0.392	0.263	2.58	27.226	0.000	23.322
9.744	0	0	0	0.00	7.782	0.000	6.823
6.845	0	0	0	0.00	5.805	0.000	4.793

NUM	DEN	
2.25	0.62	
6.26	2.48	
7.22	3.53	<b>F</b>
15.88	9.84	0.95
14.27	11.35	
15.58	12.80	
16.03	17.44	<b>F</b>
16.05	20.55	
15.77	20.84	
15.03	20.96	
19.17	27.23	
5.73	7.78	
4.15	5.80	
<b>153.38</b>	<b>161.21</b>	<b>0.95</b>

 Submerged slices  
 Trial Value of F

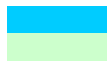
Land Slide 5 - Residual Strength Parameters - Bishop Modified Method - H=0.15 m

strip	b <sub>i</sub> (m)	α <sub>i</sub> (deg)	sin α <sub>i</sub>	cos α <sub>i</sub>	h <sub>i</sub> (m)	A <sub>i</sub> (m <sup>2</sup> )	Δl <sub>i</sub> (m)
1	0.57	26	0.438	0.899	0.10	0.057	0.63
2	0.60	25	0.423	0.906	0.33	0.198	0.66
3	0.60	27	0.454	0.891	0.52	0.312	0.67
4	0.44	29	0.485	0.875	0.66	0.290	0.50
5	0.75	31	0.515	0.857	0.74	0.555	0.87
6	0.60	34	0.559	0.829	0.91	0.546	0.72
7	0.60	37	0.602	0.799	0.96	0.576	0.75
8	0.60	39	0.629	0.777	0.98	0.588	0.77
9	0.60	42	0.669	0.743	0.94	0.564	0.81
10	0.76	47	0.731	0.682	0.76	0.578	1.11
11	0.43	46	0.719	0.695	0.62	0.267	0.62
12	0.60	51	0.777	0.629	0.50	0.300	0.95
13	0.60	54	0.809	0.588	0.19	0.114	1.02

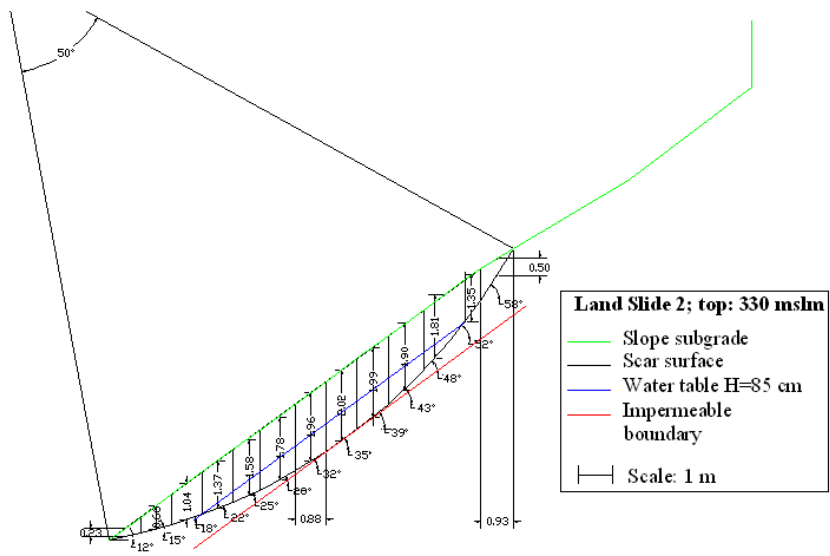
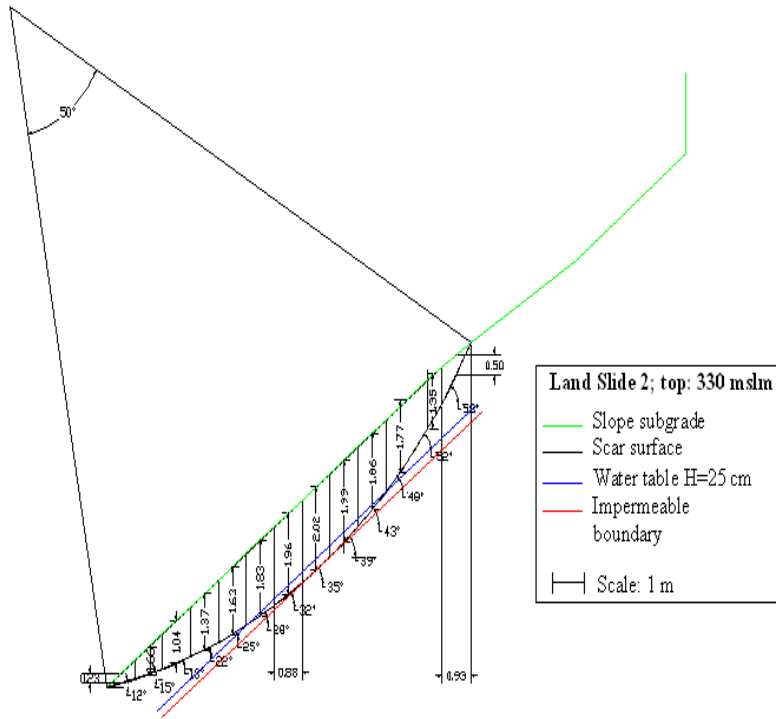
γm(kPa/m)	γ (kPa/m)	tg φ'	φ'	β	cos β	H(m)
20.000	16.000	0.754	37.0	37	0.80	0.150

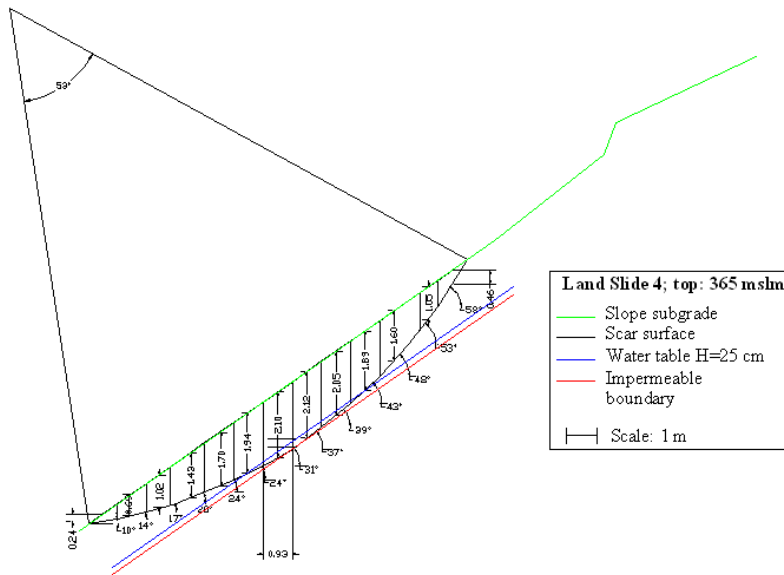
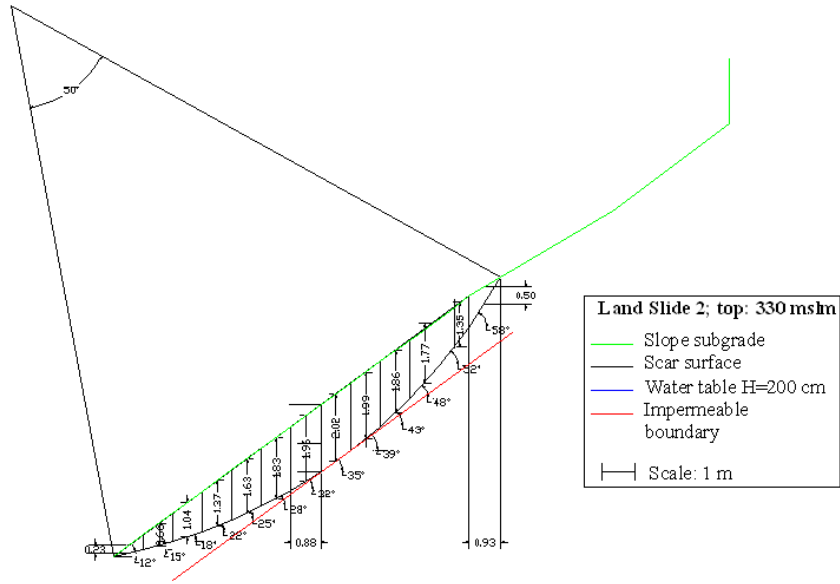
w <sub>i</sub> (kN/m)	C <sub>i</sub> (kPa)	h' <sub>p<sub>i</sub></sub> (m)	hp <sub>i</sub> (m)	u <sub>i</sub> (kPa)	w <sub>i</sub> sin α <sub>i</sub>	c <sub>i</sub> Δl <sub>i</sub> cos α <sub>i</sub>	(w <sub>i</sub> - u <sub>i</sub> Δl <sub>i</sub> cos α <sub>i</sub> )tan φ'
0.912	0	0	0	0.00	0.400	0.000	0.687
3.168	0	0	0	0.00	1.339	0.000	2.387
4.992	0	0	0	0.00	2.266	0.000	3.762
4.646	0	0	0	0.00	2.253	0.000	3.501
8.880	0	0	0.000	0.00	4.574	0.000	6.692
9.096	0	0.086	0.055	0.54	5.086	0.000	6.611
9.576	0	0.142	0.091	0.89	5.763	0.000	6.814
9.768	0	0.150	0.096	0.94	6.147	0.000	6.936
9.384	0	0.121	0.077	0.76	6.279	0.000	6.729
9.242	0	0	0.000	0.00	6.759	0.000	6.964
4.266	0	0	0	0.00	3.068	0.000	3.214
4.800	0	0	0	0.00	3.730	0.000	3.617
1.824	0	0	0	0.00	1.476	0.000	1.374

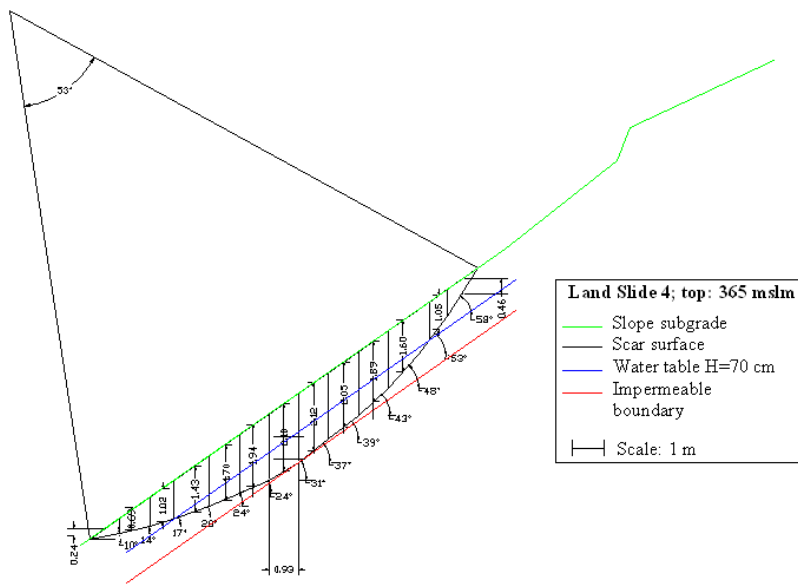
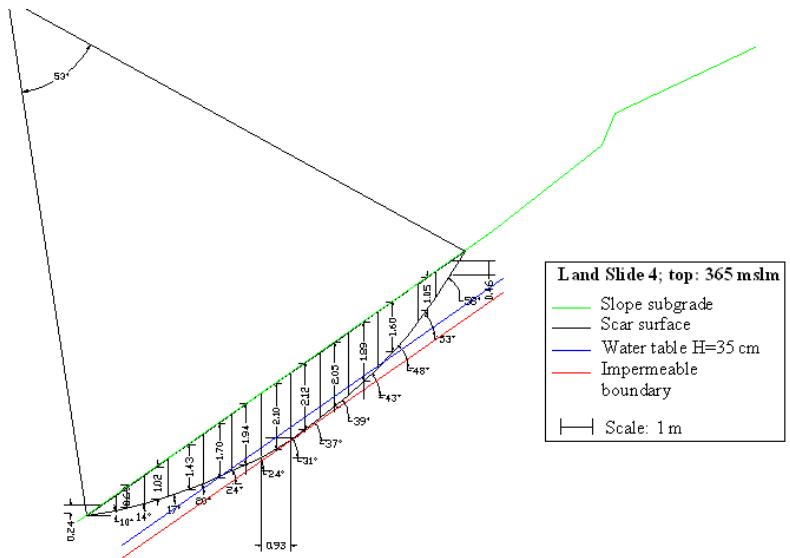
NUM	DEN	
0.55	0.40	
1.92	1.34	
3.01	2.27	<b>F</b>
2.78	2.25	0.95
5.29	4.57	
5.19	5.09	
5.34	5.76	<b>F</b>
5.43	6.15	<b>0.95</b>
5.28	6.28	
5.52	6.76	
2.54	3.07	
2.90	3.73	
1.12	1.48	
<b>46.88</b>	<b>49.14</b>	

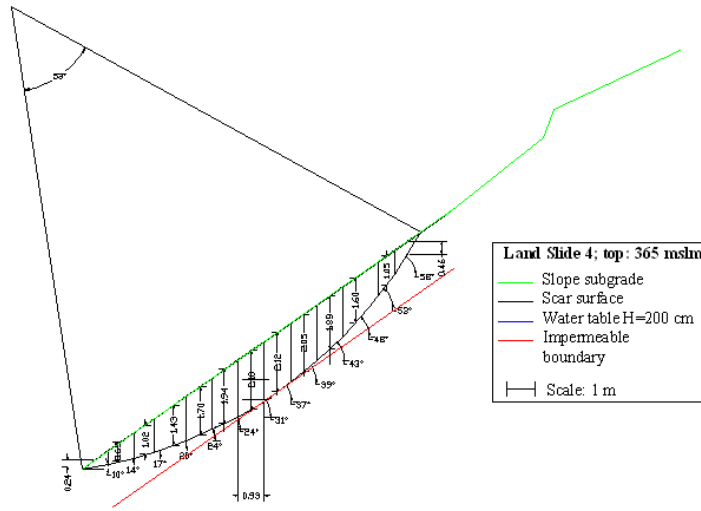


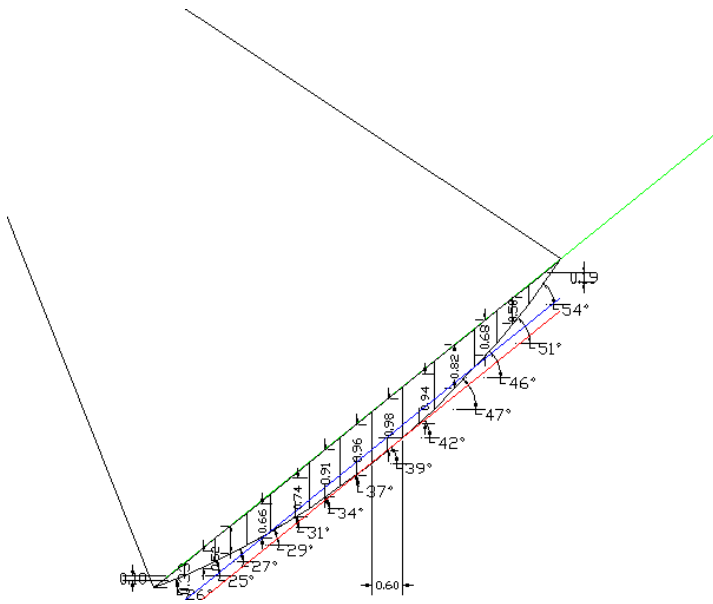
Submerged slices  
Trial Value of F











**Land Slide 5; top: 350 mslm**

- Slope subgrade
- Scar surface
- Water table H=25 cm
- Impermeable boundary
- |—| Scale: 1 m

## BIBLIOGRAPHY

Alarcon-Guzman, A., Leonards, G.A., and Chameau, J.L. (1988). “*Undrained monotonic and cyclic strength of sands.*” *Journal of Geotechnical Engineering, ASCE*, 114(10), 1089–1109.

Amoozegar A. (1989). “A compact constant head permeameter for measuring saturated hydraulic conductivity of the vadose zone”. *Soil Sci. Soc. Am. J.*, 53, 1356-1361.

Anderson M.G. & Brut T.P. (1977). “Automatic monitoring of soil moisture conditions in a hillslope spur and hollow”. *Journal of Hydrology*, 33, 27-36.

Anderson, S. A. & Sitar, N. (1995). “Analysis of rainfall-induced debris flow”. *J. Geot. Eng.* 121(7), 544-552.

ASTM D 2487. Annual book of ASTM standards, vol. 04-08

Bingham, E.C. (1916) “*An Investigation of the Laws of Plastic Flow*” U.S. Bureau of Standards Bulletin, 13, 309-353

Bishop A.W. (1955). “*The use of the slip circle in stability analysis of slope.*” *Geotechnique*, London, 5(1), 7-17

Bishop A.W. & Bjerrum L. (1960). “*The relevance of triaxial test to the solution of stability problem*” *Proc. of Research conference on shear strength UCB-ASCE*, 437-501.

Brooks R.H. & Corey A.T., (1966). “*Properties of porous media affecting fluid flow*” *J. Irrig. Drain. Proc. ASCE*, 4855 (IR2), 61-88.

Budetta P. & De Riso R. (2004). “*The mobility of some debris flow in pyroclastic deposits of the northwestern campanian region (southern Italy)*”. *Bulletin of Engineering Geology and Environment*, 63, 293-302.

Campbell, R. H. (1975). “*Soil slips, debris-flow and rainstorms in the Santa Monica mountains and vicinity, Southern California*”. *Prof. Paper, U. S. Geological Survey*, Washington, D. C., 851 51p.

Casagrande, A. (1940). “*Characteristics of cohesionless soils affecting the stability of slopes and earth fills*”. Contribution to soil mechanics, 1925-1940, Boston Society of Civil Engineers, Oct. 1940.

Cascini L., Guida D., Nocera N., Romanzi G. and Sorbino G. (2000). “*A preliminary model for the landslides of May 1998 in Campanian Region*”. Proceedings 2nd International Symposium on Geotechnics of Hard Soil-Soft Rock, Napoli. Balkema, 1623-1649.

Celico P. & Guadagno F.M. (1998). “*L’instabilità delle coltri piroclastiche delle dorsali carbonatiche in Campania: conoscenze attuali*”. Quaderni di Geologia Applicata, 1, 75-133

Celico P., De Vita P., Fabbrocino S. & Piscopo V. (2001). “*Primi risultati dell’analisi dei debris flows nei versanti dei rilievi carbonatici peri-vesuviani: aspetti idrogeologici predisponenti e condizioni idrologiche critiche*”. Atti dei Convegni Lincei n. 181 “Il dissesto idrogeologico: Inventario e prospettive” Accademia nazionale dei Lincei - 5 giugno 2001.

Chiesa S., Civetta L., De Lucia M., Orsi G. & Poli S. (1987) “*Volcanological evolution of the Island of Ischia*” Rend. Acc. Scienze Fis. E Mat., Special Issue “The volcanoclastic rocks of Campania (southern Italy)” P. Di Girolamo editors. Liguori Editore

Corominas (1996). “*The angle of reach as a mobility index for small and large landslides*”. Canadian Geotechnical Journal, 22, 260-271.

Coulomb C.A. (1773). “*Sur une application des règles, de maximis et minimis à quelque problèmes de statique, relatifs à l’architecture*”

Crosta G. & Dal Negro P. (2003). “*Observation and modelling of soil slip-debris flow initiation processes in pyroclastic deposits: the Sarno 1998 event*”. Natural Hazards and Earth System Sciences, 3, 53-69.

- Cruden D.M. & Varnes D.J. (1996) - *Landslides Types and Processes*. In: "Landslides: Investigation and Mitigation". Transportation Research Board. National Academy of Sciences.
- De Vita P. (2000). "*Fenomeni di instabilità delle coperture piroclastiche dei monti Lattari, di Sarno e di Salerno (Campania) ed analisi degli eventi pluviometrici*". Quaderni di Geologia Applicata, 7-2,
- De Vita P. and Piscopo V. (2002). *Influences of hydrogeological conditions on debris flows in peri- vesuvian hillslopes*. Natural Hazards and Earth System Sciences, 2, 1-9.
- De Vita P. and Reichenbach P. (1998). "*Rainfall-triggered landslides: a references list*". Environmental Geology, 35, 219-233.
- De Vita, P., Agrello, D. & Ambrosino, F. (2006). "*Landslide susceptibility assessment in ash-fall pyroclastic deposits surrounding Mount Somma-Vesuvius: Application of geophysical surveys for soil thickness mapping*" Journal of Applied Geophysics 59, 126-139.
- De Vita P., Di Clemente E., Rolandi M. & Celico P. (2007). "*Engineering geological models of the initial landslides occurred on April 30 2006, at Mount di Vezzi (Ischia Island, Italy)*". Italian Journal of Engineering Geology and Environment, 2, 119-141.
- Dietrich W.E., Reneau S.L. and Wilson C.J. (1986). *Hollows, colluvium and landslides in soil-mantled landscapes*. In: Hillslope processes, Abrahams, A.D. ed., Allen and Unwin, 361-388.
- P. Di Girolamo, G. Nardi, G. Rolandi, D. Stanzione (1976). "*Occurrence of calc-alkaline two pyroxene andesites from deep bore-holes in the Phlegraen Phield . Petrographic and petrochemical data.*" Rend. Acc. Sc. Fis. Mat. - Napoli Serie IV, vol. XLIII.
- Duncan, J.M. and Wright, S.G., (2005). "*Soil strength and slope stability,*" Wiley New York.
- Duncan, J.M., and Stark, T.D. (1992). "*Soil strength from back analysis of slope failures.*" Proc. ASCE Geotech. Conf. on Slopes and Embankments, Berkeley, 890-904.

- Esposito L. and Guadagno F.M. (1998). “*Some special geotechnical properties of pumice deposits*”. Bulletin of Engineering Geology and the Environment, 57, 41–50.
- Guadagno F.M., Forte R., Revellino P., Fiorillo F. and Focareta M. (2004). “*Some aspects of the initiation of debris avalanches in the Campania Region: The role of morphological slope discontinuities and the development of failure*”. Geomorphology, 66, pp. 237-254.
- Guzzetti, F., Cardinali, M., Reichenbach, P., (1994). “*The AVI Project: A bibliographical and archive inventory of landslides and floods in Italy.*” Environmental Management 18: 623-633
- Guzzetti, F., (2000). “*Landslide fatalities and evaluation of landslide risk in Italy.*” Engineering Geology 58: 89–107
- Harr R.D. (1977). “*Water flux in soil and subsoil on a steep forested slope*” Journal of Hydrology, 33, 37-58.
- Hungr O., Evans S.G., Bovis M.J. & Hutchinson J.N. (2001). “*A review of the classification of landslides of flow type*”. Env. Eng. Geos.,7(3), 221-238.
- Hutchinson, J. and Bhandari, R. (1971). “*Undrained loading, a fundamental mechanism of mudflows and other mass movements*”. Géotechnique, 21, 353-358.
- Ishihara K. (1993). “*Liquefaction and flow failures during earthquakes.*” *Geotechnique*, 43(3), 351-415.
- Johnson, K. A. & Sitar, N. (1990). “*Hydrologic conditions leading to debris-flow initiation*”. Can. Geotech J., 27(6), 789-801.
- Kramer, S. & Seed, H. B. (1988). “*Initiation of soil liquefaction under static conditions*”. J. Geotech. Engrg., ASCE, 114(4), 412-430.
- Lampitello (2003). “*Resistenza non drenata e suscettibilità alla liquefazione di ceneri vulcaniche della Regione Campania*”. Tesi di dottorato seconda Università di Napoli.
- Lee, K. L. and Seed, H. B. (1967). “*Drained strength characteristics of sands*”. J Soil Mech.& Found. Eng. 93(SM6), 117-141.

- Lowe, J. (1966). “*Stability analysis of embankments*”. Stability and performance of slopes and embankments, ASCE, New York, N.Y., 1-33.
- Olivares, L., Picarelli, L., Andreozzi, L., Avolio, L., Damiano, E., Lampitello, S., (2002). “*Scenari di pericolosità di frana in terreni sciolti di natura piroclastica*” – Proc. XXI Convegno Nazionale di Geotecnica, l’Aquila, 173-181.
- Olivares, L., Picarelli, L., Andreozzi, L., Damiano, E., Lampitello, S., (2003). “*Meccanismi di innesco delle colate di fango in terreni piroclastici sciolti: il caso di Cervinara*”. Atti del workshop di Anacapri, 205-223.
- Preston N.S.J. and Crozier M.J. (1999). “*Resistance to shallow landslide failure through root-derived cohesion in east coast hill country soils, north island, New Zealand*”. Earth Surface Processes and Landforms – 24, 665-675.
- Pulos, S.J. (1981). “*The steady state of deformation*”. J. Geotech. Engrg. Div., ASCE, 107(GT5), 553-562.
- Rolandi, G., Bertolini, F., Cozzolino, G., Esposito, N., Sannino, D., (2000). “*Sull’origine delle coltri piroclastiche presenti sul versante occidentale del Pizzo D’Alvano*.” Quaderni geologia applicata, 7-1, 38-47.
- Rolandi G., Bellucci F., Heizler M. T., Belkin H. E. and De Vivo B (2003). “*Tectonic controls on the genesis of ignimbrites from the Campanian volcanic zone, southern Italy*.” Mineralogy and Petrology, 79: 3-31.
- Rosi G., Sbrana A., (1987). *Phlegraean Fields. Quaderni de La ricerca Scientifica, 114, 9: 1-175.*
- G. Rolandi, G. Mastrolorenzo, A. M. Barrella, A. Borrelli (1993). “*The Avellino Plinian Eruption of Somma-Vesuvius (3760 Y B.P.): The progressive evolution from Magmatic to hydromagmatic style*.” Journ. Volcanol. and Geoth. Res., 58: 67-88.
- Rowe, P. W. (1962). “*The stress dilatancy for static equilibrium of an assembly of particle in contact*”. Proceedings, Royal Society, London, Series A, Vol. 269, 500-527.

- Sasitharan, S., Robertson, P.K., Sego, D.C. & Morgensten, N.R. (1993). "*Collapse behavior of sand*" Can. Geotech. J. 30: 569-577
- Sassa, K. (1985). "*The mechanism of debris flow*". Proceedings of XI International Conference on Soil Mechanics and Foundation Engineering, San Francisco, 1173-1176. A.A. Balkema, Rotterdam, the Netherlands.
- Sladen, J.A., D'Hollander, R.D., Krahn, J. (1985). "*The liquefaction of sand a collapse surface approach.*" Can Geotech. J. 22: 564-578
- Sassa, K. (1989). "*Geotechnical classification of landslides*". Landslide News. 3, 39-43.
- Selby M.J. (1993). "*Hillslope materials and processes*". Oxford University Press, New York, p. 451.
- Tanaka, T., M. Yasuhara, H. Sakai, and A. Marui (1988). "*The Hachioji experimental basin study—storm runoff processes and the mechanism of its generation*". Journal of Hydrol., 102, 139–164, 1988.
- Taylor, D. W. (1948). "*Fundamentals of soil mechanics*", John Wiley & Sons, Inc., New York, N.Y., 1948, 346-346.
- Terribile Di Gennaro A., Aronne G., Basile A., Buonanno M., Mele G. & Vigiani S. (1998). "*The soil of landslides of Sarno and Quindici*". Proc. Symp. Degradation processes in volcanic soils, University of Naples – pp. 48-64.
- Terzaghi, K. (1942). "*Theoretical Soil Mechanics.*" Wiley, New York,
- USDA (1998). "*Keys to soil taxonomy.*" USDA-Nat, Res. Cons. Service, 8th ed.: p. 328
- Vezzoli L. (1988). *The island of Ischia*. CNR Quaderni de "La Ricerca Scientifica", 114: 1-122, Roma, Italia.
- Whitan A.J. & Sparks R.S.J (1986). "Pumice". Bulletin of Volcanology, 48, 209-223.